

**FABRICATION OF POLYMERIC ULTRAFILTRATION
MEMBRANES USING IONIC LIQUIDS AS GREEN SOLVENTS**

XING DINGYU

(B. Eng, Zhejiang University, P.R. China)

**A THESIS SUBMITTED
FOR THE DEGREE OF DOCTOR OF PHILOSOPHY
DEPARTMENT OF CHEMICAL AND BIOMOLECULAR
ENGINEERING**

NATIONAL UNIVERSITY OF SINGAPORE

2012

DECLARATION

I hereby declare that this thesis is my original work and it has been written by me in its entirety. I have duly acknowledged all the sources of information which have been used in the thesis.

This thesis has also not been submitted for any degree in any university previously.

A handwritten signature in black ink, reading "Xing Dingyu". The signature is written in a cursive style with a large, stylized 'X' and 'D'.

Xing Dingyu
31-Jan-2013

ACKNOWLEDGEMENT

I would like to acknowledge the people who made the journey of my PhD study a wonderful and rewarding experience. First, I want to thank my academic advisor, Professor Chung Tai-Shung. He has given me every opportunity to learn about membrane science and provided well equipped facilities to carry out my research. The journey to the accomplishment of the PhD degree is certainly full of challenges; Prof. Chung has impelled me to achieve what I never imagine and trained me as an independent researcher. His attitude towards work is helpful to my growth in areas extending beyond research work. I wish to express my sincere appreciation to Prof. Chung for his teaching and guidance.

Thanks are dedicated to Professor Jiang Jianwen and his staffs for their great help on simulation works. Special thanks are due to all the team members in Prof. Chung's research group. Dr. Peng Na is especially recognized for her guidance and help in my research works from the first day I joined this group. With her support in both research and life, I could progressively make the way in these four years. I would like to convey my appreciation to Dr. Wang Kaiyu, Dr. Su Jincai, Dr. Teoh May May, Dr. Wan Yan, Dr. Ge Qingchun and Dr. Xiao Youchang for their valuable advice to my work, and for sharing their knowledge and technical expertise with me. My gratitude extends to Ms Zhang Sui, Ms Zhong Pei Shan and Ms Wang Huan for their suggestions and support in the past years. It is my treasure to make so many friends here. All members in Prof.

Chung's group are cheerful and helpful to me which have made my study in NUS enjoyable and memorable.

I gratefully acknowledge the research scholarship by the National University of Singapore. I would like to thank the NUS initiative grant for life science (R-279-000-249-646), the NRF CRP grant for energy development (R-279-000-261-281), and GlaxoSmithKline-Economic Development Board (GSK-EDB) Trust Fund for the project entitled "New membrane development to facilitate solvent recovery and pharmaceutical separation in pharmaceutical syntheses" with the grant number R-706-000-019-592. I also thank BASF, Eastman and PBI Performance Products, Inc. for the provision of materials.

Last but foremost, I wish to thank my family and friends for their constant support, love and encouragement throughout my candidature.

TABLE OF CONTENTS

| | |
|---|-------------|
| ACKNOWLEDGEMENT..... | i |
| TABLE OF CONTENTS | iii |
| SUMMARY | viii |
| LIST OF TABLES | xi |
| LIST OF FIGURES | xii |
| NOMENCLATURE..... | xvii |
| Chapter 1 Introduction..... | 1 |
| 1.1 Characteristics and advantages of ionic liquids | 2 |
| 1.2 Applications of ionic liquids in recent polymer science | 5 |
| 1.3 Application of ionic liquids in membrane science | 7 |
| 1.4 Research objectives | 7 |
| Chapter 2 Literature Review on Membrane Technology | 10 |
| 2.1 Development of polymeric membrane for liquid separation | 10 |
| 2.2 Theoretical background on phase inversion in membrane formation | 13 |
| 2.2.1 Phase diagrams and phase inversion..... | 13 |
| 2.2.2 Fabrication of flat sheet and hollow fiber membranes..... | 17 |
| Chapter 3 Fundamentals and characteristics of membrane formation via phase inversion for cellulose acetate membranes using an ionic liquid, [BMIM]SCN, as the solvent..... | 23 |
| 3.1 Introduction | 23 |

| | |
|---|-----------|
| 3.2 Experimental | 24 |
| 3.2.1 Materials | 24 |
| 3.2.2 Phase diagrams, dope preparation and viscosity measurements..... | 24 |
| 3.2.3 Fabrication of flat asymmetric membranes..... | 26 |
| 3.2.4 Fabrication of hollow fibers..... | 26 |
| 3.2.5 Morphology study..... | 27 |
| 3.2.6 Ultrafiltration tests for pure water flux and pore size distribution..... | 27 |
| 3.2.7 Membrane porosity | 30 |
| 3.2.8 Recovery and reuse of [BMIM]SCN | 30 |
| 3.3 Results and discussion..... | 30 |
| 3.3.1 Solubility, viscosity curves and phase diagrams of CA in ionic liquids..... | 30 |
| 3.3.2 The effects of solvents on CA flat sheet membranes..... | 33 |
| 3.3.2.1 The morphology of CA flat sheet membranes | 33 |
| 3.3.2.2 Porosity, pure water permeability, pore size and its distribution of CA flat sheet membranes | 37 |
| 3.3.3 Fabrication of CA hollow fiber membranes from [BMIM]SCN and the morphology study | 40 |
| 3.3.4 Recovery and reuse of [BMIM]SCN for membrane fabrication | 43 |
| 3.4 Conclusions | 44 |
| Chapter 4 Investigation of unique interactions between cellulose acetate and ionic liquid, [EMIM]SCN, and their influences on hollow fiber ultrafiltration membranes | 46 |
| 4.1 Introduction | 46 |
| 4.2 Experimental | 48 |

| | |
|--|-----------|
| 4.2.1 Materials | 48 |
| 4.2.2 Dope characterizations - FTIR, rheology, phase inversion kinetics and phase diagrams | 49 |
| 4.2.3 Molecular simulation by Materials Studio..... | 50 |
| 4.2.4 Fabrication of CA flat sheet and hollow fiber membranes | 51 |
| 4.3 Results and discussion..... | 52 |
| 4.3.1 The molecular interactions between CA and ionic liquids | 52 |
| 4.3.2 The rheology of CA/[EMIM]SCN solutions | 55 |
| 4.3.3 Phase inversion of CA/[EMIM]SCN in different coagulants | 58 |
| 4.3.4 Hollow fiber membrane morphology and ultrafiltration characterizations | 64 |
| 4.3.4.1 Effects of dope flow rate and dope temperature..... | 66 |
| 4.3.4.2 Effects of air-gap distance | 70 |
| Chapter 5 Molecular interactions between polybenzimidazole and [EMIM]OAc, and derived ultrafiltration membranes for protein separation..... | 74 |
| 5.1 Introduction | 74 |
| 5.2 Experimental | 77 |
| 5.2.1 Materials | 77 |
| 5.2.2 Dissolution experiments..... | 78 |
| 5.2.3 Molecular simulation by Materials Studio..... | 78 |
| 5.2.4 Rheological measurements of PBI/ionic liquid solutions..... | 79 |
| 5.2.5 Fabrication of flat asymmetric membranes..... | 79 |
| 5.2.6 Thermal treatment and chemical cross-linking of PBI membranes..... | 80 |
| 5.2.7 Protein separation performance | 80 |
| 5.3 Results and discussion..... | 81 |

| | | |
|--|---|-----|
| 5.3.1 | Dissolution of PBI in ionic liquids..... | 81 |
| 5.3.2 | Molecular dynamic simulation of PBI/ionic liquid systems..... | 84 |
| 5.3.3 | The rheological behavior of PBI/[EMIM]OAc solutions | 86 |
| 5.3.4 | Morphology of PBI asymmetric membranes..... | 89 |
| 5.3.5 | Protein separation performance | 91 |
| 5.4 | Conclusions | 95 |
| | | |
| Chapter 6 Fabrication of porous and interconnected PBI/P84 ultrafiltration membranes using [EMIM]OAc as the green solvent | | |
| 6.1 | Introduction | 97 |
| 6.2 | Experimental | 99 |
| | | |
| 6.2.1 | Materials | 99 |
| 6.2.2 | Dope characterizations - Rheological measurements, phase inversion kinetics of PBI/ionic liquid solutions | 101 |
| 6.2.3 | Fabrication of flat asymmetric membranes..... | 102 |
| 6.2.4 | Fourier transformed infrared spectroscopy (FTIR)..... | 102 |
| 6.2.5 | Differential Scanning Calorimetry (DSC) | 102 |
| 6.3 | Results and discussion..... | 103 |
| | | |
| 6.3.1 | Solubility of selected polyimides in [EMIM]OAc..... | 103 |
| 6.3.2 | Interactions in the P84/[EMIM]OAc solution | 103 |
| 6.3.3 | Miscibility of P84 and PBI in [EMIM]OAc | 105 |
| 6.3.4 | The rheological behavior of PBI/P84/[EMIM]OAc solutions..... | 109 |
| 6.3.5 | Morphology and ultrafiltration performance of PBI/P84 blend membranes | 111 |
| 6.3.5.1 | Effects of polymer composition | 111 |

| | |
|---|------------|
| 6.3.5.2 Effects of casting temperatures | 116 |
| 6.4 Conclusions | 118 |
| Chapter 7 Conclusions and recommendations..... | 120 |
| Chapter 8 References..... | 127 |

SUMMARY

Ionic liquids have gained worldwide attention as green solvents in the last decade. This study explored, for the first time, the fundamental science and engineering of using ionic liquids as a new generation of solvents to replace the traditional organic solvents for the fabrication of flat sheet membranes and hollow fiber membranes. The fundamentals and characteristics of membrane formation of cellulose acetate (CA) membranes have been investigated using 1-butyl-3-methylimidazolium thiocyanate ([BMIM]SCN) as the solvent via phase inversion in water. For elucidation, other solvents, i.e. *N*-Methyl-2-pyrrolidinone (NMP) and acetone, were also studied. It is found that [BMIM]SCN has distinctive effects on phase inversion process and membrane morphology compared to NMP and acetone because of its unique nature of high viscosity and the high ratio of [BMIM]SCN outflow to water inflow. Membranes cast or spun from CA/[BMIM]SCN have a macrovoid-free dense structure full of nodules, implying the paths of phase inversion are mainly nucleation growth and gelation, followed possibly by spinodal decomposition. The recovery and reuse of [BMIM]SCN have also been demonstrated and achieved. The derived flat sheet membranes made from the recovered [BMIM]SCN show similar morphological and performance characteristics with those from the fresh [BMIM]SCN.

To further investigate the molecular interactions between ionic liquid, 1-ethyl-3-methylimidazolium thiocyanate ([EMIM]SCN) and cellulose acetate (CA), we employed not only experimental characterizations including FTIR and rheological tests, but also

molecular dynamics simulations. Due to the electronic nature of ionic liquids, [EMIM]SCN interacts with CA molecules through pronounced hydrogen bonding, coulombic forces and van der Waals interactions, which play an important role in dissolving CA and also greatly contribute to a three-region flow curve of the CA/[EMIM]SCN solutions under shear stress. The charge-ordered network in CA/[EMIM]SCN solutions as well as the affinity and unique solvent exchange characteristics between non-solvents and [EMIM]SCN are found to greatly influence the phase inversion paths of membranes. In addition, the effects of dope flow rate, dope temperature and air-gap distance on hollow fiber formation have been elucidated and correlated to the interactions between CA and [EMIM]SCN and the phase inversion mechanisms. By fine-tuning the spinning conditions, CA hollow fiber membranes are successfully fabricated for ultrafiltration with a PWP value of 90.10 (L/m² bar h) and a mean effective pore diameter of 16.68nm.

Ionic liquid, 1-ethyl-3-methylimidazolium acetate ([EMIM]OAc), was found to be a promising green solvent to fabricate polybenzimidazole (PBI) membranes for water reuse and protein separation. [EMIM]OAc exhibits superior efficiency in dissolving PBI under much lower temperature and pressure compared to the traditional toxic *N,N*-dimethylacetamide (DMAc) because the acetate anions of [EMIM]OAc could form hydrogen bonding with PBI chains and effectively break up the interchain hydrogen bonding in PBI molecules, verified by molecular simulations. The PBI/[EMIM]OAc solution also displays unique rheological properties significantly deviated from the traditional Cox-merz rule, and the shear thinning rheology at low shear rates implies a

strong charge-ordered structure resulting from the intense hydrogen bonding. PBI ultrafiltration membranes are prepared from PBI/[EMIM]OAc solutions by non-solvent induced phase separation method. The high dope viscosity and a high ratio of [EMIM]OAc outflow to water inflow facilitate the formation of a relatively thick sponge-like structure with a few macrovoids. After thermal treatment in ethylene glycol at 140°C and chemical cross-linking by dichloro p-xylene, derived PBI ultrafiltration membranes achieved a high separation factor of 94.55 for a binary protein mixture containing bovine serum albumin and hemoglobin.

In order to facilitate the fabrication of PBI membranes with a higher water flux by using a less amount expensive PBI material, five commercially available polyimides and polyimide-amides were screened and P84 co-polyimide was chosen to blend with PBI because it formed miscible blends with PBI and interacted closely with [EMIM]OAc. The incorporation of P84 in the blend system not only lowered the overall viscosity for easier membrane fabrication but also delayed the phase inversion process favorably to form a macrovoid-free morphology. PBI/P84 blend membranes were therefore fabricated for ultrafiltration via non-solvent induced phase inversion method. Compared to plain PBI ultrafiltration membranes, the newly developed PBI/P84 blend membranes exhibit an open cell structure and a reduced thickness which result in an increase of the PWP to around 200 (L/m² bar h), as well as an increase of the mean effective pore diameter.

LIST OF TABLES

| | |
|--|-----|
| Table 1-1 Structures of ionic liquids most extensively employed [10]..... | 3 |
| Table 2-1 Membrane Separation Processes and Membrane Characteristics [51]..... | 11 |
| Table 3-1 Properties of solvents and non-solvent | 26 |
| Table 3-2 Spinning conditions for CA/[BMIM]SCN membranes..... | 27 |
| Table 3-3 Solubility parameters of solvents, non-solvent and cellulose acetate..... | 31 |
| Table 3-4 Comparison of various parameters (porosity, pore size and pore size distribution) and PWP performance of CA flat sheet membranes..... | 38 |
| Table 4-1 Spinning conditions for CA membranes..... | 52 |
| Table 4-2 Solubility parameters of solvents, cellulose acetate and non-solvents at 20°C | 55 |
| Table 4-3 Viscosities and diffusivities of water and IPA..... | 58 |
| Table 4-4 Comparison of various parameters and PWP of CA hollow fiber membranes | 66 |
| Table 5-1 Molecular simulation results of PBI/ionic liquid systems | 85 |
| Table 5-2 Properties of [EMIM]OAc, DMAc and water | 90 |
| Table 5-3 Comparison of PWP, mean pore diameter and geometric standard deviation for PBI membranes calculated from neutral solute rejection | 92 |
| Table 5-4 BSA/Hb separation performance of PBI membranes at different pH values .. | 93 |
| Table 5-5 Basic properties of BSA and Hb..... | 93 |
| Table 6-1 Solubilities of PBI, polyimides and polyamide-imides in [EMIM]OAc at 120 °C..... | 100 |
| Table 6-2 T_g values of the PBI/P84 blend systems from the Fox equation and experimental results | 105 |

| | |
|---|-----|
| Table 6-3 Physicochemical properties of [EMIM]OAc and water..... | 111 |
| Table 6-4 Solubility parameters of PBI and P84 at 298K calculated according to Hoy's table, Fedors' and Matsuura's methods | 114 |
| Table 6-5 Comparison of PWP values and pore diameters of PBI/P84 blend membranes | 115 |

LIST OF FIGURES

| | |
|--|----|
| Figure 1-1 A two-dimensional simplified schematic of 1,3-dialkyl imidazolium ionic liquids showing the hydrogen bonds between the imidazolium cation (C+) and the anion (A-) (one cation is surrounded by three anions and vice-versa) [13] | 4 |
| Figure 2-1 A conceptual ternary phase diagram of the polymer–solvent–nonsolvent system | 14 |
| Figure 2-2 Schematic illustration of a phase separation by the nucleation and growth mechanism [52]..... | 16 |
| Figure 2-3 Schematic illustration of a phase separation by spinodal decomposition mechanism [52]..... | 17 |
| Figure 2-4 Schematic diagram of a hollow fiber spinning line [5]..... | 19 |
| Figure 2-5 A simplified schematic comparison of solvent/non-solvent exchange during the fabrication of (a) flat sheet membrane and (b) hollow fiber membrane [51] | 20 |
| Figure 2-6 A hypothetical mechanism of the conformation changes of polymer chains induced by elongation and shear rates [73]..... | 22 |

| | |
|--|----|
| Figure 3-1 The structure of (a) [BMIM]SCN and (b) [BMIM][MeSO ₄] | 25 |
| Figure 3-2 Schematic diagram of the measuring instrument for water flux and separation performance of UF hollow fiber membranes [5] | 28 |
| Figure 3-3 Viscosity vs. CA concentration for CA/[BMIM]SCN and CA/NMP dope solutions. | 32 |
| Figure 3-4 Phase diagrams of CA/solvents/water systems at 25°C | 33 |
| Figure 3-5 The cross section morphology of flat sheet membranes prepared from [BMIM]SCN, acetone and NMP (CA concentration: 10wt%; Thickness of casting knife: 100µm) | 35 |
| Figure 3-6 The surface morphology of flat sheet membranes prepared from [BMIM]SCN, acetone and NMP (CA concentration: 10wt%, thickness of casting knife: 100µm) | 36 |
| Figure 3-7 Pore Size distribution probability density curve for CA/[BMIM]SCN and CA/NMP flat sheet membranes | 39 |
| Figure 3-8 The morphology of the CA/[BMIM]SCN hollow fiber membrane (Free-fall wet-spun hollow fibers with a bore fluid of NMP/water=5/5) | 41 |
| Figure 3-9 Thermal gravimetric analysis of recycled [BMIM]SCN | 43 |
| Figure 3-10 Comparison of the morphology of flat sheet membranes prepared from fresh [BMIM]SCN (a) and recovered [BMIM]SCN (b) (CA concentration: 10wt%, thickness of casting knife: 100µm) | 44 |
| Figure 4-1 The structure of (a) [EMIM]SCN and (b) CA-398-30 | 48 |
| Figure 4-2 The FTIR spectra of pure [EMIM]SCN, 12%CA/[EMIM]SCN and CA membrane | 53 |

Figure 4-3 Shear viscosity of CA/[EMIM]SCN solutions with different CA concentration at 23 °C (n is the power law index of initial shear thinning regions)..... 56

Figure 4-4 The cross section morphology of flat sheet membranes cast from 12/88 wt% CA/[EMIM]SCN and coagulate in (a) water (b) IPA 59

Figure 4-5 The phase diagrams of CA/[EMIM]SCN/non-solvent systems at 23±1 °C 60

Figure 4-6 The phase inversion kinetics of flat sheet membranes cast from 12/88 wt% CA/[EMIM]SCN and coagulate in (a) water (b) IPA 61

Figure 4-7 Observation of non-solvent intrusion ((a) water, (b) IPA) in 12/88 wt% CA/[EMIM]SCN thin film under PLM 63

Figure 4-8 The morphologies of CA hollow fiber membranes DR-2.5 (dope:2.5ml/min, bore fluid:1.0ml/min, air gap=0.5cm, free fall) 65

Figure 4-9 Effects of dope flow rate on the PWP and mean effective pore diameter of hollow fiber membranes spun from 12/88 wt% CA/[EMIM]SCN (a constant ratio of dope flow rate to bore fluid flow rate, air gap = 0.5cm, free fall) 66

Figure 4-10 (a) Shear rate profile along with the radial length at the outlet of 2.0/0.9 (o.d./i.d.) spinneret; and (b) shear and elongational viscosity of 12/88wt% CA/[EMIM]SCN solutions at 23 °C 68

Figure 4-11 Effects of spinneret temperature on the morphologies of hollow fiber membranes spun from 12/88 wt% CA/[EMIM]SCN (dope:2.5ml/min, bore fluid:1.0ml/min, air gap=0.5cm, free fall) 69

Figure 4-12 Effects of air gap distance on (a) the morphologies of the enlarged cross section near the outer surface; (b) the PWP and mean effective pore diameter of hollow

| | |
|---|-----|
| fiber membranes spun from 12/88 wt% CA/[EMIM]SCN (dope:2.5ml/min, bore fluid:1.0ml/min, free fall). | 70 |
| Figure 5-1 The structures of ionic liquids and PBI..... | 77 |
| Figure 5-2 Observation of a fully dissolved 20/80 wt% PBI/[EMIM]OAc solution cooling from 120 to 23 °C under PLM..... | 82 |
| Figure 5-3 Schematic of the possible mechanism for the dissolution of PBI in [EMIM]OAc | 83 |
| Figure 5-4 Comparison of shear viscosity η (○) and complex viscosity $ \eta^* $ (■) of 8/92 wt% PBI/[EMIM]OAc solution as a function of shear rate or angular frequency at 23°C | 86 |
| Figure 5-5 Shear viscosity of PBI/[EMIM]OAc solutions with different PBI concentrations at 23°C | 88 |
| Figure 5-6 Morphology of PBI-AC(as-cast) asymmetric membrane | 89 |
| Figure 5-7 Pore size distribution curves of newly developed PBI membranes | 92 |
| Figure 5-8 Schematic of protein separation environments with PBI membranes at (a) pH=4.8, (b) pH=6.8..... | 95 |
| Figure 6-1 The FTIR spectra of P84 co-polyimide, [EMIM]OAc and their solution.... | 104 |
| Figure 6-2 The enlarged FTIR spectra of PBI/P84 blend membranes at wave numbers of (a) 1690 – 1800 cm^{-1} and (b) 2500 – 4000 cm^{-1} | 107 |
| Figure 6-3 Possible intermolecular hydrogen bonding among PBI, P84 and [EMIM]OAc | 108 |
| Figure 6-4 Shear viscosity of PBI/P84/[EMIM]OAc solution with different polymer ratios at 80°C | 109 |

| | |
|--|-----|
| Figure 6-5 Comparison of the morphology of PBI/P84 blend membranes prepared at | 113 |
| Figure 6-6 The phase inversion kinetics of PBI/P84/[EMIM]OAc solutions in water (casting temperature 80 ⁰ C)..... | 114 |
| Figure 6-7 Pore size distribution curves of developed PBI/P84 blend membranes (casting temperature 80 ⁰ C)..... | 116 |
| Figure 6-8 Comparison of the morphology of 10/10 wt% PBI/P84 blend membranes cast at different temperatures | 117 |
| Figure 6-9 Shear viscosity of 10/10/80 wt% PBI/P84/[EMIM]OAc solution at different temperatures..... | 118 |

NOMENCLATURE

| | |
|---------------|--|
| A | Effective filtration area (m^2) |
| C_f | Solute concentrations in the feed solutions (ppm) |
| C_p | Solute concentrations in the permeate (ppm) |
| D | Diffusion coefficient (cm^2/s) |
| d_s | Solute diameter (nm) |
| d_p | Mean effective pore diameter (nm) |
| ΔP | Trans-membrane pressure (bar) |
| Q | Water permeation rate (L/h) |
| R | Rejection (%) |
| T | Light transmittance |
| α | Protein separation factor |
| γ | Shear rate (s^{-1}) |
| ε | Porosity of porous membrane (%) |
| σ_p | Geometric standard deviation (nm) |
| δ_d | Dispersive solubility parameter ($\text{MPa}^{1/2}$) |
| δ_{ES} | Electrostatic solubility parameter ($\text{MPa}^{1/2}$) |
| δ_h | Hydrogen bonding solubility parameter ($\text{MPa}^{1/2}$) |
| δ_p | Polar solubility parameter ($\text{MPa}^{1/2}$) |
| δ_t | Total solubility parameter ($\text{MPa}^{1/2}$) |
| τ | Shear stress (N m^{-2}) |

Chapter 1 Introduction

In separation technologies, membranes are used as selective barriers to separate fluid mixtures into two parts with different compositions and are fabricated into modules as an operation unit. Membrane separation technology has undergone rapid developments and the resultant membranes have been employed in chemical, environmental and refinery industries [1, 2] since Loeb and Sourirajan fabricated the first cellulose acetate reverse osmosis membranes by immersing nascent membranes in ice water [3]. Membranes have been commercialized as diverse membrane configurations such as hollow fibers, spiral wounds and plate-and-frame modules depending on separation requirements. As one of the most important configurations, hollow fiber membranes made of polymeric materials have been widely studied because of easy fabrication, self-mechanical support, large surface area to volume ratio, high module packing density, and relatively low cost [4-6]. However, during the fabrication of polymeric membranes, a great amount of traditional organic solvents are used, which will certainly cause severe waste solvent pollution and also other problems to the environment. Because of their undesirable impact on the environment, these traditional organic solvents should be deducted in the foreseeable future, and alternative green solvents to replace them have to be found.

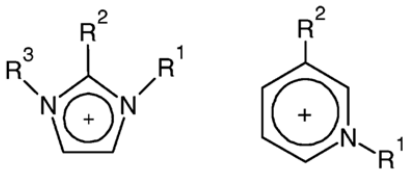
One kind of green solvent is ionic liquid that contain only ions and emerge to replace the traditional volatile organic solvents for industrial uses. The unique characteristics of ionic liquids, such as their negligible volatility, thermal and chemical stability, non-inflammability and recyclability, make it possible to lessen chemical waste and losses

during many processes. Therefore, ionic liquids have been employed in numerous applications and are also receiving great attention in the field of membrane separation technologies [7]. Some imidazolium-based ionic liquids, those with good capability in dissolving macromolecules and miscibility with water, are suitable to replace some organic solvents as a new generation of solvents for membrane fabrication. The study of ionic liquids as an alternative for volatile organic solvents in membrane fabrication is quite an interesting and promising field. To understand fundamental mechanisms of using ionic liquids as a solvent for membrane formation, the interactions between polymer and ionic liquids and their effects on membrane formation need to be studied. In addition, one may expect different solution rheology, spinning characteristics, process parameters and separation performance for hollow fiber membranes spun from polymer and ionic liquid systems.

1.1 Characteristics and advantages of ionic liquids

Ionic liquids are fluids composed entirely of ions and have been considered as a group of environmentally-friendly solvents [8, 9]. Structures of extensively employed ionic liquids are listed in Table 1-1 [10]. They have several unique characteristics. First of all, most used and preferred ionic liquids have relatively a low melting point that is always below 100°C. This is because the small charge of ions (always +1 or -1) and the large size of cations in ionic liquids lead to large distances between the ions with reduced charge density [10, 11]. These features contribute to a low lattice enthalpies and large entropy changes, and therefore, the liquids state is thermodynamically favorable [7, 8, 12]. As a result, room temperature ionic liquids can retain their liquid state.

Table 1-1 Structures of ionic liquids most extensively employed [10]

| Cation | Anion |
|---|---|
|  | Halide SCN^- BF_4^- PF_6^- CF_3COO^- $\text{C}_6\text{H}_5\text{COO}^-$ $(\text{CF}_3\text{SO}_2)_2\text{N}^-$ $\text{CH}_3\text{OSO}_3^-$ $(\text{CN})_2\text{N}^-$ |
| $\text{R}^1 = \text{Alkyl, Alkenyl}$ $\text{R}^2 = \text{H, CH}_3$ $\text{R}^3 = \text{CH}_3$ | |

In the liquid state, ionic liquids maintain a kind of three-dimensional arrangement through hydrogen bonding, π - π stacking and electrostatic interactions [13]. Figure 1-1 illustrates the possible hydrogen bonds between the imidazolium cation (C^+) and the anions (A^-) of 1,3-dialkyl imidazolium ionic liquids. It is reported in some X-ray studies that in the solid state, one imidazolium-based cation is always surrounded by at least three anions and accordingly one anion is surrounded by at least three cations [14-17]. Therefore, 1,3-dialkyl imidazolium ionic liquids are possible to form chains of imidazolium rings and anions, respectively [16]. They may provide hydrophilic and hydrophobic regions with a high polarizability based on the properties of their structures [18, 19]. Such pronounced self-organization in ionic liquids still sustains to a great extent in the liquid state as a result of the hydrogen bonds and Coulombic forces. The self-

organized structure of ionic liquids is one of the unique qualities that distinguish them from the molecular organic solvents and the classical ion aggregates.

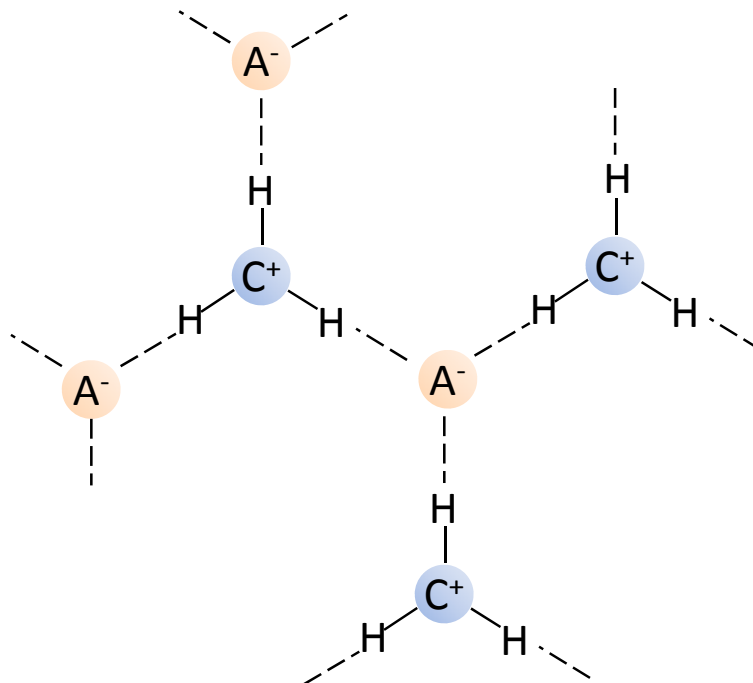


Figure 1-1 A two-dimensional simplified schematic of 1,3-dialkyl imidazolium ionic liquids showing the hydrogen bonds between the imidazolium cation (C^+) and the anion (A^-) (one cation is surrounded by three anions and vice-versa) [13]

Another important characteristic of ionic liquids is the versatility in cations, anions and their combinations, which make their properties designable according to different requirements. The alkyl chain length and anion may influence the density, viscosity, surface tension and melting points of ionic liquids. For instance, the imidazolium-based ionic liquids with hydrophilic anions such as chloride, iodide and nitrate are usually miscible with water [20]. Their miscibility with water, hydrophilicity and viscosities are varied with the alkyl chain length of imidazolium cations. Additionally, ionic liquids also have the characteristics of negligible volatility, thermal and chemical stability due to the

stronger interactions, i.e. Coloumbic forces, among ionic liquids than the van der Waals forces among traditional molecular solvents. Ionic liquids are also non-inflammable and recyclable, which is a result of the features of their chemical structure and interactions [21, 22].

Environmental problems such as air pollution, waste chemicals, and water shortage have been emerging with the fast expansion of chemical industries. By employing ionic liquids to replace the traditional volatile organic solvents, it is possible to minimize chemical waste and losses during many processes in order to protect the environment. Ionic liquids appear to be a clean-up solution for industrial uses, and they have shown promising applications in many aspects including electrochemistry, organic synthesis, catalysis, as well as separations [23-25].

1.2 Applications of ionic liquids in recent polymer science

Currently in polymer science, ionic liquids are not only promoted as polymerization media but also used in preparation of functional polymer materials considering the inherent ionic pattern of ionic liquids [25]. This pattern is expected to alter or facilitate reaction paths involving charge-separated intermediates or transition states [16]. For instance, polymer gels based on ionic liquids have been developed into mainly three types: doping polymers in ionic liquids [26], in situ polymerization of vinyl monomers in ionic liquids [27], and polymerization of polymerizable ionic liquids [28]. Porous materials were also fabricated by polymerization of microemulsions stabilized by surfactant ionic liquids that consisted of an imidazolium cation polar group and a

hydrophobic tail [29]. The new class of advanced materials shows great potential as electrolyte matrixes due to excellent ionic conductivity.

Another major application of ionic liquids is to dissolve macromolecules which have limited solubility in common solvents. Some types of ionic liquids, compared to traditional solvent systems, are very powerful to dissolve biopolymers at higher concentrations [10, 30]. One successful case is cellulose processing, in which hydrophilic imidazolium-based ionic liquids are used. This successful application may be due to the facts that cellulose is the most abundant renewable source but very difficult to be dissolved in organic solvents, and hydrophilic imidazolium-based ionic liquids can simplify the dissolving process without creating environmental problems.

Swatloski et al. [31] were the first group to report that ionic liquids were effective solvents for cellulose and microwave heating could effectively accelerate the dissolution. Their ionic liquids contained 1-butyl-3-methylimidazolium cations ($[BMIM]^+$) and anions such as Cl^- , SCN^- , Br^- . Solutions in $[BMIM]Cl$ containing 3 wt% and 10 wt% cellulose were prepared at 70°C and 100°C, respectively. A subsequent NMR study by the same group confirmed that the high chloride concentration and activity in $[BMIM]Cl$ can effectively break the hydrogen bonding present in cellulose and lead to the ability to dissolve a higher concentration of cellulose than the traditional solvents [32]. Zhang et al. [33, 34] explored the solubility of cellulose in 1-allyl-3-methylimidazolium chloride ($[AMIM]Cl$), and prepared transparent cellulose films and cellulose/multiwalled-carbon-nanotube composite fibers from $[AMIM]Cl$ by coagulation in water. The residue ionic

liquids in the coagulation bath could be easily recycled by evaporation to remove the water [35], thus providing an effective way to minimize chemical waste and losses.

1.3 Application of ionic liquids in membrane science

The unique characteristics of ionic liquids allow them to be employed in certain membranes which have become a popular separation technology over the past decade [36-38]. For example, Snedden et al. [39] prepared porous catalytic membranes through in situ polymerization in imidazolium-based ionic liquids followed by the removal of ionic liquids which behaved as the porogen. Fuel cell membranes consisting of ionic liquids [40] or directly synthesized by ionic liquids [41] exhibited better conductivity.

It is found that ionic liquids are particularly promising in the capture of CO₂ due to the enhanced solubility and preferred transport of CO₂ in ionic liquids with amine functional groups. For instance, Scovazzo et al. used ionic liquids to replace the traditional solvents in supported liquid membranes, and was able to obtain a long-term, continuous separation performance for CO₂/CH₄ and CO₂/N₂ mixed gases [42]. Polymer/ionic liquid membranes [43, 44] and poly(ionic liquid)/ionic liquid composite membranes [45] have been prepared for CO₂ capture.

1.4 Research objectives

As described in the preceding section, ionic liquids show a good capability in dissolving macromolecules and can be designed to have excellent miscibility with water, thus making it highly possible to employ ionic liquids to replace the organic solvents in

membrane technology. Nevertheless, research on this area is quite limited and the gaps are summarized below:

- Although ionic liquids are employed to dissolve several kinds of polymeric materials, until now few studies have focused on fabrication of polymeric membranes employing ionic liquids as a kind of solvent.
- The interactions between polymer and ionic liquids and their effects on membrane formation have yet to be explored and understood.
- Solution rheology, spinning characteristics, process parameters and separation performance for hollow fiber membranes spun from ionic liquids may vary from those spun from commonly used organic solvents. However, the influences of the above parameters on hollow fiber membranes spun from ionic liquids have not been systematically studied.

Therefore, the objectives of this research were to:

- explore the feasibility of using ionic liquids to replace the organic solvent to prepare asymmetric flat sheet membranes and hollow fiber membranes using the phase inversion method.
- examine the differences in the fundamentals of membrane formation by comparing with traditional organic solvents during the phase inversion process.
- investigate the molecular interactions between ionic liquids and polymers interrelated to the chemical structure and properties of the employed ionic liquids.

- study the spinning conditions to fabricate hollow fiber membranes suitable for ultrafiltration.

Our research focused on the polymer and ionic liquid systems that meet the requirements for membrane fabrication. Since the fabrication of membranes in an environmentally benign process has become increasingly important and the development of polymeric membranes from ionic liquid solutions is likely to be an inevitable trend, it is envisioned that the results of this work may provide the fundamentals and new insights on the use of ionic liquids as green solvents for future manufacturing of polymeric membranes. The subsequent sections provide an overview of the background of membrane formation mechanism and recent developments in membrane technology for liquid separation.

Chapter 2 Literature Review on Membrane Technology

2.1 Development of polymeric membrane for liquid separation

In the industry, membranes, which are fabricated into modules as an operation unit, are selective barriers that can be used to separate fluid mixtures, e.g., liquids or gases, into two phases with different compositions [46]. Membrane-based separation is energy efficient and cost effective compared to traditional separation processes as it is a kind of non-thermal separation and able to overcome efficiency limitations on heat utilization [47, 48]. The chemical potential difference between the two separated phases, which can result from pressure difference, concentration difference, and electrical potential difference or their combinations, is the driving force for membrane separation and is often used to categorize membrane processes.

In membrane processes for liquid separation, pressure difference is the driving force. When a pressurized feed solution flows through a selective membrane, the solvent permeates through the membrane while solute is retained adjacent to of the membrane [49]. Membranes are classified into four categories, i.e., microfiltration (MF), ultrafiltration (UF), nanofiltration (NF) and reverse osmosis (RO), according to their pore size and pore size distribution as shown in Table 2-1. In this classification, the UF membranes with a effective pore diameter of 10-1000 Å have the advantages of relative high throughput of product, ease of scale-up and ease of equipment cleaning and sanitization, and therefore have a broad variety of applications in the food and beverage

industries, protein bioseparations and wastewater treatment for fractionation, concentration, diafiltration processes [50].

Table 2-1 Membrane Separation Processes and Membrane Characteristics [51]

| Membrane process | Separation mechanism | Nominal pore size or Intermolecular size (Å) | Transport regime |
|-------------------------|-----------------------------|---|-------------------------|
| Microfiltration | Size exclusion | 500-50000 | Macropores |
| Ultrafiltration | Size exclusion | 10-1000 | Mesopores |
| Nanofiltration | Size exclusion | 5 - 20 | Micropores |
| | Electrical exclusion | | Molecular |
| Reverse Osmosis | Size exclusion | <5 | Micropores |
| | Solution/diffusion | | Molecular |

Membrane separation technology has played a vital role in liquid separation as well as other areas; therefore, it is imperative to search for alternative green solvents that can be employed in the membrane fabrication process to minimize the damage to the environments.

Membranes for liquid separation are fabricated from a wide range of materials, from organic polymeric materials to inorganic materials. Compared to inorganic membranes, polymeric membranes show advantages in the mild environment of their higher productivity and flexibility in the application. The chemical engineering of polymeric

membranes for liquid separation can be fundamentally focused on (1) membrane material selection, (2) membrane fabrication procedures, (3) membrane characterization and evaluation and (4) membrane module design and separation performance. In order to achieve diverse separation purposes, the membrane material selection, the interactions between materials and solvents and the membrane fabrication procedure must be cautiously determined. The chemistry of adopted materials along with the formation mechanisms occurring during membrane preparation will control the permeation flux and the separation efficiency of the resulted membranes [51]. The following section will zoom into membrane formation mechanisms.

2.2 Theoretical background on phase inversion in membrane formation

2.2.1 Phase diagrams and phase inversion

Polymeric membranes can be classified into asymmetric and symmetric membranes based on their distinct type of morphology. Asymmetric membranes have a gradient of pore density while symmetric membranes have a uniform structure. The majority of polymeric membranes are prepared by the phase inversion of homogeneous polymer solutions. Phase inversion of the polymer dope is generally induced by variations in temperature, pressure or composition of the mixture [52]. A phase change from a liquid to a solid state would happen in a controlled manner and result in various membrane structures. There are four main techniques to induce the phase inversion for membrane fabrication: solvent-evaporation induced precipitation, vapor-induced precipitation, thermal precipitation and immersion precipitation [47].

Normally, polymeric asymmetric membranes can be fabricated through phase inversion technique via immersion precipitation from an initially thermodynamically stable polymer solution. When a nonsolvent is introduced in the polymer solution, the compositions of the mixture undergo a range of variations and achieve a state with the lowest free energy. The ternary phase diagram of polymer (P) – solvent (N) – nonsolvent (NS) is commonly used to represent the states and equilibrium compositions of polymer solutions. As shown in [Figure 2-1](#), a conceptual isothermal ternary phase diagram indicates three regions (i) the stable region, located between the polymer/solvent axis and the binodal curve, (ii) the metastable region, located between the binodal curve and

spinodal curve, and (iii) the unstable region, located between the spinodal curve and the non-solvent/solvent axis [47].

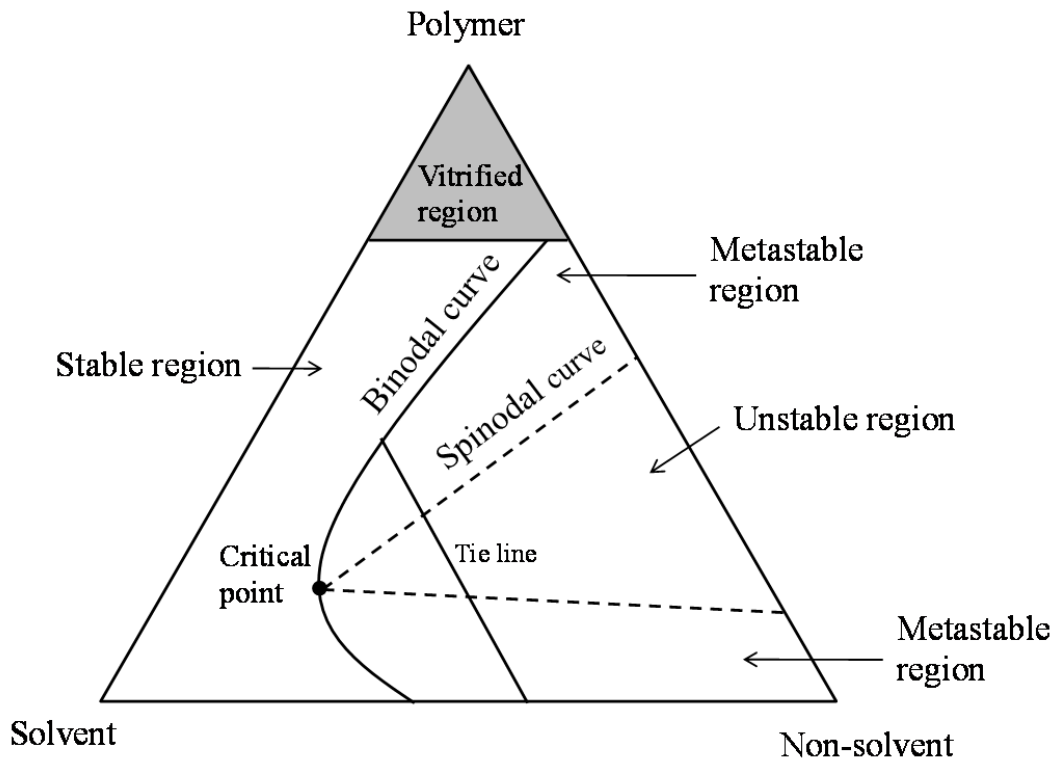


Figure 2-1 A conceptual ternary phase diagram of the polymer–solvent–nonsolvent system

By the penetration of non-solvent, the polymer solution becomes visually opaque and separates into two conjugative liquid phases at equilibrium, forming the binodal curve. Physically, the tie lines describe phase equilibrium between two phases, which means the chemical potentials in two phases have to be equivalent to each species. The spinodal curve signifies the situation where all possible concentration fluctuations lead to instability, and phase separation occurs spontaneously. For a ternary system, the binodal curve and the spinodal curve meet at the critical point. The location of critical point

determines whether the polymer-rich phase and polymer-poor phase evolves a new phase. In the metastable region between spinodal and binodal curves, small perturbations will decay, and phase decomposition can only happen when there is a sufficiently large perturbation. Within the spinodal curve, any small perturbation will cause phase inversion of the system [51].

Since Loeb and Sourirajan [3] developed the phase inversion process to fabricate membranes in late 1950s, the issues related to membrane formation have been heavily studied and debated. There exists a rich literature on the formation of asymmetric membranes by the phase inversion process using traditional organic solvents for polymeric materials [4, 47, 53-55]. Generally, there are four distinguished structural elements that have been addressed, e.g. nodules, cellular structure, bicontinuous structure and macrovoids. With the in-depth exploration, scientists proposed different mechanisms of phase inversion including liquid-liquid demixing, gelation or vitrification, nucleation and growth, spinodal decomposition and even their combinations in time and in space. Some theoretical mass transfer models have also been developed to describe these processes based on simple polymer solutions [56-58]. The mechanisms of nucleation growth and spinodal decomposition have been widely employed to explain membrane formation processes [52, 59].

Nucleation is the formation of the initial fragments of a new and more stable phase within a metastable mother phase [52]. Figure 2-2 illustrates the growth process of nuclei from the mother phase.

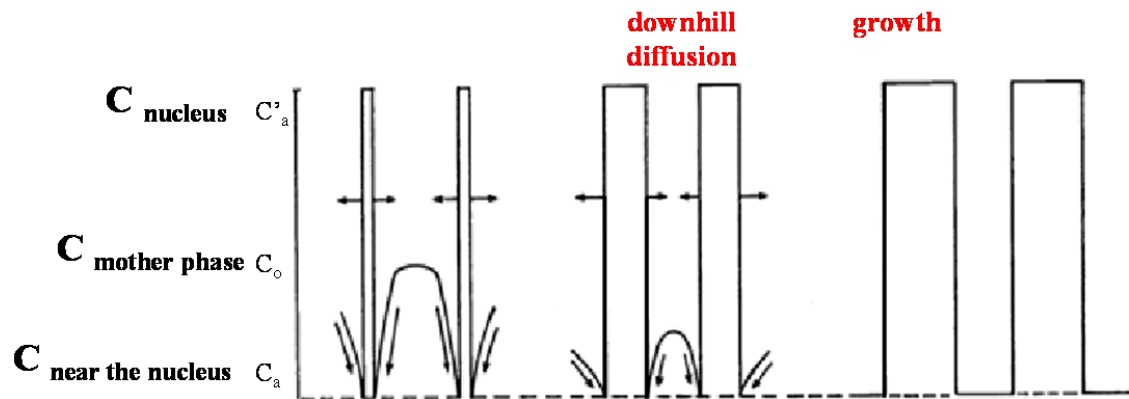


Figure 2-2 Schematic illustration of a phase separation by the nucleation and growth mechanism [52]

Any small perturbation around the metastable concentration c_0 leads to the appearance of two phases and also results in higher free energy. A nucleus with an excess of surface energy is developed and aggregates as a new phase. Once the nuclei are formed, the system begins to separate with a decline in free energy and the nuclei grow. Since the molecules composing the nucleus are held strongly together and are unable to diffuse out, the individual molecules within the mother phase would diffuse into the region, resulting in the growth of nuclei. Nuclei keep growing within the same mother phase and a dispersed two-phase system is subsequently formed. The final sizes of nuclei and the distances between them are determined by the rate of mutual diffusion and phase separation.[52]

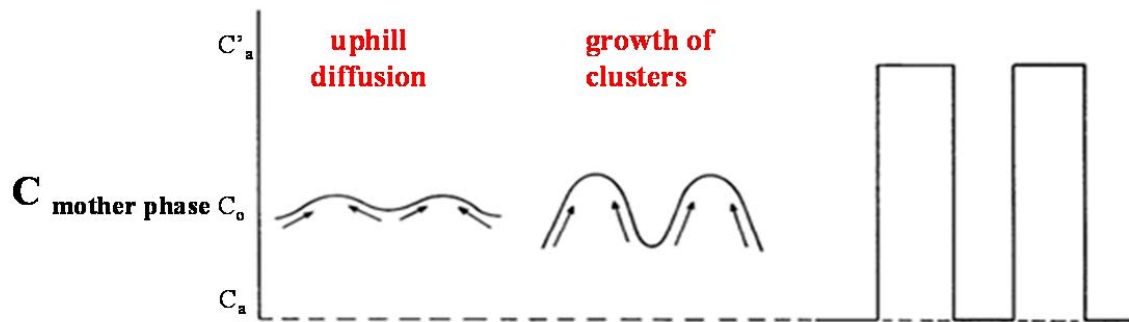


Figure 2-3 Schematic illustration of a phase separation by spinodal decomposition mechanism [52]

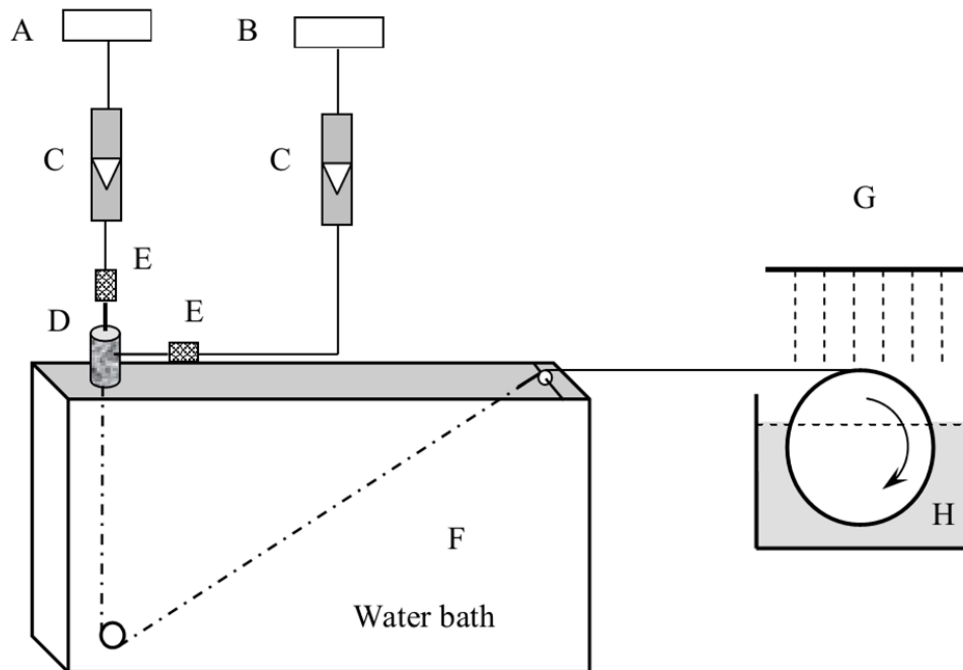
On the other hand, spinodal decomposition is a kinetic process of generating a spontaneous and continuous growth of another phase within an unstable mother phase. As shown in Figure 2-3, the growth is not from nuclei but from small amplitude of composition fluctuations where the individual molecules are subject to favorably join permanent clusters.[52] As the cluster region is a low energy region [60], diffusion occurs uphill from the low concentration region surrounding the fluctuation into the cluster, which statistically promote continuous and rapid growth of the sinusoidal composition modulation [52]. This process needs no activation energy and tends to minimize its system energy by minimizing the interface area, forming inter-connective structure.

2.2.2 Fabrication of flat sheet and hollow fiber membranes

The morphology and separation performance of asymmetric flat sheet membranes are determined by not only the chemical and physical properties of polymer, solvent and non-solvent but also the fabrication conditions. Membrane scientists have well demonstrated

that proper choice of solvents and coagulant media can affect the phase inversion pathways and hence control the membrane structure and separation performance [61-63]. Ruaan et al. defined an index Φ calculated from solubility parameters as an indicator of membrane structure, and found that the finger-like macrovoids always occurred at high Φ value, while sponge-like structure were prone to form at low Φ value [64]. Different combinations of polymer, solvents and non-solvents could alter both the thermodynamics of the polymer solution and the kinetics of the transport process, resulting in distinguished membrane structures.

In comparison to flat sheet membranes, the hollow fiber configuration is preferred for modules in membrane separation because of the following advantages: 1) a larger membrane area per unit volume of membrane module, and hence resulting in a higher productivity; 2) self-mechanical support which can be back flushed for liquid separation and 3) good flexibility and easy handling during the module fabrication and in the operation [5]. Nowadays, hollow fiber membranes are widely used in the membrane separation fields including gas separation, reverse osmosis, ultrafiltration, pervaporation and dialysis.



A: Bore fluid tank B: Dope solution tank C: Syringe pump D: Spinneret
E: Filter F: Coagulation bath G: Water sprinkling H: Fiber collecting bath

Figure 2-4 Schematic diagram of a hollow fiber spinning line [5]

The experimental set-up hollow fiber spinning is shown in Figure 2-4. After the polymer dope extrudes from the spinneret, the nascent fiber first experiences the air gap region, and then enters the coagulation bath and finally wound on a take-up roller. However, the formation mechanisms in many cases still remain hypothetical and experimental because of the complexity of hollow fiber spinning compared to the casting of flat sheet membranes. The structure of the resultant hollow fiber membranes is strongly related to the composition of polymer dope solution, the bore fluid solution and the spinning conditions. Firstly, during the spinning process, the fibers experience two phase inversion processes at both the lumen and shell side. A schematic comparison of solvent/non-

solvent exchange during the fabrication of flat sheet membranes and hollow fiber membranes is shown in Figure 2-5. The nascent fibers are prone to undergo different phase inversion kinetics and interfacial mass transfer at the same time. Secondly, the spinneret design, the bore fluid chemistry and flow rate, the dope flow rate as well as the outer coagulant chemistry greatly affect the fiber morphology and thus performance [5, 61, 62, 65]. The other factors like dope viscosity, temperature, air gap distance and take-up speed [4, 53, 66] are also crucial for hollow fiber spinning.

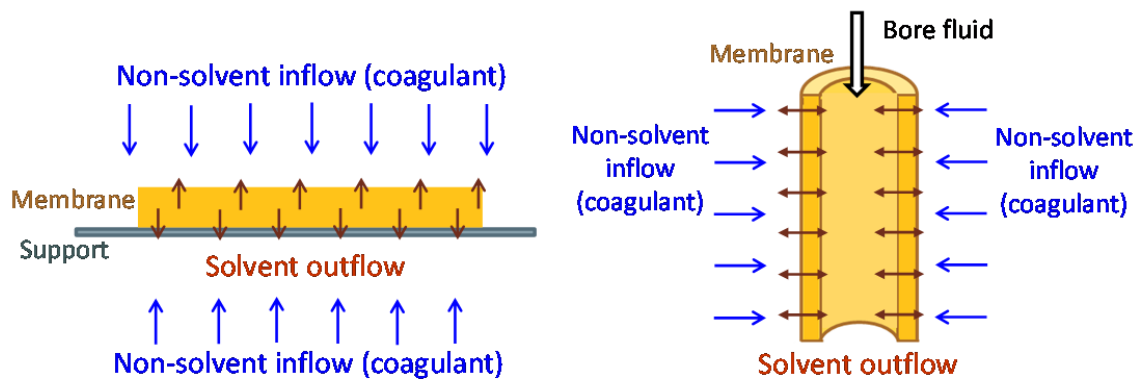


Figure 2-5 A simplified schematic comparison of solvent/non-solvent exchange during the fabrication of (a) flat sheet membrane and (b) hollow fiber membrane [51]

Flory–Huggins solution theory is extensively used to describe the thermodynamic behavior of the phase inversion process during the formation of asymmetric flat membranes by considering change of the Gibbs free energy [67]. In view of complexity of the phase inversion process of hollow fiber membranes, Chung pointed out that at least two items had to be added in Flory-Huggins theory to describe the Gibbs free energy for polymer solutions during hollow fiber spinning, and they were a work done by the external stresses on the nascent hollow fibers and an extra enthalpy change induced by

these stresses [60]. When a pressurized viscous polymer solution is extruded from a complicated channel within a tube-orifice spinneret, it may go through extra stresses compared to flat sheet membranes, such as shear stress induced by shear rate within the spinneret and elongation stress caused by gravity and drawing force in the air gap region and the coagulation bath. These rheological parameters will influence the morphology and the separation performance of the resultant hollow fiber membranes.

Researchers have found that this dope rheology play an important role on membrane morphology and separation performance. Aptel et al. explored the effect of dope extrusion rate on performance of polysulfone hollow fiber UF membranes by the dry-jet wet spinning process [68]. Ismail et al. have investigated the effect of shear rate on morphology and performance of hollow fiber membranes for gas separations [69, 70]. Chung and Cao et al. focused on studying the effect of shear rate on properties of hollow fiber UF membranes and gas separation membranes [71-73]. They all reported that the water or gas permeability of hollow fibers declined and the rejection or selectivity increased with an increase in the shear rate, because the molecular chain orientation was enhanced during the spinning and the polymer chains tended to align themselves with each other under shear and/or elongation stresses in the flow direction, resulting in a tightened skin layer. A hypothetic mechanism of the conformation changes of polymer chains induced by elongation and shear stresses is shown in Figure 2-6. Qin et al. observed that the molecular orientation induced at the outer skin of the nascent fiber by shear stress within the spinneret could be frozen into the wet-spun fiber but relaxed in a small air gap region for the dry-jet wet-spun fiber [74]. In terms of the roles of spinneret

design and additives in polymer solution, Peng et al further studied the effects of shear and elongation viscosities on the formation of ultra-thin hollow fiber membranes for gas separation [65, 75].

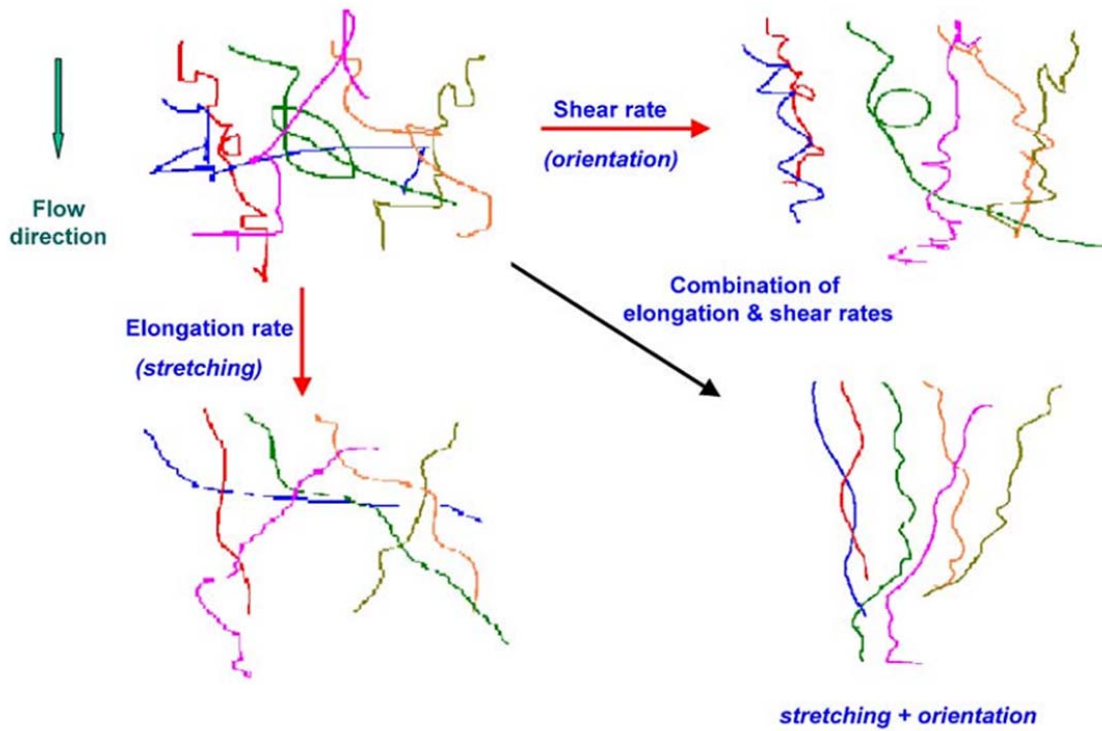


Figure 2-6 A hypothetical mechanism of the conformation changes of polymer chains induced by elongation and shear rates [73]

Chapter 3 Fundamentals and characteristics of membrane formation via phase inversion for cellulose acetate membranes using an ionic liquid, [BMIM]SCN, as the solvent

3.1 Introduction

Based on the introduction of ionic liquids in Chapter 1, the good capability of ionic liquids in dissolving macromolecules and the miscibility of ionic liquids with water inspire us to employ ionic liquids as a new generation of solvents to replace the organic solvents for membrane preparation. The recyclability and reusability of ionic liquids make the green fabrication of polymeric membranes feasible. We aim at 1) exploring the feasibility of using ionic liquids to replace the organic solvent to prepare asymmetric flat sheet membranes and hollow fiber membranes; 2) examining the differences in the fundamentals of membrane formation between using ionic liquids and traditional organic solvents, i.e. N-Methyl-2-pyrrolidinone (NMP) and acetone, during the phase inversion process; and 3) studying the feasibility to recycle and reuse ionic liquids. Membrane scientists have well demonstrated that proper choice of solvents and coagulant media can affect the phase inversion pathways and hence control the membrane structure and separation performance [61, 62, 65]. However, few studies have focused on systematically understanding polymer/ionic liquid interactions and their effects on membrane formation.

This is the first work in the literature that explores the usage of ionic liquids to membrane fabrication and studies the fundamentals of phase inversion of polymer/ionic liquid solutions. It is believed that this work can provide insight of membrane formation

mechanism and bring membrane research into a brand new area. 1-butyl-3-methylimidazolium thiocyanate ([BMIM]SCN) is chosen as one of the ionic liquids being studied in this work because [BMIM]SCN has a lower melting point ($<-20\text{ }^{\circ}\text{C}$) and a lower viscosity at room temperature than [BMIM]Cl whose melting point is $70\text{ }^{\circ}\text{C}$. These advantages of [BMIM]SCN make it more feasible to cast membranes and spin hollow fibers from polymer/[BMIM]SCN solutions at room temperature. Cellulose acetate is selected as the membrane material because it has excellent hydrophilicity and reasonably good resistance to solvents. It is also a classical material widely used in aqueous based separation, gas separation and biomaterial separation for decades [2].

3.2 Experimental

3.2.1 Materials

Cellulose acetate (CA-398-30, acetyl content 39.8%) was purchased from Eastman Chemical Company, USA. The ionic liquids including 1-butyl-3-methylimidazolium thiocyanate ([BMIM]SCN, $>95\%$) and 1-butyl-3-methylimidazolium methyl sulfate ([BMIM][MeSO₄], $>95\%$), as shown in Figure 3-1, was obtained from BASF, Germany, acetone ($>99.5\%$) was purchased from Tedia, USA, and *N*-Methyl-2-pyrrolidinone (NMP, $>99.5\%$) was purchased from Merck, USA. All the solvents were used as received.

3.2.2 Phase diagrams, dope preparation and viscosity measurements

CA powder was first dried in a vacuum oven at $120\text{ }^{\circ}\text{C}$ overnight to remove the moisture before use. Small samples of CA solutions with the CA concentration ranging from 2wt%

to 12wt% were prepared in both [BMIM]SCN and [BMIM][MeSO₄]. The viscosity of CA/ionic liquid solutions as a function of polymer concentration was measured by an ARES Rheometric Scientific Rheometer (TA instruments, USA) in the range of 1–100 s⁻¹ with a 25mm cone plate at 23±1 °C.

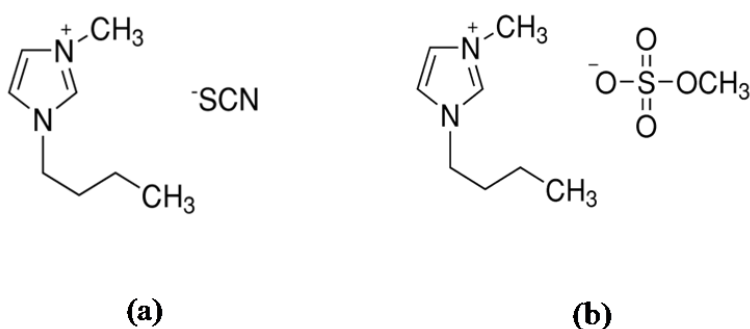


Figure 3-1 The structure of (a) [BMIM]SCN and (b) [BMIM][MeSO₄]

CA/NMP and CA/acetone solutions were prepared by stirring CA powder and solvents for 12 hours at room temperature. As the ionic liquid has a relatively higher viscosity compared to acetone and NMP as seen from [Table 3-1](#), CA powder was dispersed slowly into chilled [BMIM]SCN (0–3 °C), and stirred continuously with a high speed mechanical stirrer at room temperature (23±1 °C) as described elsewhere to reduce powder agglomeration [71]. Then, the mixture was stirred at 50 °C for five hours until CA is fully dissolved. The solution was kept quiescence for 3 days and then degassed by a sonicator (Elmasonic S 30H, Germany) at 30°C for 0.5 hour before use.

Table 3-1 Properties of solvents and non-solvent

| Solvent | [BMIM]SCN | [BMIM][MeSO ₄] | NMP | Acetone | Water |
|---|-----------|----------------------------|-------|---------|-------|
| Density(g/cm ³) (20°C, 1atm) | 1.070 | 1.213 | 1.028 | 0.792 | 0.998 |
| Viscosity (cP) (20°C) | 54 | 213.8 | 1.7 | 0.32 | 0.89 |
| $D_{w-s} \times 10^6$ (cm ² /s) (20°C) ^a | 0.97 | — | 18 | 88.6 | — |
| $D_{s-w} \times 10^6$ (cm ² /s) (20°C) ^b | 5.77 | — | 8.9 | 11.7 | — |
| D_{s-w} / D_{w-s} | 5.95 | — | 0.494 | 0.132 | — |

^aData obtained from material data sheets provided by the corresponding manufacturers

^bThe diffusion coefficient of water in almost pure solvent

^cThe diffusion coefficient of solvent in almost pure water

3.2.3 Fabrication of flat asymmetric membranes

The dope solution was cast on a horizontal glass plate to form a film of substantially uniform thickness by a casting knife with a thickness of 100µm. After casting, the nascent membrane was immediately immersed into a water bath together with the glass plate. After peeled off from the glass automatically, the resultant asymmetric membrane was immersed in water for at least 2 days to thoroughly remove the residual solvents. All procedures were performed at room temperature.

3.2.4 Fabrication of hollow fibers

The experimental set-up and general spinning procedure have been described in Chapter 2. [Table 3-2](#) lists the spinning conditions for the CA / [BMIM]SCN system and all the procedures were conducted at room temperature. The as-spun hollow fibers were immersed in tap water for three days to thoroughly remove the residual solvents. In order

to have a better mechanical strength, the hollow fibers were heated in hot water at 70°C for 1h and then immersed in tap water for further usage.

Table 3-2 Spinning conditions for CA/[BMIM]SCN membranes

| | |
|---|---------------------------|
| Dope composition | 10wt% CA/[BMIM]SCN |
| Spinneret dimension (ID/OD) (mm) | 0.8/1.2 |
| Bore fluid | NMP:water = 0:1, 5:5, 9:1 |
| Dope flow rate (ml/min) | 1 |
| Bore fluid flow rate (ml/min) | 0.4 |
| Air gap distance (cm) | 0–2 |
| Coagulation bath | Water |
| Take up rate (m/min) | Free fall |

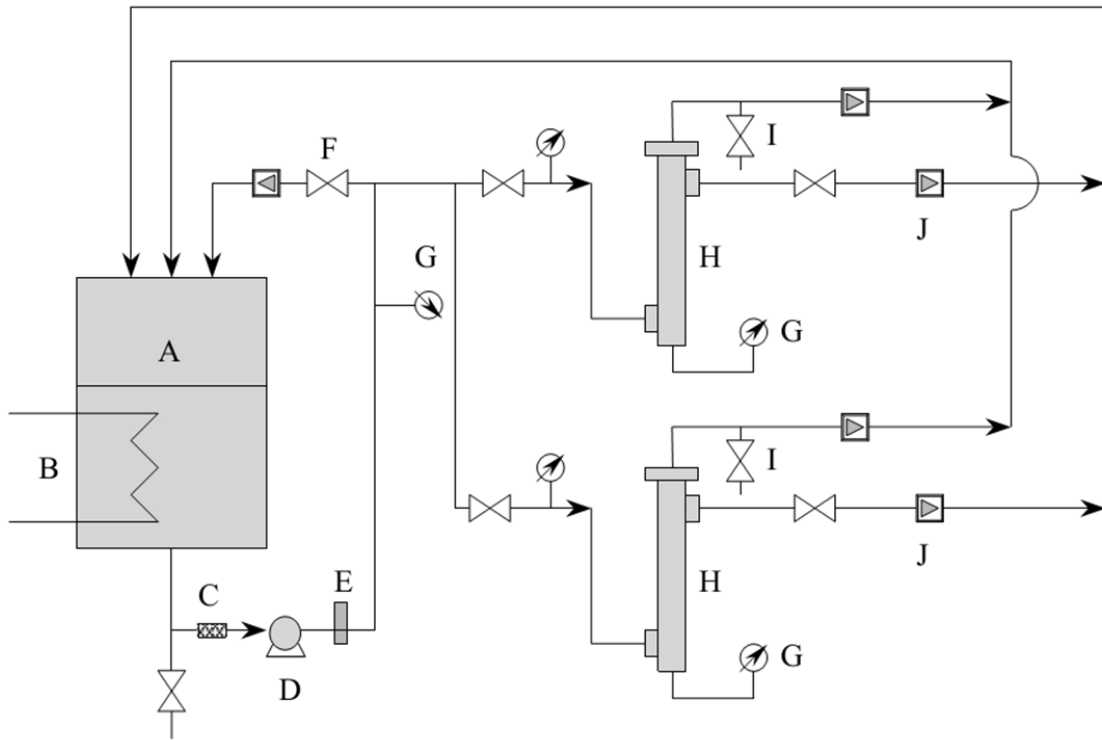
3.2.5 Morphology study

The flat sheet membranes and the hollow fibers were dried by a freeze dryer (ModulyoD, Thermo Electron Corporation, USA) for 12 hours for morphology study. The dry membranes were immersed in liquid nitrogen, fractured and then sputtered with platinum using a JEOL JFC-1300 Platinum coater (Japan) with a coating thickness of 15-20nm. The cross-section and the surface of the samples were observed under a field emission scanning electron microscope (FESEM, JEOL JSM-6700F, Japan).

3.2.6 Ultrafiltration tests for pure water flux and pore size distribution

Wet hollow fibers were kept in water all the time until they were dipped in a 50wt% glycerol aqueous solution for 48h and dried in air at room temperature before module

preparation. The ultrafiltration experimental set-up is schematically presented in [Figure 3-2](#) and the method have been described elsewhere [\[5\]](#).



A = Feed tank, B = Cooling coil, C = Filter, D = High pressure pump, E = Pulsation damper, F = Bypass valve, G = Pressure gauge, H = Permeation cell, I = Sampling valve, J = Rotameter

Figure 3-2 Schematic diagram of the measuring instrument for water flux and separation performance of UF hollow fiber membranes [\[5\]](#)

After glycerol was flushed out by Milli-Q DI water, two modules containing ten hollow fibers each were characterized in a cross-flow filtration mode by the pure water flux and neutral solute rejection with different dimensional PEG or PEO solutes that were dissolved in the distilled water. The feed concentration was kept at around 200ppm and

the trans-membrane pressure was about 0.6 bar. The normalized pure water permeability (PWP, L/m² bar h) was calculated by the following equation:

$$\text{PWP} = \frac{Q}{A \Delta P} \quad (1)$$

where Q is the water permeation rate (L/h), A denotes the effective filtration area (m²) and ΔP is the trans-membrane pressure (bar).

The concentrations of the feed and permeate solutions were determined by a total organic carbon analyzer (Shimadzu ASI-5000A, Japan) during the experimental running. The solute rejection was calculated by the following equation:

$$R(\%) = \left(1 - \frac{C_p}{C_f}\right) \times 100 \quad (2)$$

where C_p and C_f are the solute concentrations in the permeate and feed solutions (ppm), respectively. The solute rejection R as a function of the solute diameter d_s was plotted on a log-normal probability graph, which yields a straight line. The mean effective pore diameter d_p acquired at $R=50\%$ and the geometric standard deviation σ_p obtained as the ratio of d_s at $R=84.13\%$ and $R=50\%$ were further used to estimate pore size distribution of membranes as illustrated elsewhere [5]. All experiments were conducted at room temperature ($23 \pm 1^\circ\text{C}$).

To measure the pure water flux and the pore size distribution of the flat sheet membranes, a permeation cell was used with N₂ providing the pressure to make the feed permeate through the membrane. The calculation methods of the PWP and the solute rejection are the same as that for hollow fiber membranes.

3.2.7 Membrane porosity

Three samples for each type of membranes were tested to estimate the porosity of the membranes after freeze dry. The membrane mass m_m (g) was measured by a digital microbalance, and the membrane volume v_m (cm³) was calculated from the surface area and the thickness. The difference between the membrane volume v_m and the volume of polymer matrix is the volume of pores. Therefore, the porosity (ε) was calculated by the following equation:

$$\varepsilon = \frac{v_m - m_m/\rho_p}{v_m} \quad (3)$$

where ρ_p represents the density of the neat cellulose acetate (1.31g/cm³).

3.2.8 Recovery and reuse of [BMIM]SCN

The [BMIM]SCN was recovered by the evaporation of water at low pressures from the mixture taken from the coagulate bath using a Heidolph rotary evaporator (Laborota 4010, Germany). The recovered [BMIM]SCN was reused to prepare CA flat asymmetric membranes under the same procedure as described in Section 3.2.3 and the morphology, pure water permeability and porosity of the resultant membranes were characterized.

3.3 Results and discussion

3.3.1 Solubility, viscosity curves and phase diagrams of CA in ionic liquids

The dissolution of CA is much slower in [BMIM][MeSO₄] because the viscosity of [BMIM][MeSO₄] is nearly three times greater than that of [BMIM]SCN as shown in

Table 3-1. Thus [BMIM]SCN is chosen as the ionic liquid solvent in this work. Table 3-3 summarizes the solubility parameters of CA, different solvents and water. The calculated results using Material Studio are comparable with those of Ref. [76]. As indicated in Table 3-3, the difference in solubility parameter between CA and NMP is smaller than that between CA and [BMIM]SCN, which implies [BMIM]SCN has poorer solvency than NMP, thus the polymer chains are supposed to have a smaller random coil size or tighter intra-molecular state in [BMIM]SCN.

Table 3-3 Solubility parameters of solvents, non-solvent and cellulose acetate

| Chemicals | Solubility parameters δ_{sp} (cal ^{1/2} cm ^{3/2}) | Solubility parameters δ_{sp} (cal ^{1/2} cm ^{3/2}) |
|-----------------------|--|--|
| [BMIM]SCN | — | 9.35 ^b |
| NMP | 11.21 ^a | 11.92 ^b |
| Acetone | 9.77 ^a | 9.53 ^b |
| Water | 23.5 ^a | — |
| Cellulose acetate-398 | 12.7 ^a | — |

^a The Hildebrand solubility parameter from Ref. [76]

^b Calculation using Material studio based on the equation $\delta = \sqrt{\sum E_{coh,i}/V_i}$

Figure 3-3 illustrates the viscosity of CA/[BMIM]SCN and CA/NMP dope solutions at the shear rate of 10s⁻¹ as a function of CA concentration. CA/[BMIM]SCN solutions have obviously higher viscosity than CA/NMP solutions at the same CA concentration within the measurement range. The 10/90 wt% CA/[BMIM]SCN solution was chosen for hollow fiber spinning as it has a reasonably high viscosity, and hence the CA concentration was kept at 10wt% in NMP or acetone for the comparison purpose. Figure

3-4 exhibits the ternary phase diagrams of CA/ solvents/water systems with different solvents at room temperature. The binodal curve for the CA/[BMIM]SCN/water system is much closer to the polymer-water axis compared to the CA/NMP and CA/acetone systems. This indicates that the CA/[BMIM]SCN solution can tolerate more water content than the CA/NMP solution. As a result, the former has a slower phase inversion rate than the latter during the phase inversion, and they may also have different phase separation kinetics.

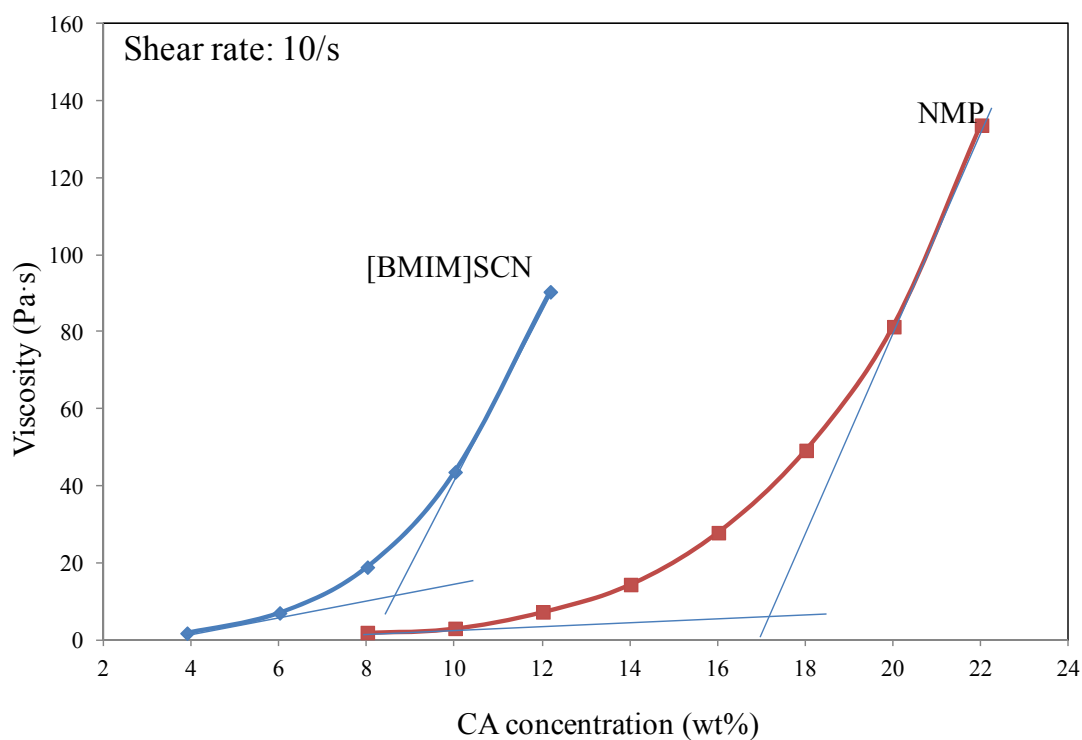


Figure 3-3 Viscosity vs. CA concentration for CA/[BMIM]SCN and CA/NMP dope solutions.

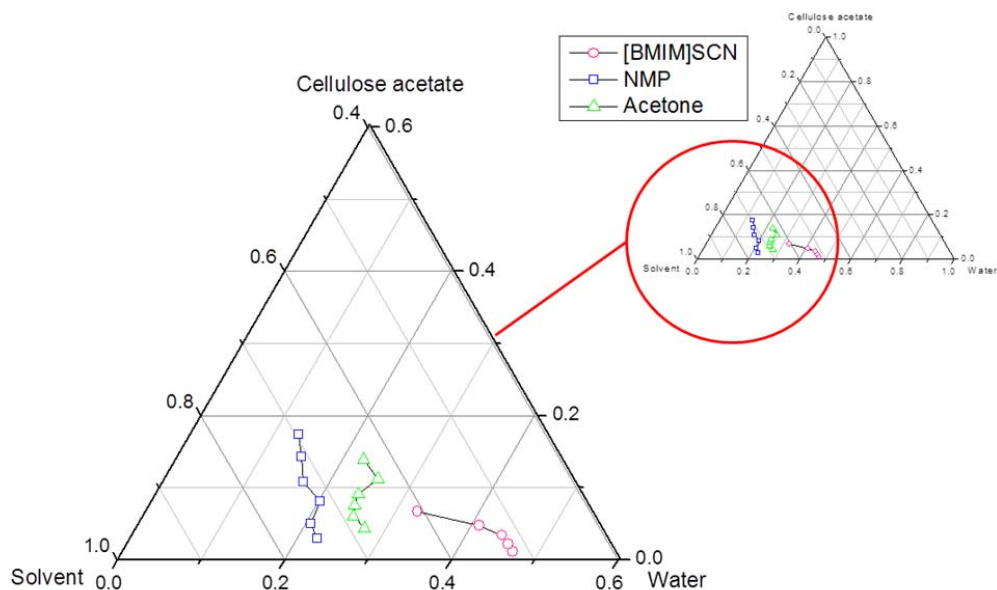


Figure 3-4 Phase diagrams of CA/solvents/water systems at 25°C

3.3.2 The effects of solvents on CA flat sheet membranes

3.3.2.1 The morphology of CA flat sheet membranes

The fresh membranes prepared from the 10/90 wt% CA/[BMIM]SCN solution were freeze dried, and Energy dispersive X-ray spectroscopy(EDX) by a scanning electron microscope (JEOL JSM-5600LV, Japan) and X-ray photoelectron spectroscopy(XPS) by an AXIS HSi spectrometer (Kratos, England) were used to detect whether there was any residue [BMIM]SCN in the membranes. No nitrogen and sulfur elements were detected on the cross section (by EDX) or the membrane surface (by XPS). Therefore it is believed that the [BMIM]SCN solvent has been fully removed from the membrane.

[Figure 3-5](#) and [Figure 3-6](#) depict the effect of different solvents on the morphology of CA flat sheet membranes. Several distinctive phenomena can be observed: 1) the cross-

section of membranes cast from the CA/[BMIM]SCN solution is of entirely nodular structure, while those from the CA/NMP or CA/acetone solution are relatively porous; 2) membranes cast from the CA/[BMIM]SCN solution and CA/acetone solution are macrovoid-free, while the membranes cast from CA/NMP exhibit numerous big macrovoids almost across the whole membrane cross-section; and 3) the thickness of membranes cast from CA/[BMIM]SCN (8.72 μm) is thinner than that from CA/acetone (11.61 μm), and much thinner than that from CA/NMP (55.7 μm) if when the same casting knife was used. These interesting and distinct morphologies reveal that CA in [BMIM]SCN behaves differently from that in NMP and acetone during the phase inversion process. The causes of these differences will be discussed in the following sections.

The diverse morphologies of cross sections are due to different phase inversion kinetics and precipitation paths. In the CA/NMP system, water can quickly diffuse and convectively advance into the 10/90 wt% CA/NMP solution because of low polymer concentration, low viscosity (Figure 3-3) and easy phase separation (Figure 3-4). This results in spinodal decomposition and produces a membrane structure consisting of a thin top layer and an open-cell substructure disrupted by macrovoids as discussed in our previous work [77]. Regarding the 10/90 wt% CA/acetone system, the highly volatile and easy outflow nature of acetone would increase the local polymer concentration at the membrane top layer, while the slow phase inversion characteristics (Figure 3-4) and fast water diffusivity in acetone (Table 3-1) may firstly induce delayed liquid-liquid demixing

via nucleation growth and then possibly spinodal decomposition, thus result in a porous cellular structure [78, 79].

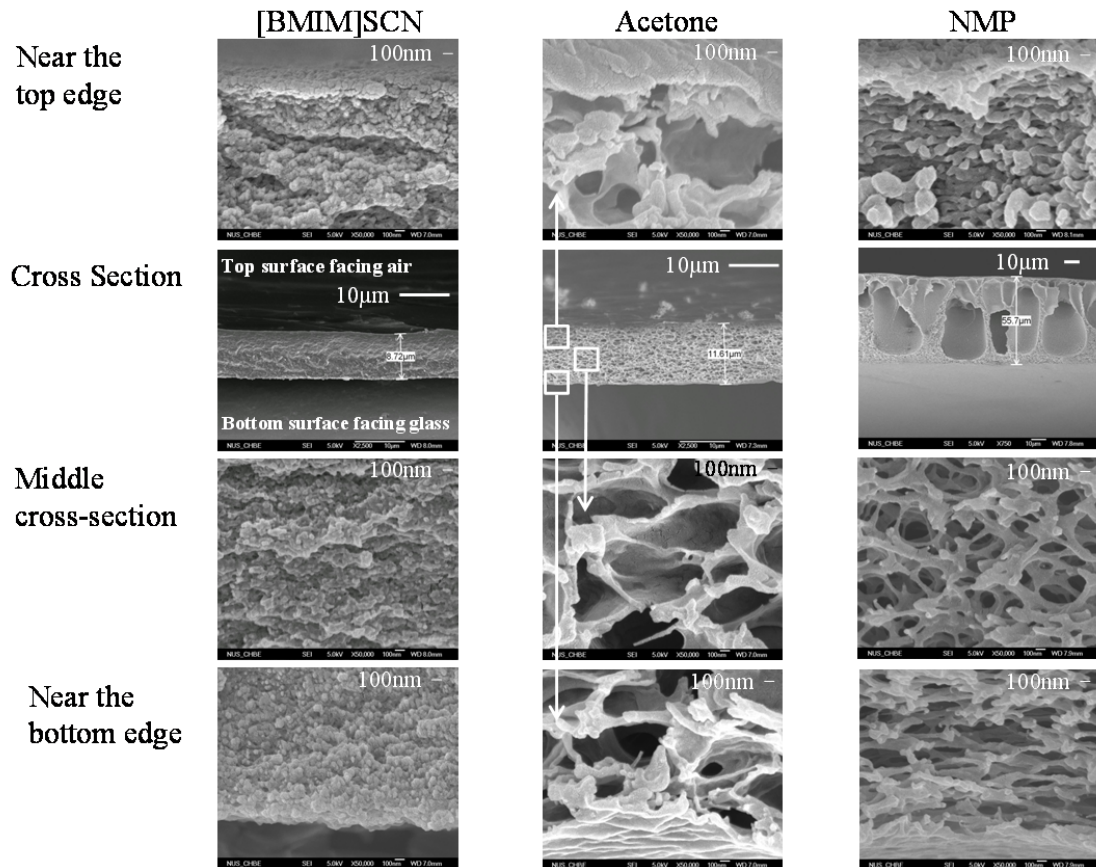


Figure 3-5 The cross section morphology of flat sheet membranes prepared from [BMIM]SCN, acetone and NMP (CA concentration: 10wt%; Thickness of casting knife: 100µm)

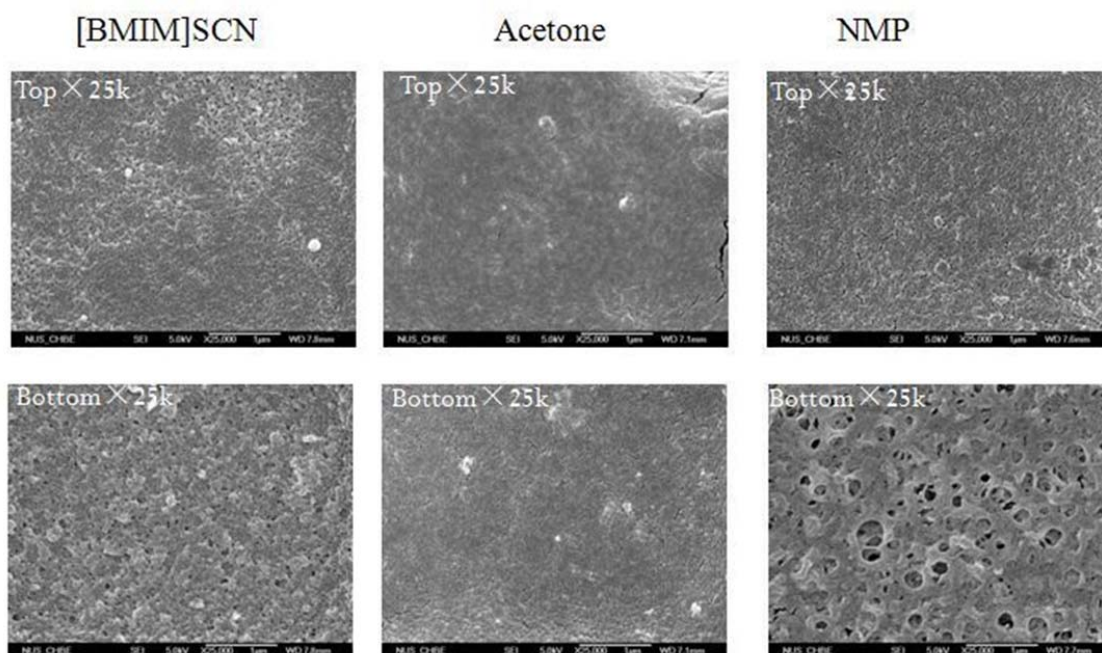


Figure 3-6 The surface morphology of flat sheet membranes prepared from [BMIM]SCN, acetone and NMP (CA concentration: 10wt%, thickness of casting knife: 100 μ m)

In contrast, a distinctive precipitation path take place in the CA/[BMIM]SCN system and a dense nodular structure membrane is formed, which may probably arise from the following causes. Diffusion coefficient is a good indicator of the ability of one substance diffusing into another. [Table 3-1](#) summarizes the diffusion coefficients of the solvents used in this work calculated from the Wilke-Chang equation [80]. The diffusion coefficients of water with respect to the solvents follow the order $D_{\text{water-acetone}} \gg D_{\text{water-NMP}} \gg D_{\text{water-[BMIM]SCN}}$, while the diffusion coefficients of solvents with respect to water obey the order $D_{\text{acetone-water}} > D_{\text{NMP-water}} > D_{\text{[BMIM]SCN-water}}$. This clearly implies that the ratio of solvent outflow to coagulant inflow defined by Yilmaz, and McHugh [56, 57] is much greater than one and is the highest in the CA/[BMIM]SCN system, followed by the CA/acetone system, and then the CA/NMP system. As a result, flat asymmetric

membranes cast from CA/[BMIM]SCN has the thinnest thickness (8.72 μm), followed by those from CA/acetone (11.61 μm), and then from CA/NMP (55.7 μm).

Since water diffuses very slowly into the nascent CA/[BMIM]SCN membrane and since the binodal curve for the CA/[BMIM]SCN/water system is much closer to the polymer-water axis compared to the CA/NMP and CA/acetone systems, nucleation growth and gelation may dominate the phase inversion paths in the beginning, and followed possibly by the spinodal decomposition and then solidification, thus resulting in a membrane cross-section structure full of nodules. In addition, the low water inflow rate and high viscosity of the CA/[BMIM]SCN solution play important roles to retard the macrovoid formation even though the system has a very low polymer concentration. It has been known that macrovoids can be formed by various mechanisms [4, 47, 53, 54, 60, 66, 81-84]. However, surface instability, non-solvent intrusion and localized supersaturation [85, 86] have been often cited as the main causes. As in the CA/[BMIM]SCN system, the low water inflow rate and high dope viscosity prevent the rapid intrusion of the external coagulant into the nascent membrane and thus eliminate any chance of localized supersaturation for the macrovoid formation.

3.3.2.2 Porosity, pure water permeability, pore size and its distribution of CA flat sheet membranes

Table 3-4 shows the porosities of membranes cast from various systems. Consistent with the membrane morphology discussed in the previous section, membranes cast from CA/[BMIM]SCN has the smallest porosity (6.21%), followed by CA/acetone (50.84%)

and then CA/NMP (84.30%). Moreover, they have quite different pure water permeabilities (PWP). As illustrated in Table 3-4 and Figure 3-7, the CA/NMP membrane has a much larger PWP value than the CA/[BMIM]SCN membranes.

Table 3-4 Comparison of various parameters (porosity, pore size and pore size distribution) and PWP performance of CA flat sheet membranes

| Solvent | Porosity (%) | Testing Pressure (bar) | Pure Water Permeability (L/(m ² h bar)) | Mean pore size μ_p (nm) | Standard deviation σ_p |
|--------------------|--------------|------------------------|--|-----------------------------|-------------------------------|
| Fresh [BMIM]SCN | 6.21 ± 2.76 | 1.5 | 114.14 | 39.16 | 2.428 |
| NMP | 84.30 ± 0.71 | 1.5 | 983.49 | 41.01 | 1.818 |
| Acetone | 50.83 ± 1.54 | 1.5 | 0 | — | — |
| Acetone | — | 4 | 0 | — | — |
| Recycled [BMIM]SCN | 7.03 ± 1.89 | 1.5 | 119.68 | — | — |

It is known that the PWP values of membranes are not determined only by their pore sizes, but also by other pore characteristics, such as porosity and pore interconnectivity [87]. Compared to the membranes cast from CA/[BMIM]SCN, the much higher PWP of membranes cast from CA/NMP is not only due to the bigger pore size and broader pore size distribution, but also due to its higher porosity, as listed in Table 3-4. In addition, the CA/NMP membrane has formed a much more open cell structure compared to the CA/[BMIM]SCN membrane because of different precipitation paths during the phase inversion process, which can be indicated by the morphology in Figures 3-5 and 3-6.

Therefore, even though the thickness of the CA/NMP membrane is 5 times bigger than that of the CA/[BMIM]SCN membrane and the big macrovoids across the CA/NMP membrane may be subjected to deformation and thus reduce the flux under the testing pressure, the PWP value of the former is still much larger than that of the latter.

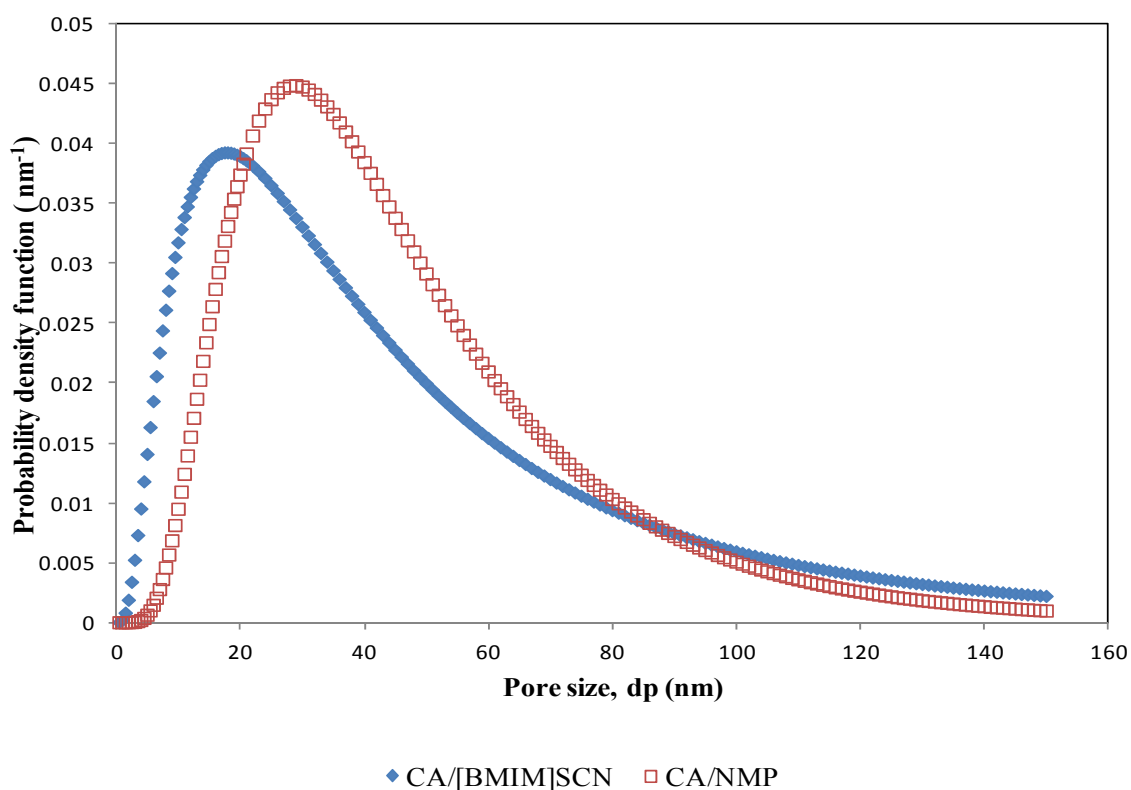


Figure 3-7 Pore Size distribution probability density curve for CA/[BMIM]SCN and CA/NMP flat sheet membranes

Interestingly, under the same casting conditions, the CA/acetone membrane has no water permeability even the trans-membrane pressure is elevated to 4 bar. This is due to the highly volatile nature of acetone and the delayed demixing, which lead to form the

densest top surface among these three kinds of membranes. SEM pictures shown in [Figure 3-6](#) confirm our hypothesis.

3.3.3 Fabrication of CA hollow fiber membranes from [BMIM]SCN and the morphology study

Even though the CA/[BMIM]SCN solution has a reasonably high viscosity, it's difficult to fabricate hollow fibers from the CA/[BMIM]SCN solution owing to its low precipitation rate as shown in the phase diagrams in [Figure 3-4](#). Transparent and white hollow fibers can be fabricated only by carefully adjusting the spinning parameters.

Firstly, several bore fluids with different NMP content were tried. It is known that as the NMP content increases in the bore fluid, delayed demixing occurs at the lumen side and more porous structure can be achieved [[5](#), [88](#), [89](#)]. However, a high NMP content in bore fluid may lower the viscosity and strength of the nascent fiber and thus induce spinning instability. A mixture of 50 wt% NMP in water was found suitable to maintain a stable spinning process of the CA/[BMIM]SCN solution. In the case of using 90 wt% NMP in bore fluid, the fiber cannot be solidified even the wet spinning process is adopted.

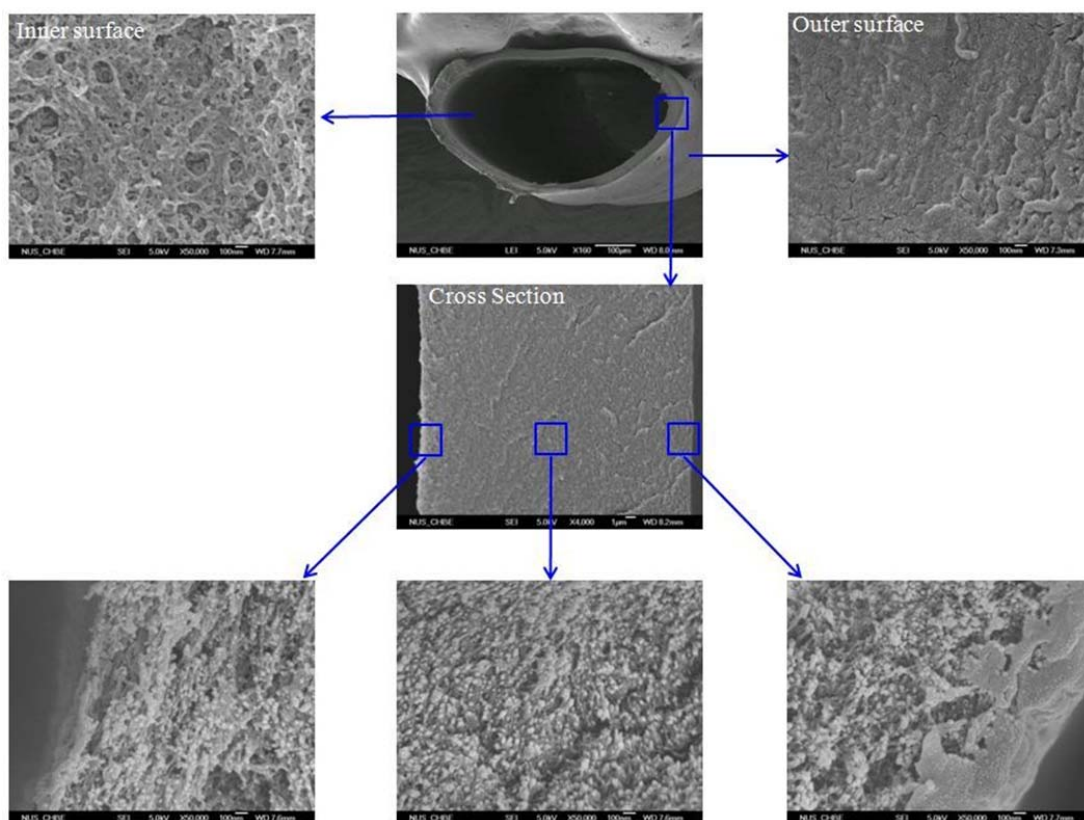


Figure 3-8 The morphology of the CA/[BMIM]SCN hollow fiber membrane (Free-fall wet-spun hollow fibers with a bore fluid of NMP/water=5/5)

The wet spinning process is preferred for the fabrication of hollow fiber membranes from the CA/[BMIM]SCN solution because it has a very slow phase inversion process. [Figure 3-8](#) displays the SEM pictures of the entire hollow fiber morphology prepared from [BMIM]SCN. Similar to the flat sheet membranes, these hollow fibers exhibit a macrovoid-free structure with an extreme thin wall because of a low polymer concentration, a high ratio of solvent outflow to water inflow, and an extreme low precipitation rate. The resultant hollow fiber has an asymmetric structure consisting of a porous inner surface and a relative dense outer surface. However, the whole cross section shows a looser interconnected nodular structure compared to that of the flat sheet

membrane cast from 10/90 wt% CA/[BMIM]SCN. This difference may arise from the following fact. Firstly, since the hollow fiber faces two coagulants at the outer and lumen sides after exiting from the spinneret and the two coagulants are of various compositions in this work, the coagulation rates in the outer and lumen sides must be different, which would affect the membrane formation [66]. Secondly, compared with the flat sheet membranes, the hollow fibers are subjected to more shear stress within the spinneret and elongation stresses induced by gravity and its own weight. The polymer chains may be under different states of shear and elongation stresses before the phase inversion, and these factors may contribute to the looser interconnected nodular structure as discussed in the literature [60].

A high dope viscosity alone cannot eliminate macrovoids in CA hollow fibers. In Peng et al. previous work [4], the hollow fibers were fabricated from a 18/82 wt% CA/NMP solution which has a comparable viscosity value with the 10/90 wt% CA/[BMIM]SCN solution. However, Peng et al's fibers still have macrovoids on the cross-section even at a take-up speed of 10m/min and an air-gap distance of 1 cm. This may be another proof that [BMIM]SCN has unique characteristics to facilitate the formation of macrovoid-free hollow fibers at a fairly low CA concentration due to its high viscosity and fast diffusivity to water. However, the thin wall fibers must be carefully handled because of the relatively poor mechanical strength. Future works will be aimed to overcome these issues.

3.3.4 Recovery and reuse of [BMIM]SCN for membrane fabrication

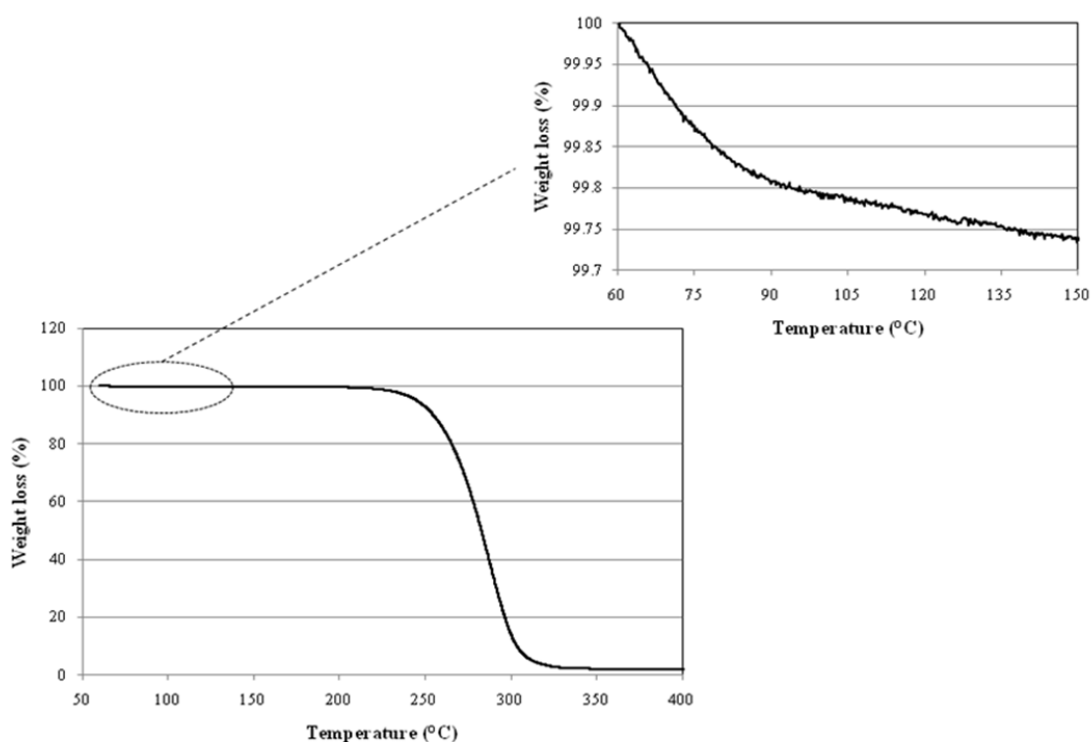


Figure 3-9 Thermal gravimetric analysis of recycled [BMIM]SCN

The coagulation bath for flat membranes was collected and water was evaporated from the water and [BMIM]SCN mixture. According to the thermal gravimetric analysis as shown in [Figure 3-9](#), the weight loss of the recovered [BMIM]SCN is less than 0.3wt% at 150 °C which is acceptable for reuse. The recycled [BMIM]SCN was reused for CA flat sheet membranes. [Figure 3-10](#) shows a morphological comparison of CA flat sheet membranes prepared from the fresh and recycled [BMIM]SCN, while [Table 3-4](#) compares their porosity and PWP values. The morphology, porosity and pure water permeability are all quite comparable, indicating ionic liquids are truly environmental-benign solvents that can be recovered and reused.

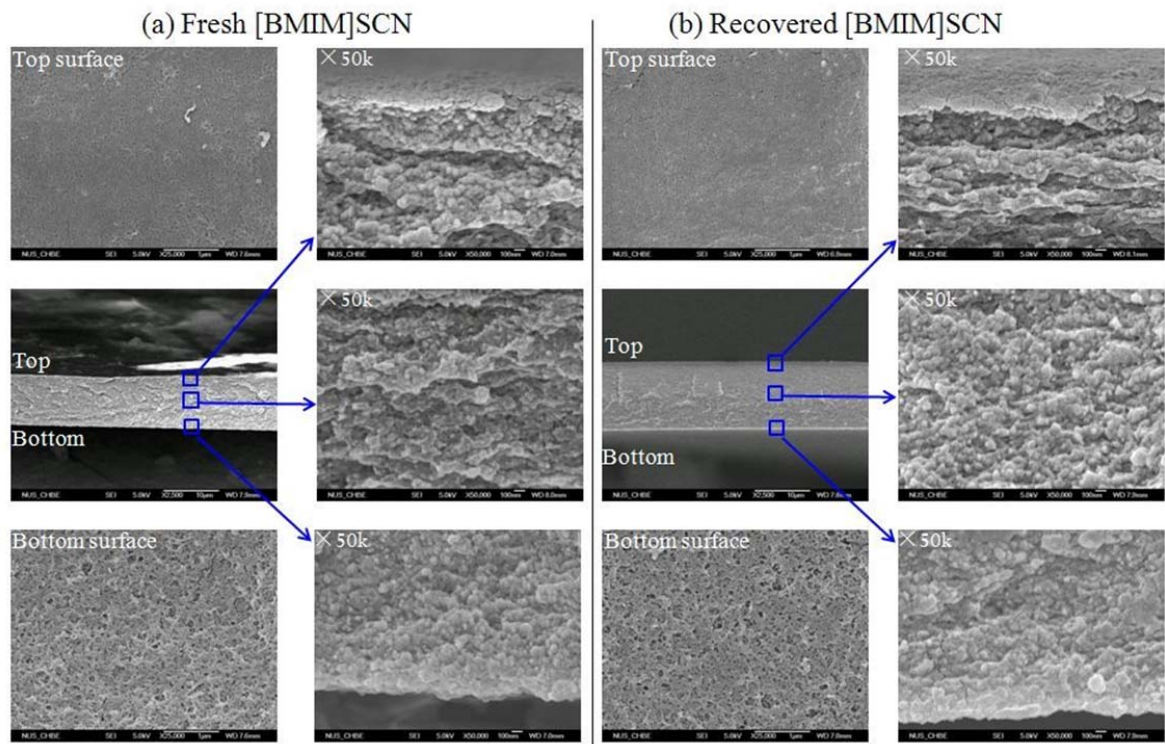


Figure 3-10 Comparison of the morphology of flat sheet membranes prepared from fresh [BMIM]SCN (a) and recovered [BMIM]SCN (b) (CA concentration: 10wt%, thickness of casting knife: 100 μ m)

3.4 Conclusions

We have conducted a pioneering study of the fundamentals of membrane formation for flat asymmetric and hollow fiber membranes using environmental-benign ionic liquids as the solvent and CA as the polymer via phase inversion. The following conclusions can be made:

1. Key factors affecting the membrane formation have been explored. CA flat membranes cast from the 10/90wt% CA/[BMIM]SCN solution exhibit a macrovoid-free and a relatively dense structure full of nodules, which is quite dissimilar with the

membranes cast from 10/90wt% CA/acetone or 10/90wt% CA/NMP. The use of ionic liquid caused far slower but even more uniform nucleation and gelation, leading to trivial asymmetry nodular structure of the CA membrane. Due to a high ratio of solvent outflow to coagulant inflow, a low water diffusivity into the nascent membrane, and a high viscosity of the CA/[BMIM]SCN solution, the phase inversion of the CA/[BMIM]SCN system most likely occurs through nucleation growth and gelation followed by solidification. The resultant ultrafiltration CA flat sheet membranes from the CA/[BMIM]SCN solution have a mean pore size of 39.2nm and pure water permeability of 114.1 L/(m² h bar).

2. Under the current experimental set up, the wet spinning process is preferred for the fabrication of hollow fiber membranes made from CA/[BMIM]SCN because of a very slow phase inversion process. The resultant hollow fiber has an asymmetric structure consisting of a porous inner surface and a relative dense outer surface, but the cross-section is macrovoid-free and full of nodules.

3. The recovery and reuse of [BMIM]SCN has been demonstrated and the derived flat asymmetric membranes made from the recovered [BMIM]SCN show similar morphological, porosity and flux characteristics with those from the fresh [BMIM]SCN.

Chapter 4 Investigation of unique interactions between cellulose acetate and ionic liquid, [EMIM]SCN, and their influences on hollow fiber ultrafiltration membranes

4.1 Introduction

The phase inversion technique has undergone a rapid development and been employed in chemical and refinery industries. Polymeric hollow fiber membranes, one of the most important configurations, have been widely studied because of easy fabrication, self-mechanical support, large surface area to volume ratio, high module packing density, and relatively low cost [1, 5, 6]. However, since environmental issues such as greenhouse effects, climate changes, and waste solvent pollution are getting severe with the rapid expansion of various industries, future manufacturing must use cleaner energy, greener solvents and fabrication technologies. Therefore, the traditional organic solvents currently used in hollow fiber spinning must be deducted in the foreseeable future and it is imperative to search for alternative green solvents that can replace them. Exclusively, ionic liquids, containing only of ions, emerge to be prominent alternatives to replace the traditional volatile organic solvents for membrane fabrication.

As known, the interaction between polymers and solvents plays an important role in membrane formation during phase inversion and by far, an informative literature has explored towards using traditional organic solvents for membrane development [65, 74, 82, 90-97]. Nevertheless, research towards fundamental understanding of polymer/ionic liquid interactions and their effects on membrane formation are under-developed. Due to the inherent ionic properties such as coulombic forces in ionic liquids, the interactions

between ionic liquids and polymers are quite different from those between polymers and conventional molecular liquids (such as *N*-Methyl-2-pyrrolidone (NMP), Dimethylformamide, and Dimethylacetamide). As a result, one may expect different solution rheology, spinning characteristics, process parameters and separation performance for hollow fiber membranes spun from these two solvent systems.

In the first part of this work, We have reported and compared the characteristics of membrane formation of cellulose acetate membranes using [BMIM]SCN and conventional solvents. However, the interactions between ionic liquids and cellulose acetate were not investigated from a molecular aspect. In addition, the rheological properties of cellulose acetate in ionic liquids and their effects on membrane formation have not been explored. Therefore, the objectives of this study are to 1) molecularly examine the interactions between ionic liquids and cellulose acetate interrelated to the chemical structure and properties of the employed ionic liquids; 2) fundamentally understand how these interactions influence phase inversion mechanisms and membrane morphology during hollow fiber formation; and 3) explore the spinning conditions to fabricate hollow fiber membranes suitable for ultrafiltration.

Since the fabrication of membranes in an environmentally benign process becomes increasingly important and the development of hollow fiber membranes from polymer/ionic liquid solutions for water reuse is likely to be an inevitable trend, it is envisioned that this work will provide the fundamentals and new insights towards the use of ionic liquids as green solvents for future manufacturing of hollow fiber membranes.

4.2 Experimental

4.2.1 Materials

The ionic liquid 1-ethyl-3-methylimidazolium thiocyanate ([EMIM]SCN, >95%) obtained from BASF, Germany were studied in this work. [EMIM]SCN is chosen as the solvent being studied because it has a even lower melting point and a lower viscosity at room temperature than 1-butyl-3-methylimidazolium thiocyanate that we studied previously. These advantages of [EMIM]SCN make it more feasible to cast flat sheet membranes and spin hollow fibers from polymer/[EMIM]SCN solutions with a suitable viscosity at room temperature. Cellulose acetate-398-30 (CA, acetyl content 39.8%) was obtained from Eastman Chemical Company, USA. Figure 4-1 shows the chemical structures of [EMIM]SCN and CA. Isopropanol was purchased from Merck. All the materials were used as received.

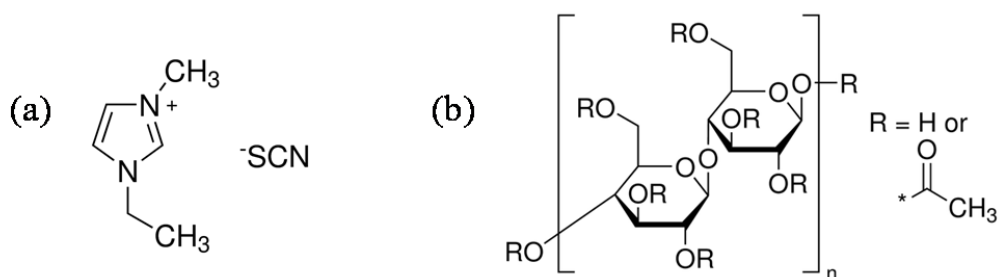


Figure 4-1 The structure of (a) [EMIM]SCN and (b) CA-398-30

4.2.2 Dope characterizations - FTIR, rheology, phase inversion kinetics and phase diagrams

12/88wt% CA/[EMIM]SCN dope was prepared using the method described in section 3.2.2. Pure [EMIM]SCN, 12/88wt% CA/[EMIM]SCN and a CA film were analyzed by a Bio-Rad FTIR FTS 135 over the range of 500-4000 cm^{-1} in the attenuated total reflectance (ATR) mode. The number of scans for each sample was 16.

The rheological studies of CA/ionic liquid solutions were conducted by a rotational rheometer (AR-G2 rheometer, TA instruments, USA) and a capillary rheometer (SMART RHEO 2000 CEASE, Italy) at 23°C. The shear viscosity of CA/ionic liquid solutions at low shear rates ranging from 0.01 to 100 s^{-1} was measured using AR-G2 rheometer under steady-state mode with a 20mm or 40mm, 1° cone geometry. The power-law expression [98] was employed to express the relationship between shear stress τ (N m^{-2}) and shear rate $\dot{\gamma}$ (s^{-1}):

$$\tau = m \cdot |\dot{\gamma}|^n \quad (4)$$

where m is the constancy index and n is the power law index.

The shear viscosity at high shear rate from 100 to 5000 s^{-1} was measured by the CEASE capillary rheometer using the two capillary stubs of a diameter of 1mm and respective length/diameter ratios of 10 and 30. The Rabinowitsch correction for non-Newtonian fluid and the Bagley correction for the end effects [98] were carried out to get the shear and elongational viscosities measured from the capillary rheometer.

The light transmittance experiments were conducted to study the phase inversion kinetics of 12/88wt% CA/[EMIM]SCN in different coagulants, i.e. water and IPA. The dope was firstly cast on a glass slide using a casting knife with a thickness of 100 μ m. The glass slide was immediately put into a plastic cuvette holding water or IPA, and the transmittance T at 600nm (water and IPA have no absorbance at this wavelength) was monitored and recorded by a UV-vis scanning spectrophotometer (Libra S32, Biochrom Ltd., England) and its built-in software. The maximum transmittance T_{max} and minimum transmittance T_{min} are used to normalize the results and get a relative light transmittance T_r using the following equation:

$$T_r = \frac{T - T_{min}}{T_{max} - T_{min}} \times 100\% \quad (5)$$

Non-solvent intrusion was observed and recorded under an Olympus BX50 polarizing optical microscope (PLM). The diffusion/convection, precipitation and solidification of the non-solvent in the nascent flat sheet CA/[EMIM]SCN films with similar thickness were recorded [65, 99]. The ternary phase diagram was determined by gradually titrating non-solvent into CA/[EMIM]SCN solutions until the solution reaches its cloud point.

4.2.3 Molecular simulation by Materials Studio

Simulation by Materials Studio 5.0 were conducted to study the interactions between CA and [EMIM]SCN. The simulation method was explored by Derecskei and Derecskei-Kovacs [100]. In our case, after the cation and anion structures were built separately using the Builder function, +1 or -1 overall charges were assigned to the ions. The full

geometry optimization of the ions was achieved by Dmol³ module on the all-electron approximation basic and then the electrostatic potential-derived charges were analyzed and assigned to all atoms. To simulate the solubility parameter of ionic liquid, three amorphous cells with the defined density were constructed with 40 cations and 40 anions respectively for molecular dynamics simulation. In order to achieve a good equilibrium of the whole system, isothermal-isobaric (NPT) and isothermal-isopyknic (NVT) dynamic running were applied at the temperature of 298K using the Forcite module in Materials Studio. The optimized system was then used for cohesive energy density and solubility parameter analysis.

4.2.4 Fabrication of CA flat sheet and hollow fiber membranes

The experimental procedures for fabricating CA flat sheet membranes and hollow fiber membranes are the same as described in Chapter 3. [Table 4-1](#) lists the spinning conditions for the CA / [EMIM]SCN system. The dope flow rate, dope temperature and air-gap distance were varied and their influences on the formation of hollow fiber membranes from [EMIM]SCN were investigated. All the procedures were conducted at room temperature (23±1°C) unless specified, and the newly prepared membranes were immersed in tap water for three days to thoroughly remove the residual solvents before they are further used. The morphology and ultrafiltration performances of resultant membranes were also explored.

Table 4-1 Spinning conditions for CA membranes

| | | | | | | | | |
|--------------------------------------|------------------------------|------|--------|------|------|------|------|------|
| Dope composition | 12wt%CA-398-30/EMIM SCN | | | | | | | |
| Bore fluid | NMP:H2O = 80:20 | | | | | | | |
| Spinneret dimension (mm) | 2.0/0.9/10 | | | | | | | |
| Spinneret temp. (°C) | Room temperature (23±1) | | | | | | | 50 |
| Dope flow rate (ml/min) | 0.5 | 1.0 | 2.5 | 5.0 | 2.5 | 2.5 | 2.5 | 2.5 |
| Bore fluid flow rate (ml/min) | 0.2 | 0.4 | 1 | 2 | 1 | 1 | 1 | 1 |
| Air gap distance (cm) | 0.5 | 0.5 | 0.5 | 0.5 | 0 | 1.0 | 5.0 | 0.5 |
| Take up rate | Free Fall | | | | | | | |
| Coagulation bath | Tap water @ room temperature | | | | | | | |
| Fiber ID * | DR-0.5 | DR-1 | DR-2.5 | DR-5 | AG-0 | AG-1 | AG-5 | T-50 |

* DR stands for dope flow rate; AG for air gap distance; T for temperature.

4.3 Results and discussion

4.3.1 The molecular interactions between CA and ionic liquids

Figure 4-2 presents the FTIR spectra of pure [EMIM]SCN, 12/88 wt% CA/[EMIM]SCN dope solution and the CA film. The assignments for wavenumbers below 1600cm^{-1} arise mostly from the imidazolium ring and $-\text{C}\equiv\text{N}$ stretching of the anion at 2048cm^{-1} , showing good agreement with previous studies [101, 102]. The broad bands in the $=\text{C}-\text{H}$ stretching region around 3100cm^{-1} and $-\text{C}-\text{H}$ stretching near 2980cm^{-1} are observed in pure [EMIM]SCN, confirming the existence of hydrogen bond between the imidazolium cation and anion. Similar observations of $-\text{C}-\text{H}$ stretching and $=\text{C}-\text{H}$ stretching have also been evidenced in other studies [13, 103]. It has been proven by both experimental and simulation works in literature that there is charge-ordered ionic structure in the imidazolium-based ionic liquids due to the nature of the coulombic interactions and hydrogen bonding between ions which facilitate the self organization in ionic liquids [13, 17-19]. Furthermore, as shown in Figure 4-2, the wavenumbers of hydrogen bonded C-H

group does not shift even when 12 wt% of CA is added into [EMIM]SCN, suggesting that the polymer chains are surrounded by the cations and ions, and that the network of ionic liquid is still continuous and maintains to a great extent. In other words, highly charge-ordered ionic structure remained in the CA/[EMIM]SCN mixture due to the hydrogen bonding and coulombic forces.

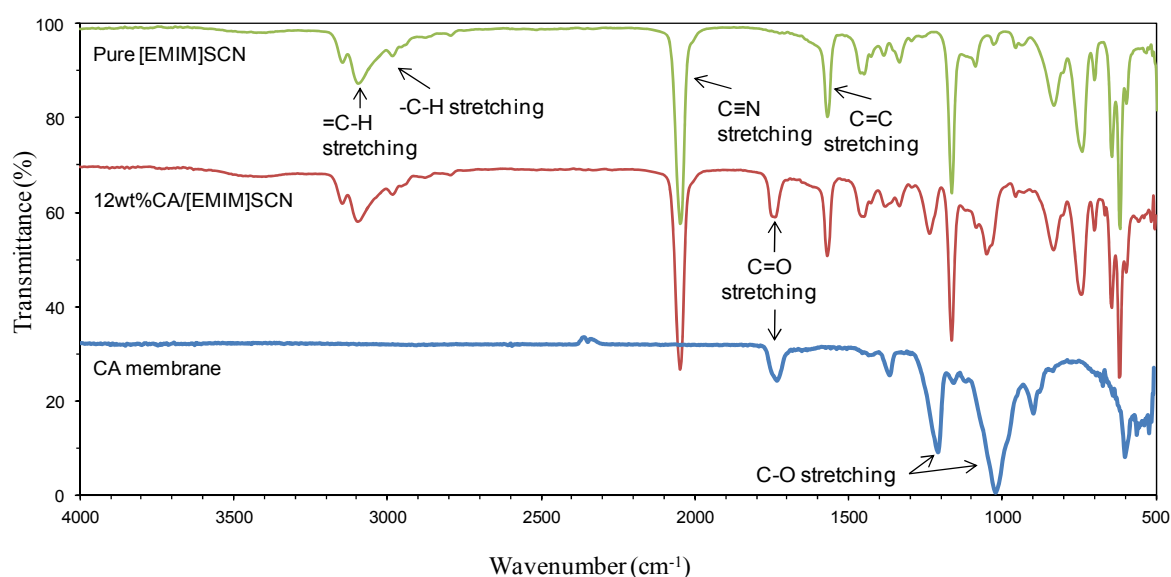


Figure 4-2 The FTIR spectra of pure [EMIM]SCN, 12%CA/[EMIM]SCN and CA membrane

The solubility parameters of [EMIM]SCN simulated by Materials Studio can also verify the existence of hydrogen bonding and coulombic forces. One factor we must take into account is that Material Studio is designed for neutral molecules and the interaction energy between neutral ion pairs is also included in the calculated cohesive energy in the case of ionic liquids. On the other hand, according to the definition of cohesive energy density as the amount of energy needed to overcome when per unit volume of molecules

are separated from their neighboring molecules to form ideal gases [2], the interaction energy between one ion pair in ionic liquids should be deducted from the total calculated cohesive energy to reveal that ionic liquids vaporize as neutral ion pairs [100]. Since Material Studio does not provide an individual parameter for hydrogen bonding, the electrostatic parameter δ_{ES} is employed instead. Table 4-2 summarizes the solubility parameters of solvents, CA and non-solvents. After the dynamic equilibrium of the [EMIM]SCN system, the simulated density of 1.110g/cm³ corresponds well to the experimental measurement of 1.114g/cm³ from BASF, indicating that the simulated amorphous cell is indeed suitable to the real case, since the spatial distance between ions is of great importance in determination of their interactions. The δ_{ES} of [EMIM]SCN which contributes greatly to the total solubility parameter, δ_t , is much larger than that of NMP, a commonly used solvent for CA. This result also proves the electrostatic nature of ionic liquids. It is possible that the ions have electrostatic interactions with CA molecules, while the imidazolium ring has close contact with CA by van der Waals interactions since their dispersive parameters δ_d are quite similar to each other as shown in Table 4-2. Although the difference in total solubility parameter between CA and [EMIM]SCN is larger than that between CA and NMP, implying that [EMIM]SCN may be not a good solvent as NMP, the hydrogen bonding and electrostatic interactions between CA and [EMIM]SCN compensate the inefficiency of solvent power and play important roles in dissolving CA and the subsequent process of membrane fabrication.

Table 4-2 Solubility parameters of solvents, cellulose acetate and non-solvents at 20°C

| Chemicals | Solubility parameter (MPa ^{1/2}) | | | | |
|-----------|--|------------|------------|--------------------|--------------------|
| | δ_d | δ_p | δ_h | δ_{ES} | δ_t |
| [EMIM]SCN | 15.03 ^a | – | – | 31.60 ^a | 34.99 ^a |
| NMP | 18.00 | 12.30 | 7.21 | 14.26 ^b | 22.90 |
| CA-398-30 | 15.55 | 16.30 | 12.95 | 21.82 ^b | 25.98 |
| Water | 15.60 | 16.00 | 42.30 | 45.25 ^b | 47.80 |
| IPA | 15.80 | 6.10 | 16.40 | 17.50 ^b | 23.50 |

δ_d , dispersive parameter; δ_p , polar parameter; δ_h , hydrogen bonding parameter; δ_{ES} , electrostatic parameter; δ_t , total solubility parameter.

^a Calculated from Materials Studio (MS);

$$^b \delta_{ES} = \sqrt{\delta_p^2 + \delta_h^2}.$$

4.3.2 The rheology of CA/[EMIM]SCN solutions

The rheological behavior is also a good indicator of the microstructure and mechanical properties of the studied systems. Figure 4-3 presents the shear viscosities of CA/[EMIM]SCN dopes with different CA concentrations as a function of shear rate. presents the shear viscosities of various CA/[EMIM]SCN dopes with different CA concentrations as a function of shear rate. The power law indices, n , of low shear thinning regions which indicate the degree of non-Newtonian behavior is calculated and listed beside the graph. It is interesting to find that all the solutions with CA concentration varying from 4wt% to 14wt% exhibit a shear thinning behavior at low shear rates ($<0.5 \text{ s}^{-1}$), followed by a Newtonian plateau and another shear thinning as the shear rate increases.

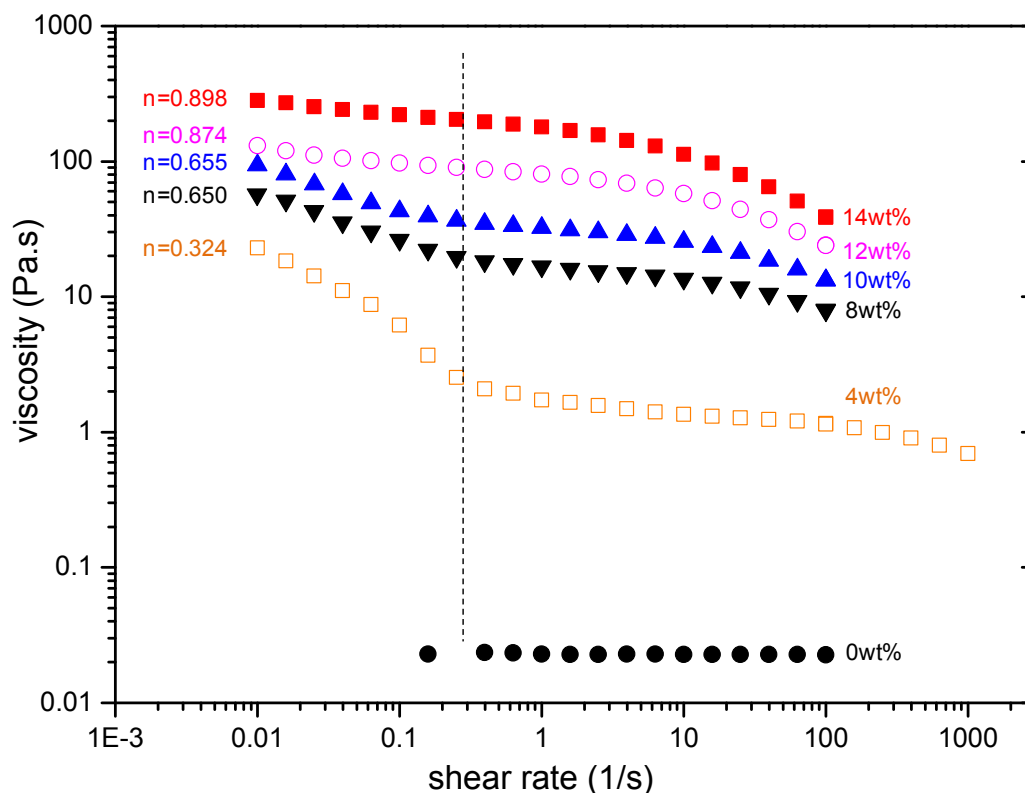


Figure 4-3 Shear viscosity of CA/[EMIM]SCN solutions with different CA concentration at 23 °C (n is the power law index of initial shear thinning regions)

Although this phenomenon is quite similar to the rheological behavior of the liquid crystals formed from rod-like molecules [104, 105], the anisotropic behavior could not be optically observed under a PLM. Contrary to the behavior of rod-like liquid crystalline polymers, the initial shear thinning is much steeper for the solution samples with low polymer concentrations but becomes less significant for the solution samples with increased CA contents. Moreover, without CA, the pure [EMIM]SCN shows a Newtonian behavior within the measurable range of $0.15\text{-}100\text{ s}^{-1}$, which is possibly because of homogeneous charge-ordered structure in pure solvent state. Thus, the three-

region flow behavior in CA/[EMIM]SCN solutions should be related to the pronounced charge-ordered ionic structure in the solutions resulting from the hydrogen bonding and electrostatic interactions as discussed previously. Moreover, there is a competition between such ordered structures and the polymer chain entanglements in CA/[EMIM]SCN solutions. At low CA concentrations such as 4 wt%, CA molecules can disperse well with little entanglements with other polymer chains and have strong interactions with surrounding ions. As a consequence, the charge-ordered local structure plays the leading role and undergoes deformations caused by shear stresses without encountering much resistance to flow and results in a shear thinning behavior at low shear rates. With the increase of CA concentration, polymer chain entanglements become progressively significant and the abovementioned local structures may be disrupted to certain extent, allowing the solution to exhibit more resistance as well as making it difficult to deform at low shear rates, resulting in a Newtonian flow.

With the increase of shear rate, movements of CA molecular chains begin to play the leading role after the effects of the charge-ordered ionic structure has been overcome. The Newtonian plateau followed by shear thinning at higher shear rates, a typical feature of a shear thinning power-law fluid, is greatly attributed to the reduction in polymer chain entanglements or the enhancement in chain orientation [78, 106]. In other words, under a relatively low shear, the random coil macromolecules have a high degree of un-oriented chain entanglements leading to a high viscosity, although they will gradually disentangle, orientate and align themselves in response to increasing shear, producing less fluid resistance and molecular friction [65, 73, 75]. The following sections will zoom into

discussions in the effects of intense interactions between CA and [EMIM]SCN as well as rheological properties of polymer dopes on membrane formation.

4.3.3 Phase inversion of CA/[EMIM]SCN in different coagulants

In order to further verify the molecular interactions in CA/[EMIM]SCN solutions and their effects on membrane formation, flat sheet membranes cast from 12/88wt% CA/[EMIM]SCN solutions were coagulated in different non-solvents, i.e. water and isopropanol (IPA), which are of different hydrogen bonding strengths as shown in [Table 4-3](#). [Figure 4-4](#) exhibits the effects of different coagulants on the morphology of CA flat sheet membranes. It is interesting to find that the CA flat membrane coagulated in water shows a dense packed nodular structure; while the one coagulated in IPA shows a closed-cell porous structure. Therefore, the membrane coagulated in water has a much thinner thickness (around 14 μm) than that coagulated in IPA (around 48 μm). These dissimilar morphologies of cross sections are due to different phase inversion kinetics and precipitation paths, which will be discussed in the following sections.

Table 4-3 Viscosities and diffusivities of water and IPA

| Chemicals | Viscosity (cP) | $D_{E-N} \times 10^6$ (cm^2/s) ^a | $D_{N-E} \times 10^6$ (cm^2/s) ^b |
|-----------|-------------------|--|--|
| Water | 1.00 | 7.29 | 2.20 |
| IPA | 2.40 | 4.21 | 0.952 |

^a The diffusion coefficient of [EMIM]SCN in almost pure non-solvent;

^b The diffusion coefficient of non-solvent in almost pure [EMIM]SCN.

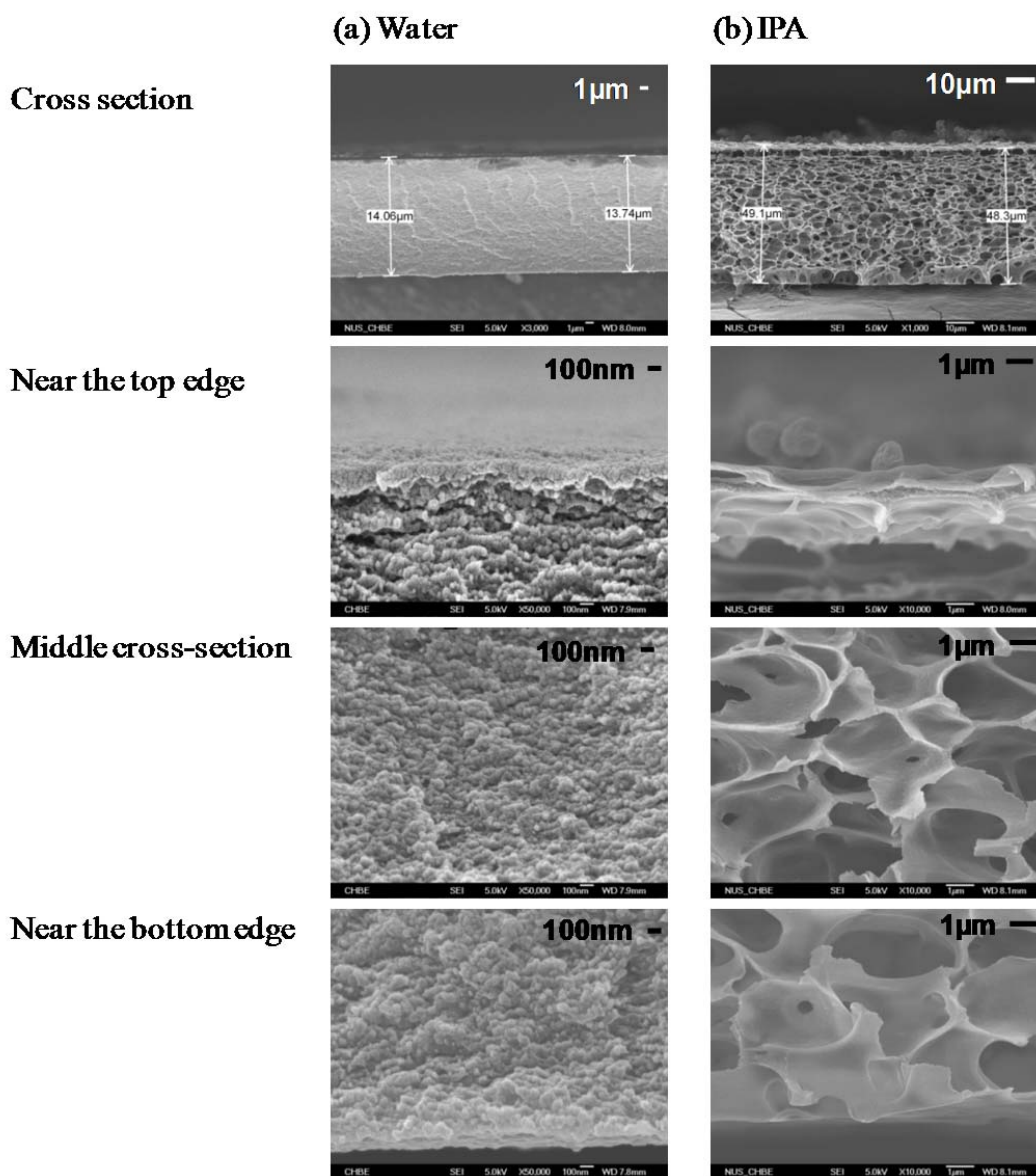


Figure 4-4 The cross section morphology of flat sheet membranes cast from 12/88 wt% CA/[EMIM]SCN and coagulate in (a) water (b) IPA

First of all, the phase diagram in [Figure 4-5](#) illustrates that the binodal curve of the CA/[EMIM]SCN/IPA system is much closer to the polymer – non-solvent axis compared to that of the CA/[EMIM]SCN/water system, which indicates that the phase inversion

rate of CA/[EMIM]SCN in IPA is much slower than that in water. The different phase inversion rates are also confirmed by the results of light transmittance tests in Figure 4-6. When using IPA as the coagulant, a noticeable decrease of light transmittance indicating the commencement of phase inversion is only observed at around 450s; while the light transmittance starts to decline at only about 10s if water is employed as the coagulant. Possible reasons may arise from the differences in solubility and diffusivity between [EMIM]SCN and two non-solvents. From the solubility parameters in Table 4-2, it is known that water and IPA have similar dispersive solubility parameters δ_d but have quite distinguishable hydrogen bonding parameters δ_h from each other. In addition, the diffusion coefficients between [EMIM]SCN and two non-solvents are calculated from the

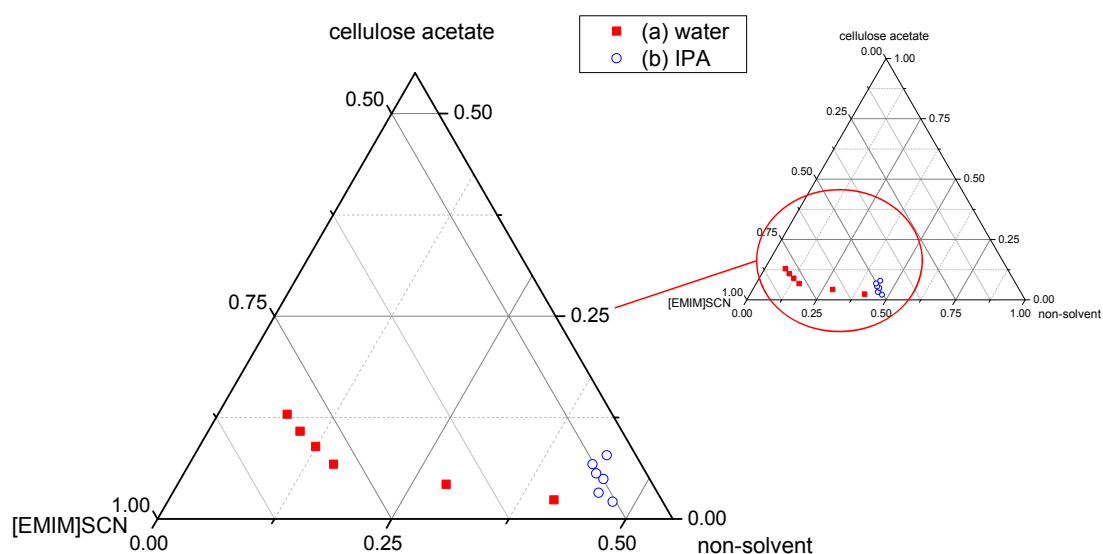


Figure 4-5 The phase diagrams of CA/[EMIM]SCN/non-solvent systems at $23\pm 1^\circ\text{C}$

Wilke-Chang equation [80] and summarized in Table 4-3. The diffusion coefficients of [EMIM]SCN with respect to non-solvents obey the order of $D_{E-water} > D_{E-IPA}$, while the diffusion coefficients of non-solvents with respect to [EMIM]SCN follow the order of $D_{water-E} > D_{IPA-E}$. These two facts also strongly indicate that [EMIM]SCN has a better affinity with water than with IPA.

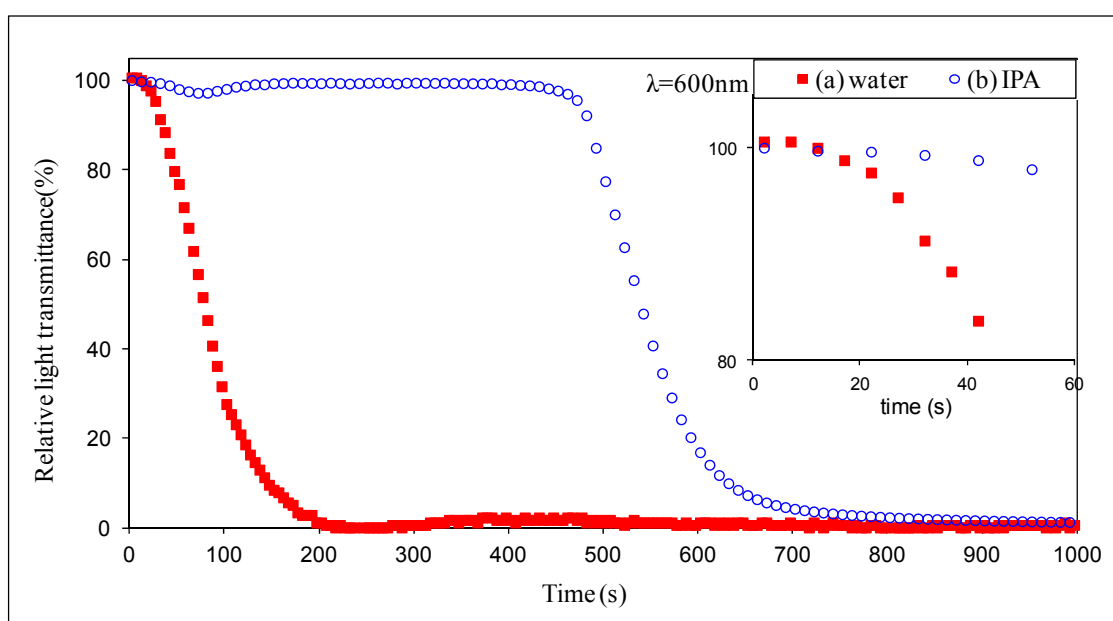


Figure 4-6 The phase inversion kinetics of flat sheet membranes cast from 12/88 wt% CA/[EMIM]SCN and coagulate in (a) water (b) IPA

As discussed in the first part of work, when water is used as the coagulant, nucleation growth and gelation may dominate the phase inversion paths because a significant amount of [EMIM]SCN tends to diffuse out while a small amount of water diffuses in. This would result in a membrane cross-section structure full of nodules. Due to the stronger hydrogen bonding in water, a less quantity of water is required to initiate the phase separation. In addition, it is easier for water to induce phase inversion of the

nascent membrane compared to IPA because the former has a high diffusivity into [EMIM]SCN than the latter. As a result, more nascent nucleus can be formed at the early stage, which evolves into the nodular structure eventually. In the case of using IPA as the non-solvent for the CA/[EMIM]SCN solution, a large amount of IPA is needed to induce phase separation, and its weak hydrogen bonding strength as well as the low diffusivity of IPA to [EMIM]SCN make it difficult for IPA to diffuse into the CA/[EMIM]SCN system consisting of a strong charge-ordered network. Consequently, a delayed liquid-liquid demixing will happen and there should be fewer nucleus formed in the polymer poor phase at the early stage compared to those formed when water is used as the non-solvent. Besides that, since the phase inversion rate is much slower in IPA, it allows more time for the pore evolution before membrane solidification. Based on the pore formation mechanism [107], because of a high diffusivity ratio of [EMIM]SCN out flow to IPA inflow (about 5:1 as shown in Table 4-3), poor affinity between IPA and [EMIM]SCN and weak coagulation strength of IPA, [EMIM]SCN in the polymer rich phase may slowly diffuse into IPA with the sluggish intrusion of IPA into the nascent CA/[EMIM]SCN membrane. As a result, the CA concentration in the polymer rich phase would gradually increase and eventually form a close-cell porous structure.

The different phase inversion kinetics and precipitation paths have also been proved by the observation of water or IPA intrusion into the 12/88wt% CA/[EMIM]SCN solution observed under PLM as shown in Figure 4-7. It can be found that in neither of these two cases, the non-solvent intrusion can be observed immediately after water or IPA is introduced. When water is used as the coagulant, the diffusion front can be observed at

5s, and as time goes on, the front of water does not go much further and the membrane solidifies without any trace of water intrusion in the CA/[EMIM]SCN solution. This is because the [EMIM]SCN outflow is more significant than water inflow during the phase inversion and the nascent membrane solidifies relatively fast, leading to the invisibility of the non-solvent intrusion. By contrast, the diffusion front is hard to recognize until 10s in the case of IPA, yet it turns out that the precipitation and diffusion/convective fronts of IPA intrusion grow clearly with time, which visualizes the pore evolution due to the poor affinity and diffusivity between IPA and [EMIM]SCN.

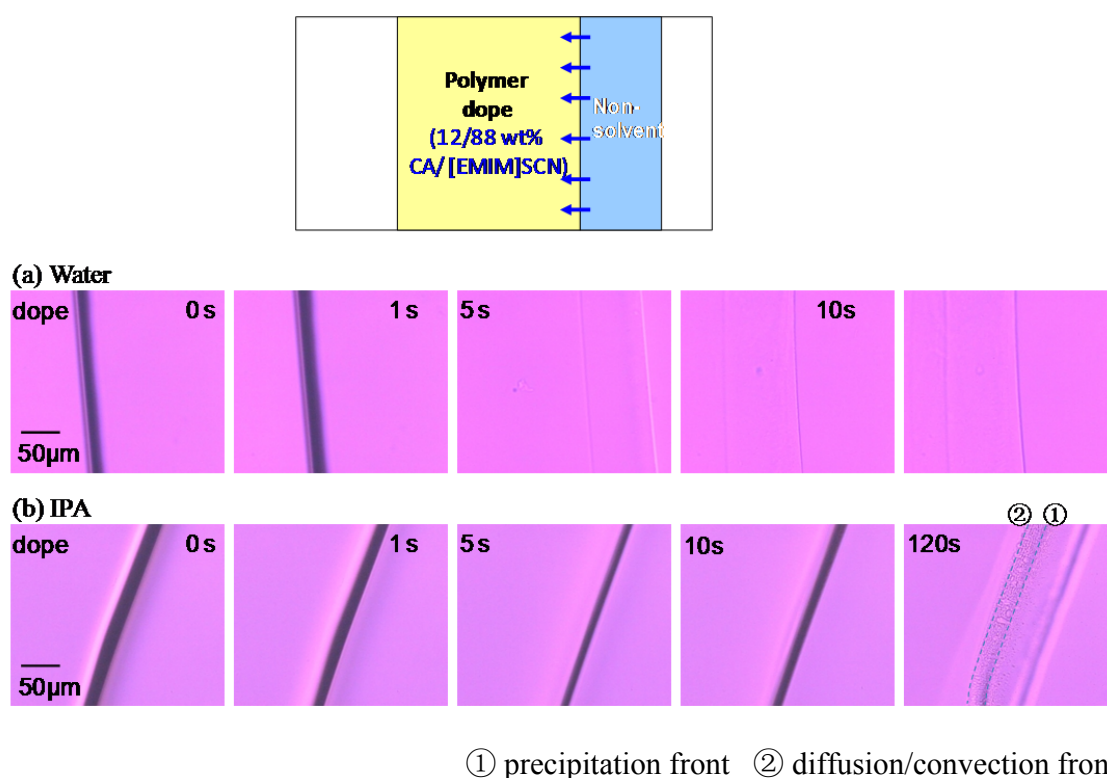


Figure 4-7 Observation of non-solvent intrusion ((a) water, (b) IPA) in 12/88 wt% CA/[EMIM]SCN thin film under PLM

The above phenomena again reinforce our hypotheses that the charge-ordered network in CA/[EMIM]SCN solutions as well as the interactions and affinity between non-solvents and [EMIM]SCN play important roles in the phase inversion process. Water with strong hydrogen bonding promotes favorable interactions between water with [EMIM]SCN and easily intrudes the charge-ordered network in CA/[EMIM]SCN solution, thus the phase inversion in water is much faster through gelation and nucleation growth but without pore evolution. Whereas, IPA with the poor hydrogen bonding strength is relatively difficult to intrude into the charge-ordered network of the CA/[EMIM]SCN solution, leading to relatively a slow phase inversion by delayed liquid-liquid demixing and allowing the growth of close-cell pores.

4.3.4 Hollow fiber membrane morphology and ultrafiltration characterizations

[EMIM]SCN can dissolve CA up to 20 wt%, yet considering the feasibility of hollow fiber spinning and the applications of the hollow fibers, 12wt% CA/[EMIM]SCN was chosen. [Figure 4-8](#) displays the typical bulk and surface morphologies of CA hollow fiber membranes using [EMIM]SCN as the solvent. Under all the conditions listed in [Table 4-1](#), the resultant hollow fibers have an asymmetric structure with a porous inner surface but a relative dense outer surface. The cross section of the fibers shows a loose interconnected nodular structure without macrovoids. The interconnected nodular structure is formed because the phase inversion probably happens through nucleation growth followed by spinodal decomposition as discussed in our previous works [\[77, 108\]](#); while no macrovoids are formed because of the high dope viscosity, a high ratio of solvent outflow to non-solvent inflow, as well as the pronounced hydrogen bonding and

charge-ordered structure in CA/[EMIM]SCN dope solutions. All of these factors retard a rapid intrusion of the external coagulant into the nascent membrane and thus reduce any chance of localized supersaturation for the macrovoid formation [4, 66, 82, 109].

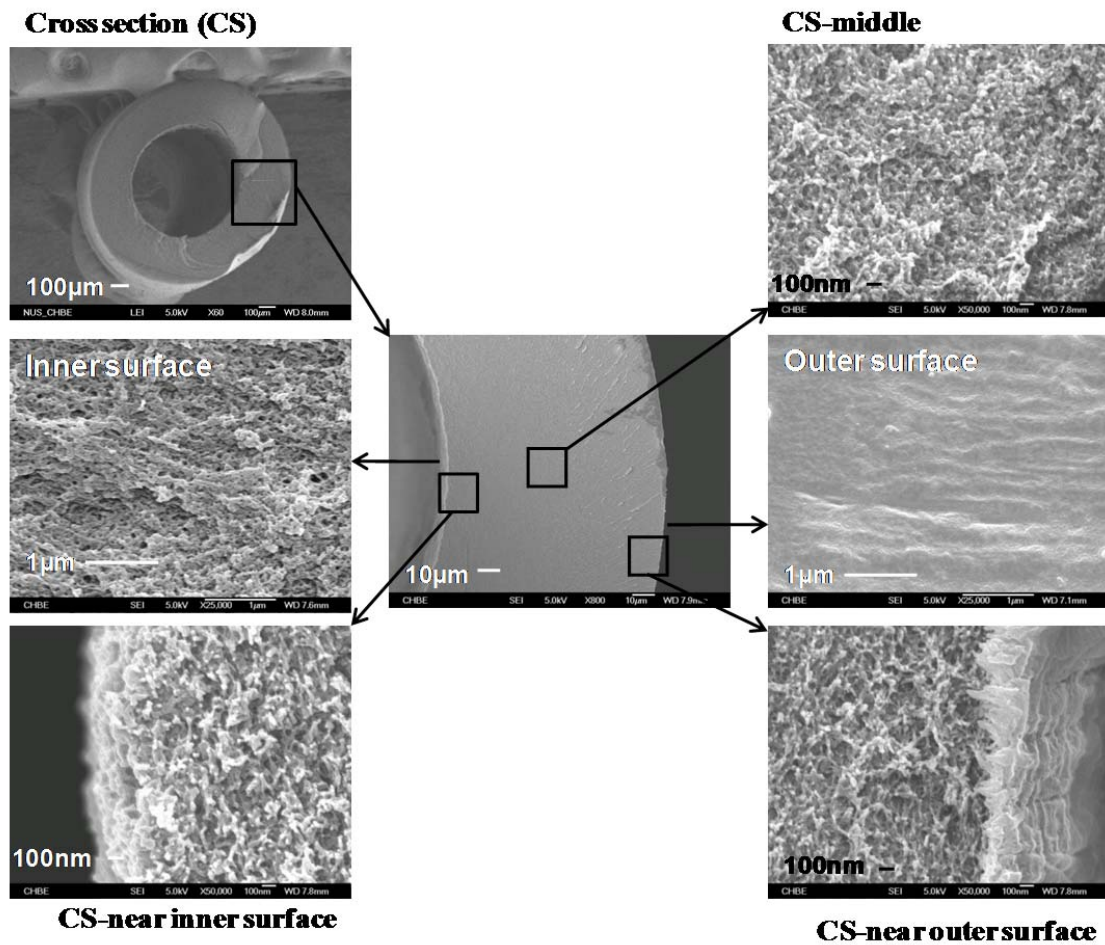


Figure 4-8 The morphologies of CA hollow fiber membranes DR-2.5 (dope:2.5ml/min, bore fluid:1.0ml/min, air gap=0.5cm, free fall)

4.3.4.1 Effects of dope flow rate and dope temperature

Table 4-4 Comparison of various parameters and PWP of CA hollow fiber membranes

| Fiber ID | DR-0.5 | DR-1 | DR-2.5 | DR-5 | AG-0 | AG-1 | AG-5 | T-50 |
|---|----------------|-----------------|-----------------|-----------------|----------------|-----------------|-----------------|-----------------|
| Fiber o.d./ i.d.(mm) | 1.268/ 0.62 | 1.330/ 0.667 | 1.456/ 0.728 | 1.586/ 0.828 | 1.953/ 0.99 | 1.193/ 0.633 | 1.024/ 0.572 | 1.149/ 0.594 |
| Wall thickness (mm) | 0.324 | 0.332 | 0.364 | 0.379 | 0.482 | 0.279 | 0.226 | 0.278 |
| PWP(L/m ² bar h) | 62.88 | 52.72 | 47.66 | 46.80 | 43.1 | 79.17 | 90.10 | 57.68 |
| μ_p (nm) The mean of effective pore diameter | 16.68 | 14.61 | 11.91 | 10.28 | 12.91 | 14.29 | 16.68 | 17.98 |
| σ_p The geometric standard deviation | 1.932 | 2.264 | 1.966 | 1.376 | 2.139 | 2.276 | 2.148 | 2.907 |

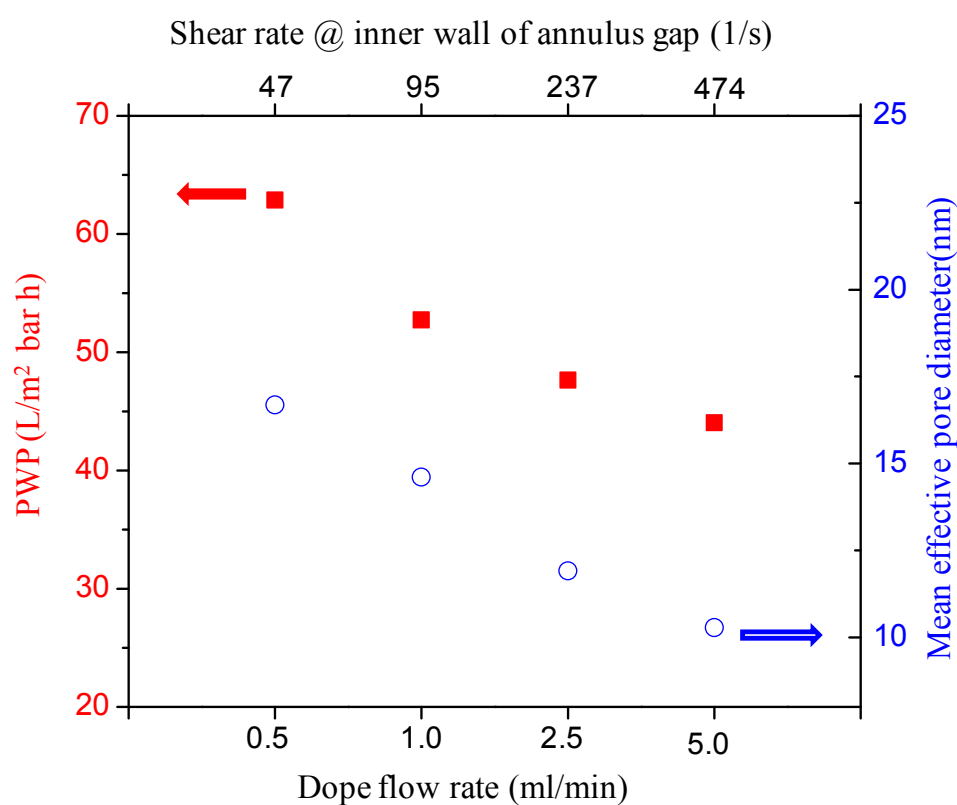
**Figure 4-9** Effects of dope flow rate on the PWP and mean effective pore diameter of hollow fiber membranes spun from 12/88 wt% CA/[EMIM]SCN (a constant ratio of dope flow rate to bore fluid flow rate, air gap = 0.5cm, free fall)

Figure 4-9 and Table 4-4 summarize the effects of dope flow rate on ultrafiltration performance of the newly developed hollow fibers. It is found that the higher the dope flow rate, the lower the PWP value and the smaller the mean effective pore diameter.

At least two reasons are proposed to explain these phenomena. Firstly, the wall thickness of hollow fibers increases with an increment in dope flow rate from 0.5 to 5.0 ml/min which may result in an enhanced transport resistance during ultrafiltration tests. Secondly, the increased shear rate within the spinneret also contributes to the reduced PWP value and pore diameter. Figure 4-10 (a) shows the effects of dope flow rate on the shear rate profile along with the radial length at the outlet of the 2.0/0.9(o.d./i.d.) spinneret, which is calculated from the computational fluid dynamics model described in Cao et al.'s work [73]. The shear rate within the spinneret increases dramatically with the dope flow rate and fall into the shear thinning region of the CA/[EMIM]SCN solution as illustrated in Figure 4-10 (b). Therefore, a higher shear rate would facilitate the development of orientation and alignment of polymer chains, adjusting the space between polymer chains and forming a closely packed polymer network [5, 71, 73, 74]. As a result, the hollow fiber DR-5.0 has the smallest mean effective pore diameter, as well as the sharpest pore size distribution and the most reduced pure water permeability.

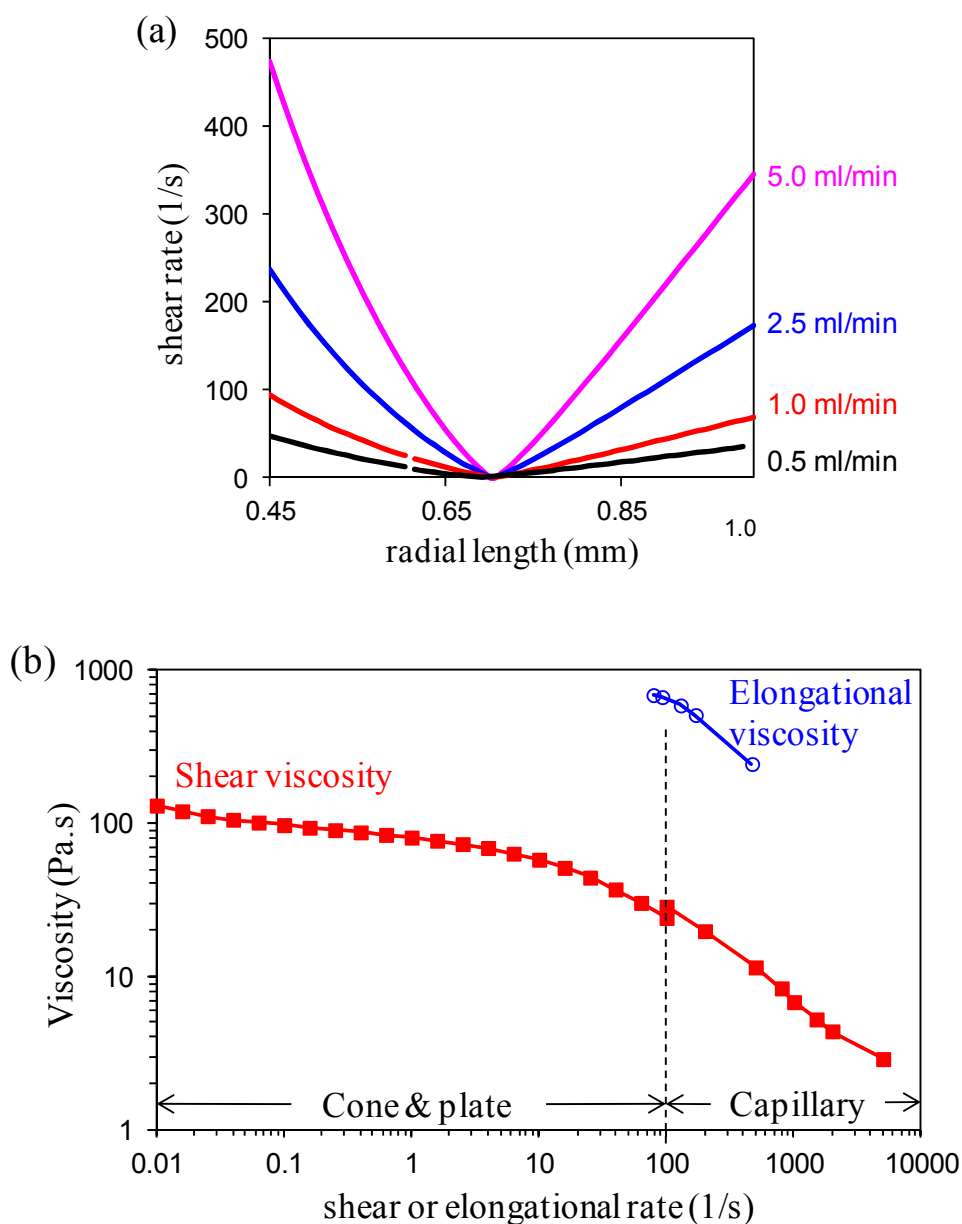
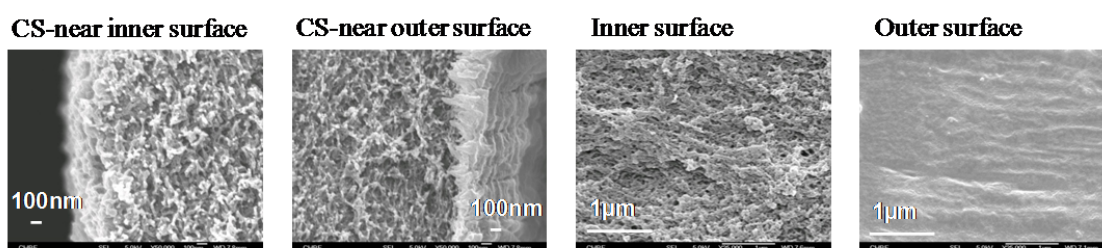


Figure 4-10 (a) Shear rate profile along with the radial length at the outlet of 2.0/0.9 (o.d./i.d.) spinneret; and (b) shear and elongational viscosity of 12/88wt% CA/[EMIM]SCN solutions at 23 °C

Figure 4-11 displays the morphologies of hollow fibers spun employing different dope temperatures. Taking DR-2.5 spun at room temperature as a reference, raising the dope temperature to 50 °C produces hollow fiber membranes with a slightly more porous cross

section and inner surface. Some tiny pores can even be observed on the outer surface of the membrane. There are at least two reasons for the formation of more porous structure at a higher temperature. Firstly, as the dope temperature increases, the CA/[EMIM]SCN dope shows a reduced shear viscosity, and the diffusion flows between non-solvent and solvent are also enhanced [65]. Meanwhile, the binodal curve would shift slightly close to the polymer – non-solvent axis, which means more water is needed to start the phase separation. Therefore, at high dope temperatures, the faster exchange between [EMIM]SCN and water as well as the softer boundary of the nascent membranes probably facilitate the spinodal decomposition and thus results in a more porous bulk structure. Consistent to the above analyses, both PWP value and mean effective pore diameter reinforce the increase with elevated dope temperature as shown in Table 4-4.

(a) DR-2.5 (spinneret at room temperature)



(b) T-50 (spinneret at 50°C)

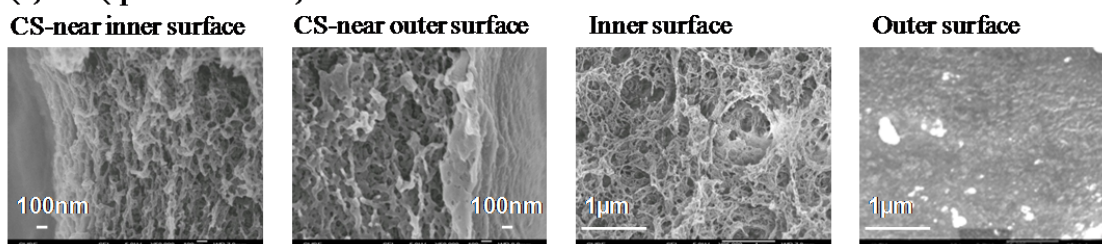


Figure 4-11 Effects of spinneret temperature on the morphologies of hollow fiber membranes spun from 12/88 wt% CA/[EMIM]SCN (dope:2.5ml/min, bore fluid:1.0ml/min, air gap=0.5cm, free fall)

4.3.4.2 Effects of air-gap distance

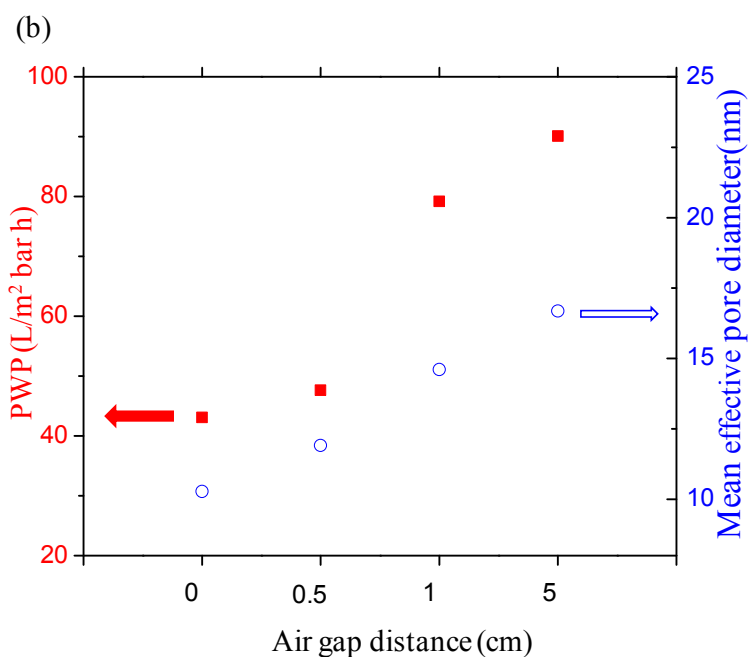
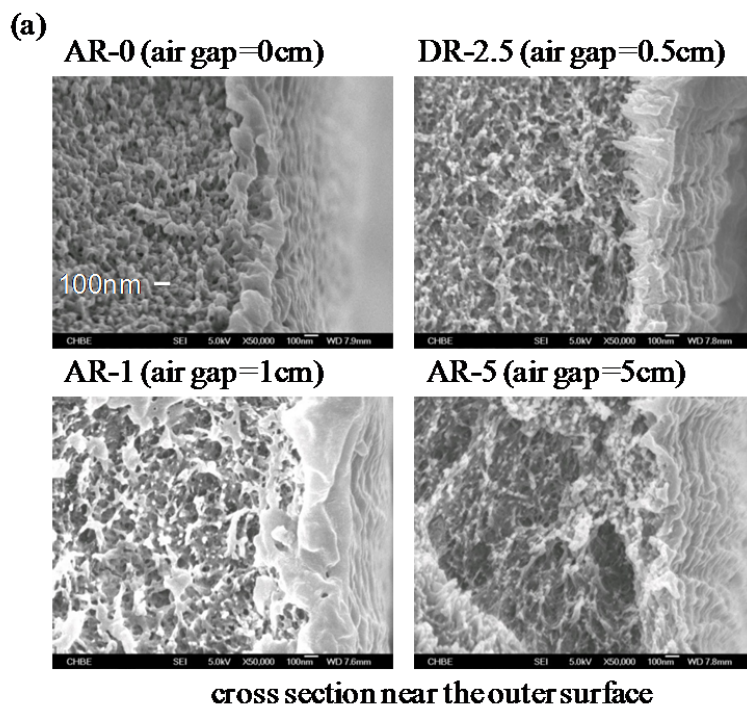


Figure 4-12 Effects of air gap distance on (a) the morphologies of the enlarged cross section near the outer surface; (b) the PWP and mean effective pore diameter of hollow fiber membranes spun from 12/88 wt% CA/[EMIM]SCN (dope:2.5ml/min, bore fluid:1.0ml/min, free fall).

The influences of air-gap distance on the morphology and ultrafiltration performance of hollow fibers are also studied. The membrane structure gradually evolves from the nodular structure of AR-0 to the more porous structure of AR-5, verified by SEM pictures in [Figure 4-12\(a\)](#) and is responsible for the larger pore diameter and enhancement of pure water permeability with an increment in air gap distance as shown in [Figure 4-12\(b\)](#).

Two hypotheses are proposed here to explain the effects of air-gap distance when using [EMIM]SCN as the solvent. One is that the hollow fibers would undergo different phase inversion paths during wet-spinning and dry-jet wet-spinning processes. The polymer dope exhibits a much lower viscosity resulted from the shear thinning and elongational thinning as referred to [Figure 4-10\(b\)](#). Meanwhile in a dry-jet wet spinning process, as discussed in Chung's work [\[60\]](#), the external forces including shear stress within the spinneret and the elongational stress during the air gap region would apply extra work on the nascent fibers, thus create extra instability and alter the kinetics and thermodynamics of phase separation. Therefore, after experiencing the extra stresses and also the moisture induced phase inversion during the air gap region in a dry-jet wet spinning process, the solvent exchange would proceed faster compared to that in a wet-spinning (AR-0) [\[53, 88, 110\]](#). The phase inversion of CA/[EMIM]SCN in water may change from the domination of nucleation growth in the wet-spinning to the domination of spinodal decomposition with better orientation of pores in the dry-jet wet-spinning process.

Therefore, the porosity of the resultant hollow fiber membranes increases with an increase in air-gap distance, leading to enhanced pure water permeability.

Another hypothesis is that the CA/[EMIM]SCN/water system shows a much slower phase inversion compared to CA/NMP/water [108] due to the electrostatic interactions and charge-ordered ionic structure in the CA/[EMIM]SCN solution, thus the whole cross section only displays trivial asymmetry as shown in Figure 4-8 and the membrane thickness plays an important role in the determination of pure water permeability of the hollow fibers. The thickness of AR-5 (0.226mm) is only about half of that of AR-0, which results in less transport resistance and leads to the higher PWP value. In this work, the highest PWP value achieved is 90.10 (L/m² bar h) with a mean effective pore diameter of 16.68nm of the CA hollow fiber AR-5.

4. Conclusions

In this work, we have explored in-depth the interactions between [EMIM]SCN and CA in relation to its efficiency of using room temperature ionic liquid, [EMIM]SCN as the solvent for CA hollow fiber fabrication. The following conclusions can be drawn:

- 1) In the CA/[EMIM]SCN solution, the highly charge-ordered ionic structure remains in the mixture with the inclusion of CA molecules due to the hydrogen bonding and coulombic forces, causing this ordered structure to play important roles in dissolving CA as well as in the membrane formation process.

2) The unique rheological characterizations of CA/[EMIM]SCN solutions are demonstrated as a three-region flow curve under shear stress, which arise from the competition between the charged-ordered structure and polymer chain entanglements in the CA/[EMIM]SCN solution.

3) The dissimilar morphologies of CA flat sheet membranes coagulated in two non-solvents, i.e. water and IPA, indicate the diverse phase inversion paths, verifying the vital role of the charge-ordered network in CA/[EMIM]SCN solutions as well as the effects of affinity and unique solvent exchange characteristics between non-solvents and [EMIM]SCN on membrane formation.

4) The effects of dope flow rate, dope temperature and air-gap distance on hollow fiber formation have been studied and correlated to the interaction between CA and [EMIM]SCN and the phase inversion mechanisms. By alteration of the spinning conditions, CA hollow fiber membranes have been successfully fabricated for ultrafiltration with a PWP value of 90.10 (L/m² bar h) and a mean effective pore diameter of 16.68nm.

As far as we know, this is the first work that applies hollow fibers fabricated from polymer/ionic liquid solution in water treatment. Future work will focus on fabricating hollow fibers with desirable separation performances, which will make the idea of using ionic liquid for membrane fabrication more promising and practical in many applications.

Chapter 5 Molecular interactions between polybenzimidazole and [EMIM]OAc, and derived ultrafiltration membranes for protein separation

5.1 Introduction

Polybenzimidazole, a type of aromatic polymeric material, is well known for its outstanding thermal and chemical stability [111]. Among the family of polybenzimidazoles, poly-2,2'-(*m*-phenylene)-5,5'-bibenzimidazole (PBI) has received most attention because it has a high glass transition temperature (417°C), stable thermal properties up to 350°C [112], and excellent chemical resistance in harsh environments. PBI has been extensively explored in the field of membrane separation technologies for fuel cell [113-115], nanofiltration [116], reverse osmosis [117], forward osmosis [118, 119], and pervaporation [120]. Nevertheless, one major problem of PBI is the difficulty of dissolving it in common solvents. PBI only has very limited solubility in a few highly polar and aprotic organic solvents, such as dimethyl sulfoxide (DMSO), *N,N*-dimethylacetamide (DMAc), *N,N*-dimethylformamide (DMF). These solvents are relatively toxic and volatile, which are hazardous to both the operators and environment. In addition, PBI can only be dissolved in abovementioned solvents under special conditions, i.e., high pressures as well as high temperatures above the boiling points of solvents [36, 111]. Not only do these shortcomings limit the growth potential of PBI materials but also cause problems such as high energy consumption and environmental pollution. Therefore, it is imperative to find better solvents for PBI.

Efforts have been made to improve PBI solubility by chemically modifying PBI molecules through either substitution at the reactive benzimidazole nitrogen sites [113, 121, 122] or employment of novel monomers for polymerization [115, 123]. However, these methods are not so convenient, economical and direct compared to the search of a novel solvent to effectively dissolve PBI.

Ionic liquids possess great potential as a new solvent for PBI due to the following reasons. Firstly, since ionic liquids are composed of entirely ions. The distinct coulombic forces among ions greatly affect their solubility characteristics [11] and significantly enhance their interactions with other substances. Secondly, ionic liquids are regarded as “green” solvents as they have very stable thermal and chemical properties and negligible volatility. Since they can be recycled and reused repeatedly [124], the use of ionic liquids would minimize chemical waste and losses during chemical processes [7, 9]. Thirdly, throughout the literature, ionic liquids have shown good capability in dissolving macromolecules which have limited solubility in traditional organic solvents [10]. A well-known case is the dissolution of highly concentrated cellulose in hydrophilic imidazolium-based ionic liquids under milder conditions [30, 31]. The strong ionic interactions are the driving force to break up the hydrogen bonding in cellulose [32]. Furthermore, ionic liquids are designable according to users’ requirements by varying cations, anions or their combinations. As a result, considering these unique properties, one of the objectives in this study is to search for suitable ionic liquids that can dissolve PBI and mitigate the hazard and pollution issues of using traditional solvents.

To fabricate asymmetric PBI membranes by the non-solvent induced phase inversion method [118, 119, 125], the suitable ionic liquids are not only required to dissolve PBI, but also have excellent miscibility with water so that phase inversion can occur and ionic liquids can be leached out from membranes and then be recycled [35, 108]. Nevertheless, research on this area is quite limited. To our best knowledge, only 1-butyl-3-methylimidazolium chloride ([BMIM]Cl) has been reported to be a solvent for PBI [126]. However, it is not an ideal solvent because [BMIM]Cl remains as solid at room temperature and has a relatively high viscosity (11,000cp) during melting. Thus, it is crucial to search for other ionic liquids with lower viscosity for easier processing during membrane fabrication. Besides, the dissolution mechanism of PBI in ionic liquids has not been fully understood. Therefore, in addition to searching for better ionic liquids for the fabrication PBI membranes, our objectives are to (1) fundamentally understand the molecular interactions between ionic liquids and PBI with the aid of molecular simulation; (2) examine the distinctive morphology of PBI membranes made from PBI/ionic liquid solutions; and (3) investigate the ultrafiltration characteristics and separation performance of the newly developed membranes for the separation of bovine serum albumin (BSA) and hemoglobin (Hb) protein mixtures [127]. In order to achieve an excellent separation performance, thermal treatment and chemical cross-linking of PBI membranes were conducted. Since “green” technologies have received increasing attention, this work may provide new insights on the development of polymeric membranes made from ionic liquids and facilitate the evolution and implement of “greener membrane fabrication” in the membrane industry.

5.2 Experimental

5.2.1 Materials

Poly-2,2'-(*m*-phenylene)-5,5'-bibenzimidazole (PBI) in the form of fine powder, with inherent viscosity of 0.50 dL/g, was kindly provided by PBI Performance Products, Inc.(United States). Three ionic liquids, 1-ethyl-3-methylimidazolium thiocyanate ([EMIM]SCN, >95%), 1-ethyl-3-methylimidazolium acetate ([EMIM]OAc) and 1-butyl-3-methylimidazolium methyl sulfate ([BMIM]MeSO₄), kindly given by BASF (Germany) were chosen to study the solubility of PBI in this work. The water content of [EMIM]OAc is less than 2 wt% according to thermal gravimetric analysis. The chemical structures of PBI and ionic liquids are shown in Figure 5-1. Poly(ethylene glycol) (PEG) of different molecular weights, bovine serum albumin (BSA) and hemoglobin (Hb) were purchased from Sigma-Aldrich. All the materials were used as received.

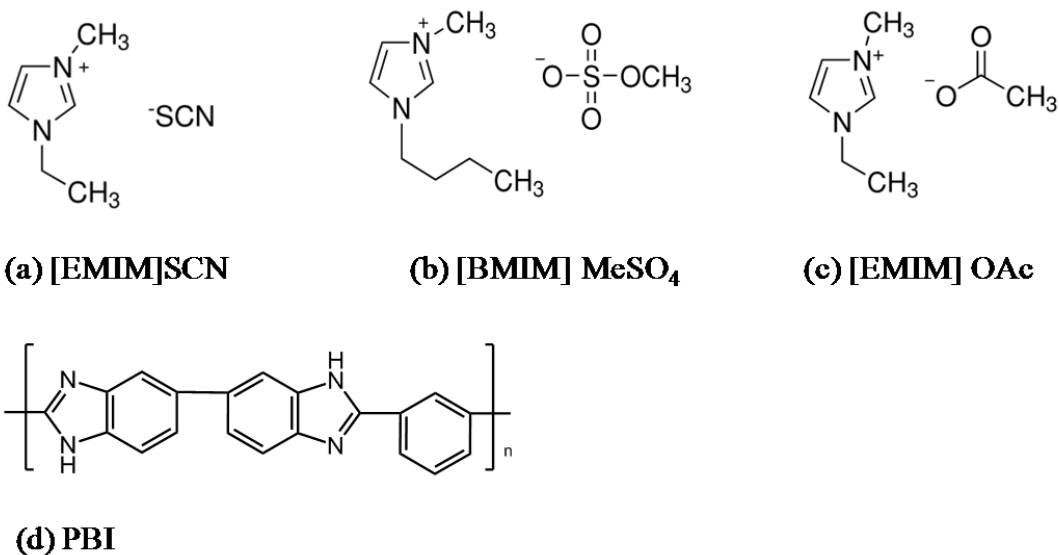


Figure 5-1 The structures of ionic liquids and PBI

5.2.2 Dissolution experiments

PBI powder was dried in a vacuum oven at 120°C overnight to remove moisture before use. Mixtures of PBI and ionic liquids were prepared by adding PBI powder to glass vials containing ionic liquids, and then heated with stirring in an oil bath. The dissolution behavior were observed and recorded under an Olympus BX50 polarizing optical microscope (PLM).

5.2.3 Molecular simulation by Materials Studio

Simulation by Materials Studio[®] 5.5 was conducted to study the interaction between PBI and ionic liquids. Ions of ionic liquids were built, geometrically optimized and then assigned with required charges as described elsewhere [100, 128]. PBI polymer chains were constructed from the repeat unit using Build function. After energy minimization using the Discover module, two polymer chains composed of 35 repeat units each were used to construct an amorphous cell of pure PBI. Similarly, amorphous cells of PBI/ionic liquid systems were constructed by mixing one polymer chain with each kind of ionic liquid, respectively, and maintained a molar ratio of repeat units to ionic liquid to be 1 to 3.6. In order to achieve a good equilibrium of the whole system, isothermal-isobaric (NPT) and isothermal-isopyknic (NVT) dynamic running were applied at the temperature of 298K using the Forcite module in Materials Studio for every amorphous cell. The optimized systems with stable densities were then used for the system total energy analysis and hydrogen bonding calculation. A Perl script was written to calculate the numbers of hydrogen bonding between PBI and different ionic liquid systems during the last 200 ps of the NVT dynamics[129]. Particularly, the criterion for hydrogen bonding

was defined as that the angle formed by the donor, hydrogen and acceptor atoms was larger than 90° and the distance between hydrogen and acceptor atoms was within the cutoff distance of 2.0 \AA according to the radial distribution function calculated in a pure PBI system[130].

5.2.4 Rheological measurements of PBI/ionic liquid solutions

The rheological studies of PBI/ionic liquid solutions were conducted by a rotational cone and plate rheometer (AR-G2 rheometer, TA instruments, USA) at 23°C . Both the shear viscosity under a steady state flow mode and the complex viscosity under a dynamic flow mode were measured using a 20mm, 1° cone geometry.

5.2.5 Fabrication of flat asymmetric membranes

The non-solvent induced phase inversion method was employed to fabricate flat asymmetric membranes. A casting knife with a thickness of $100\mu\text{m}$ and a glass casting plate were kept at 80°C in advance. After heating at 120°C , a homogeneous PBI/ionic liquid solution was cooled down to 80°C , and casted using the casting knife on a non-woven fabric which was tightly fixed on the horizontal glass plate. After casting, the nascent membrane together with the glass plate was immediately immersed into a coagulating bath filled with water at room temperature. The as-cast PBI asymmetric membrane, designated as PBI-AC, was then immersed in water for at least 3 days to remove the residual solvents.

5.2.6 Thermal treatment and chemical cross-linking of PBI membranes

For thermal treatment, some PBI-AC membranes were immersed in fresh ethylene glycol for 3 times to replace water, and then annealed in ethylene glycol at 140°C for 20mins. The resultant membranes, named as PBI-HT, were rinsed and kept in water for further usage. Chemical cross-linking modification was carried out after the thermal treatment. After solvent exchange using fresh methanol for three times, the heat treated PBI membranes were chemical cross-linked by immersing them in a 2wt% dichloro p-xylene/methanol solution at 30°C under agitation for 3 hours. The resultant membranes, designated as PBI-HT-X, were washed with fresh methanol, and kept in water for further usage. The morphology and ultrafiltration performances of resultant PBI membranes were also explored.

5.2.7 Protein separation performance

The protein separation tests were conducted using the same procedure as the neutral solute rejection tests. A BSA/Hb (0.1kg/m³: 0.1kg/m³) phosphate buffer solution with an ionic strength of 10 mM was used as the feed and tested at pH=4.8 or 6.8. The protein concentrations of the feed and permeate solutions were determined by a UV-Vis spectrometer (Biochrom Libra S32). The separation factor α is defined as following to express the separation performance of PBI membranes for BSA/Hb mixtures:

$$\alpha_{\text{BSA/Hb}} = \left(\frac{C_{\text{BSA}}}{C_{\text{Hb}}} \right)_p / \left(\frac{C_{\text{BSA}}}{C_{\text{Hb}}} \right)_f \quad (6)$$

where C_{BSA} and C_{Hb} are the concentrations (kg/m^3) of BSA and Hb, respectively, and p and f in subscription mean the concentrations of permeate and feed solutions, respectively. Similarly, the sieving coefficient is defined as

$$\text{sieving coefficient} = C_{i,p}/C_{i,f} \quad (7)$$

where i is referred as the species of BSA or Hb.

5.3 Results and discussion

5.3.1 Dissolution of PBI in ionic liquids

All mixtures of 5/95wt% PBI/ionic liquid are prepared and stirred at room temperature; however, PBI could not dissolve in any of three studied ionic liquids. When these mixtures are heated at elevated temperatures, it is found that only [EMIM]OAc is able to fully dissolve PBI as the temperature reached 120°C and a dark brown solution is yielded. On the other hand, the other two ionic liquids, [EMIM]SCN and [BMIM][MeSO₄], still could not dissolve 5wt% PBI even at 120°C. [Figure 5-2](#) shows the PLM images of a 20/80 wt% PBI/[EMIM]OAc mixture after being heated at 120°C for 1 hour and then undergoing a temperature decrease process. Addition to the fact that [EMIM]OAc could dissolve up to 20wt% PBI at 120°C and a homogeneous solution is obtained, PBI would not precipitate out from the [EMIM]OAc solution even if the solution is cooled down to 23 °C. The results indicate that among the three studied ionic liquids, only [EMIM]OAc is suitable as a solvent for PBI.

To our best knowledge, [EMIM]OAc exhibits greater efficiency in dissolving PBI compared to traditional solvents under similar conditions. For instance, when DMAc is

employed as the solvent, the dissolving process must be carried out in a high-pressure vessel at a temperature above the boiling point of DMAc (165 °C) [36, 111], which is much harsher compared to the process of dissolving PBI at 120 °C in [EMIM]OAc. In addition, one problem of PBI/DMAc solutions is that PBI phases out easily from solutions due to polymer aggregation [131]. As a result, about 1.5wt% LiCl must be added in PBI/DMAc solutions in order to stabilize the solution [111, 117].



Figure 5-2 Observation of a fully dissolved 20/80 wt% PBI/[EMIM]OAc solution cooling from 120 to 23 °C under PLM

In this study, we hypothesize a mechanism for the dissolution of PBI in [EMIM]OAc as schematically presented in Figure 5-3. It is believed that the acetate anions of [EMIM]OAc may effectively break up the interchain hydrogen bonding in PBI molecules and lead to the rapid dissolution of PBI in [EMIM]OAc. It has been confirmed by Fourier transform infrared spectroscopy (FTIR) and Nuclear magnetic resonance (NMR) that one of reasons for the low solubility of PBI is the intense molecular stacking due to hydrogen bonding and the π - π interaction [121, 131, 132]. The polymer chains have strong interactions within themselves by hydrogen bonding between $-N=$ (proton acceptor) and $>N-H$ (proton donor) on neighbouring benzimidazole rings. It has been proved that the

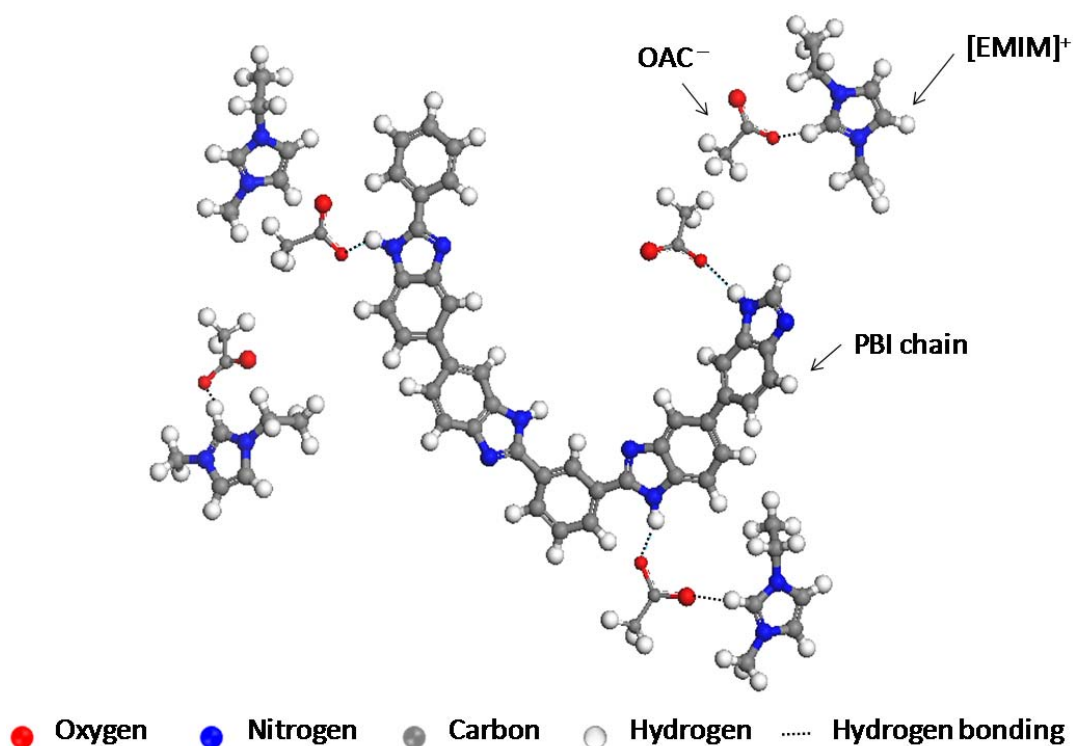


Figure 5-3 Schematic of the possible mechanism for the dissolution of PBI in [EMIM]OAc

addition of lithium chloride (LiCl) to the PBI/DMAc solution could increase the solubility of PBI and enhance the solution stability because chloride anions may have great activities to break up the hydrogen bonding in PBI [133, 134]. Therefore, it can be concluded that disrupting this interchain hydrogen bonding is essential to dissolve PBI. In the case of pure [EMIM]OAc, it has been pointed out by Bowron et al. [135] that carboxyl groups $>C=O$ of acetate anions contact intensively with imidazolium cations through $C-H\cdots O$ hydrogen-bonding. Therefore, when PBI and [EMIM]OAc are mixed together, the $>C=O$ groups of acetate anions would act as a proton acceptor and have a strong tendency to form hydrogen bonding with $>N-H$ groups of PBI as illustrated in [Figure 5-3](#). In other words, the formation of $N-H\cdots O$ hydrogen bonding between

benzimidazole rings and acetate anions could effectively disrupt the original hydrogen bonding in PBI and loosen the molecule stacking, and thus enhance the solubility of PBI in [EMIM]OAc.

5.3.2 Molecular dynamic simulation of PBI/ionic liquid systems

To verify the existence of hydrogen bonding between [EMIM]OAc and PBI, Materials Studio[®] is employed to simulate the hydrogen bonding as well as the interaction energy of PBI/ionic liquids systems as summarized in [Table 5-1](#). Considering the spatial distance among the components is of great importance in determination of their interactions, a reasonable system density is a prerequisite for the dynamic simulation. After the dynamic equilibrium of the three different systems, the simulated density of each system is quite acceptable compared to that of the corresponding ionic liquid as shown in [Table 5-1](#). This indicates that the simulated amorphous cells are indeed suitable to the real case and could be used in further simulation. In order to make the calculation of hydrogen bonding clear, this work only considers the hydrogen bonding between benzimidazole N-H groups of PBI and anions of ionic liquids, which is most probably to happen as discussed previously. [Table 5-1](#) lists the defined proton acceptors and the calculated numbers of hydrogen bonding in three PBI/ionic liquid systems if the same number of proton donors N-H is provided. Obviously, the PBI/[EMIM]OAc system has the highest probability of hydrogen bonding among these three ionic liquid systems. Hence [EMIM]OAc is inherently equipped with the strongest proton acceptor characteristics that can powerfully disrupt the original hydrogen bonding in PBI and effectively dissolve PBI even at high

concentrations. In contrast, [EMIM]SCN and [BMIM]MeSO₄ exhibit less possibility to form hydrogen bonding with PBI, leading to the poor solubility of PBI in them.

Table 5-1 Molecular simulation results of PBI/ionic liquid systems

| | PBI/ [EMIM]SCN | PBI/ [BMIM]MeSO ₄ | PBI/ [EMIM]OAc |
|--|-------------------|---------------------------------|-------------------|
| System density (g/cm ³) | 1.184 | 1.248 | 1.158 |
| Ionic liquid density (g/cm ³) | 1.114 | 1.213 | 1.103 |
| Defined proton acceptors of anions | S, N | O | O |
| Numbers of hydrogen bonding | 9.52 | 13.74 | 24.85 |
| PBI (Kcal/mol) | 31491.79 | | |
| Cation E_{cat} (Kcal/mol) | 3.93 | 80.97 | 3.93 |
| Anion E_{ani} (Kcal/mol) | 1.30 | 13.48 | -46.11 |
| System total energy E_{sys} (Kcal/mol) | -2208.95 | -3001.53 | -7219.97 |
| Interaction energy ΔE_{int} (Kcal/mol) | -33705.97 | -34597.77 | -38669.58 |

Meanwhile, the interaction energy ΔE_{int} , which reflects the energy change of the whole system resulting from the interaction between the components, also validates the strength of molecular interaction in the three PBI/ionic liquid systems. Interaction energy is defined as the difference between the system total energy and the energy of each isolated components. As shown in Table 5-1, it is notable that ΔE_{int} of the PBI/[EMIM]OAc system is the lowest among the three systems because of the intensive hydrogen bonding interaction. These results suggest that compared to [EMIM]SCN and [BMIM]MeSO₄, [EMIM]OAc tends to associate with PBI more closely through hydrogen bonding.

leading to a lower system energy and a more stable state. Based on these results, there is no surprise that [EMIM]OAc is the best solvent for PBI. The resilient hydrogen bonding between [EMIM]OAc and PBI as well as the residue hydrogen bonding in [EMIM]OAc may build up certain ordered structure, which will be further proved in the following sections.

5.3.3 The rheological behavior of PBI/[EMIM]OAc solutions

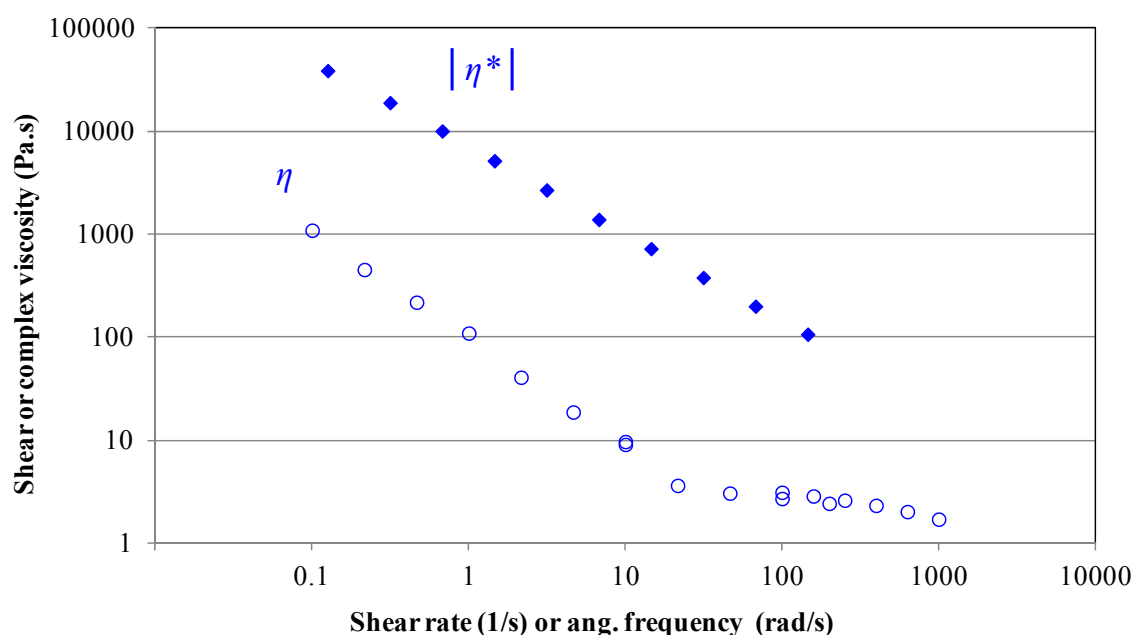


Figure 5-4 Comparison of shear viscosity η (\circ) and complex viscosity $|\eta^*|$ (\blacksquare) of 8/92 wt% PBI/[EMIM]OAc solution as a function of shear rate or angular frequency at 23°C

Rheological studies are carried out in order to get an insight into the microstructure and physicochemical interaction of PBI/[EMIM]OAc solutions under shear stresses. [Figure 5-4](#) compares the shear viscosity η and complex viscosity $|\eta^*|$ of 8/92 wt% PBI/[EMIM]OAc solution as a function of shear rate or angular frequency at room

temperature. It is obvious that η and $|\eta^*|$ are not equivalent to each other and diverge when the shear rate and angular frequency are further increased. This phenomenon is found to disagree with the Cox-merz rule [136], in which the shear viscosity η at a given shear rate should be identical to the complex viscosity $|\eta^*|$ at the corresponding angular frequency. This empirical rule has been proved to apply well for flexible polymer systems [137, 138], but normally fail for structured fluids such as rod-like liquid crystalline polymers [139, 140]. Accordingly, the inconsistency between η and $|\eta^*|$ of the PBI/[EMIM]OAc solution suggests the existence of ordered structure in the solution.

This ordered structure in PBI/[EMIM]OAc should be originated from intense hydrogen bonding between PBI and [EMIM]OAc as well as the interactions among [EMIM]OAc itself as discussed in the previous session. As proved both by experimental and simulation works [13, 17-19, 135], in imidazolium-based ionic liquids, the coulombic interactions and hydrogen bonding between ions facilitate the self organization of ions, and a sort of charge-ordered ionic structure are formed in ionic liquids. In this study, although PBI molecules are dispersed in the whole system, [EMIM]OAc still composes the main portion of the solution, thus highly charge-ordered ionic structures maintain to a large extent. Besides, the pronounced hydrogen bonding between PBI and [EMIM]OAc may also account for such ordered structure. It is the existence of this ordered structure that makes the rheological behaviors of PBI/[EMIM]OAc solutions vary from that of conventional flexible polymer solutions and show discrepancy between η and $|\eta^*|$ at the same shear rates.

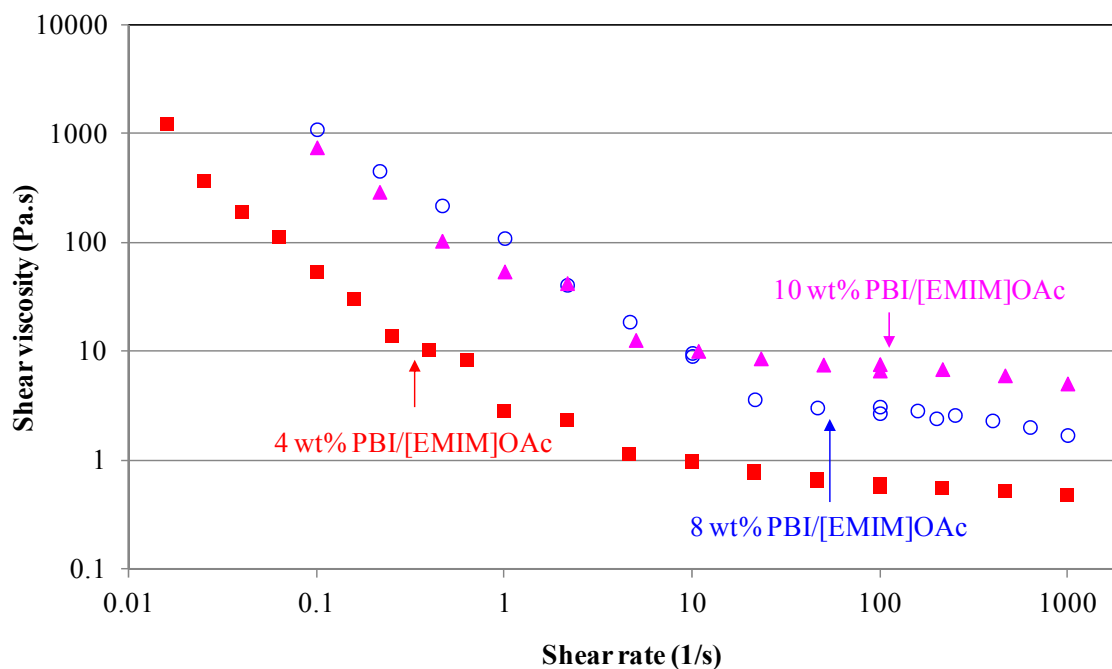


Figure 5-5 Shear viscosity of PBI/[EMIM]OAc solutions with different PBI concentrations at 23°C

Figure 5-5 presents the shear viscosities of PBI/[EMIM]OAc solutions with different PBI concentrations as a function of shear rate. It is found that all the solutions with PBI concentration varying from 4wt% to 10wt% display a shear thinning behavior at low shear rates ($<10 \text{ s}^{-1}$), followed by a Newtonian plateau within the measurable range. Such observation has never been reported when poly-2,2'-(*m*-phenylene)-5,5'-bibenzimidazole was dissolved in other solvents. It is also worth noting that no anisotropic structure could be optically observed under a PLM as shown in Figure 5-2. Similar phenomena have also been found in a CA/[EMIM]SCN system as discussed in Chapter 4. The initial shear thinning behavior should be attributed to the existence of ordered structure in PBI/[EMIM]OAc solutions. Such structure is distorted or even deformed under shear

stresses, leading to a shear thinning behavior at low shear rates. With the increase of shear rate, the effect of ordered structure is gradually mitigated while normal friction of polymeric and solvent chains begins to play a leading role in determining rheology. As a consequence, the solution exhibits a Newtonian plateau. In summary, the ordered structure resulted from strong hydrogen bonding and coulombic interactions in the PBI/[EMIM]OAc system not only facilitate the dissolution of PBI, but also account for the shear thinning rheological behavior at low shear rates.

5.3.4 Morphology of PBI asymmetric membranes

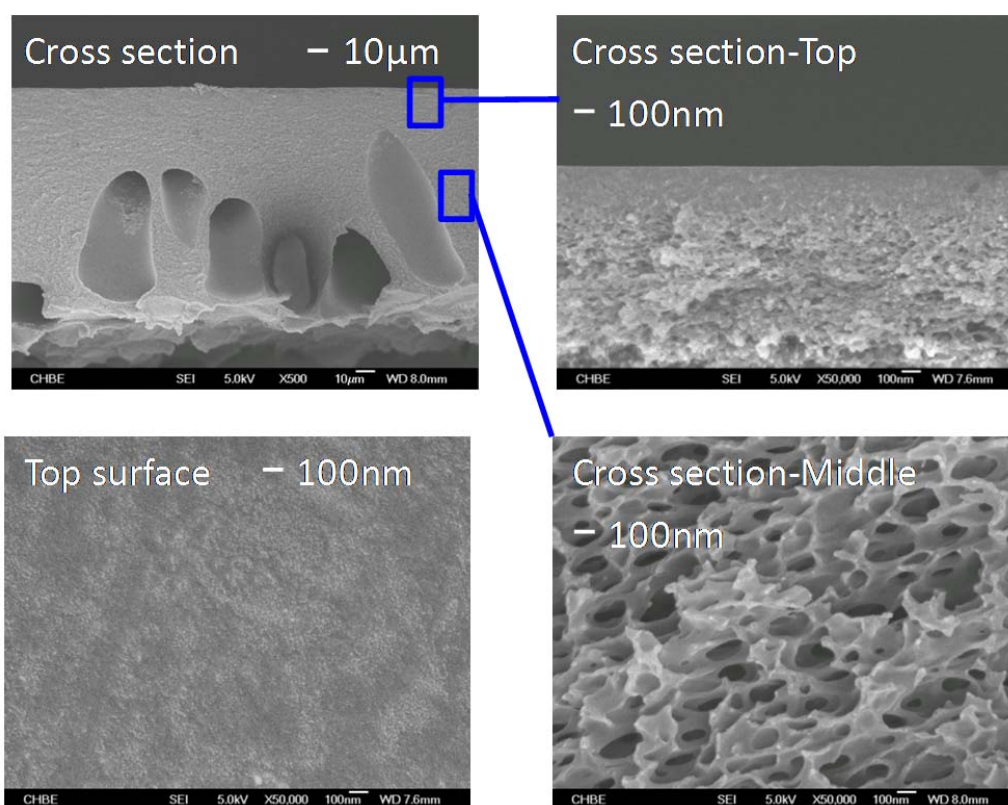


Figure 5-6 Morphology of PBI-AC(as-cast) asymmetric membrane

Asymmetric PBI membranes are cast using a 20/80wt% PBI/[EMIM]OAc solution at 80°C and coagulated in water at room temperature. In order to facilitate a green fabrication process, the residue [EMIM]OAc in the coagulant bath can be recovered by evaporation or other means to remove water [141, 142]. Figure 5-6 depicts the typical morphology of as-cast PBI (PBI-AC) membranes, which consists of a relatively dense selective layer and a sponge-like structure with some macrovoids near the bottom of the membranes. It is interesting to find that compared to PBI membranes cast from DMAc solutions by Wang et al.[118], the current PBI membranes have less macrovoids as well as a thicker layer of sponge-like structure above the macrovoids.

Table 5-2 Properties of [EMIM]OAc, DMAc and water

| Chemicals | Viscosity at 25°C (cP) | $D_{S-W} \times 10^6$ (cm ² /s) ^a | $D_{W-S} \times 10^6$ (cm ² /s) ^b | D_{S-W} / D_{W-S} |
|-----------|------------------------|---|---|---------------------|
| [EMIM]OAc | 93.00 | 7.56 | 0.52 | 14.54 |
| DMAc | 1.96 | 10.27 | 17.36 | 0.59 |
| Water | 0.89 | | | |

^a The diffusion coefficient of solvent in almost pure water;

^b The diffusion coefficient of water in almost pure solvent.

The difference may be attributed to the following facts: (1) the viscosity of the PBI/DMAc dope used in Wang et al.'s work [118] (around 200Pa•s [120]) is much lower than that of the 20/80wt% PBI/[EMIM]OAc solution (around 426Pa•s at shear rate 10 s⁻¹) at room temperature and (2) the diffusion coefficients between [EMIM]OAc and water are smaller than those between DMAc and water as calculated from the Wilke-Chang equation [80] and listed in Table 5-2. As a result, the phase inversion of the PBI/DMAc

dope is much faster than the 20/80wt% PBI/[EMIM]OAc solution. The former tends to form macrovoids, while the latter may facilitate a sponge-like structure. In addition, the large viscosity of the PBI/[EMIM]OAc solution and a high ratio of [EMIM]OAc outflow to water inflow prevent the vigorous water intrusion into the nascent membrane, thus result in less macrovoids in the PBI/[EMIM]OAc system. The thick sponge-like structure with a small quantity of macrovoids would also provide better mechanical strength under pressures.

5.3.5 Protein separation performance

Table 5-3 summarizes the PWP, mean effective pore diameter (μ_p), geometric standard deviation (σ_p) and molecular weight cutoff (MWCO) of PBI membranes after different treatments, while Figure 5-7 exhibits their pore size distributions. The PBI-AC membrane has a high pure water permeability (PWP) of 141.3 (L/(m² bar h)) with a mean pore diameter of 10.75 nm and a MWCO of 109kDa, which is practical in ultrafiltration processes for water reuse from different sources, even under harsh conditions. However, the pore diameter is too big to separate the BSA/Hb mixture. The mean pore diameter of the PBI-HT (i.e. annealed PBI-AC) membrane decreases slightly, whereas the pore size distribution of the PBI-HT-X (i.e. cross-linked PBI-HT) membrane becomes narrower with a mean pore diameter of 4.23nm. The results confirm that dichloro p-xylene [118] is an effective cross-linker that can effectively narrow down the pore diameter but with some sacrifices in the PWP value.

Table 5-3 Comparison of PWP, mean pore diameter and geometric standard deviation for PBI membranes calculated from neutral solute rejection

| Membrane | Thermal treat (°C) | Crosslink | ΔP (bar) | PWP (L/(m ² bar h)) | μ_p (nm) | σ_p | MWCO (kDa) |
|----------|--------------------|-----------|------------------|--------------------------------|--------------|------------|------------|
| PBI-AC | × | × | 2 | 141.3 | 10.75 | 1.56 | 109 |
| PBI-HT | 140 | × | 2 | 66.2 | 10.50 | 1.38 | 64 |
| PBI-HT-X | 140 | 3hr | 2 | 16.4 | 4.23 | 1.47 | 14 |

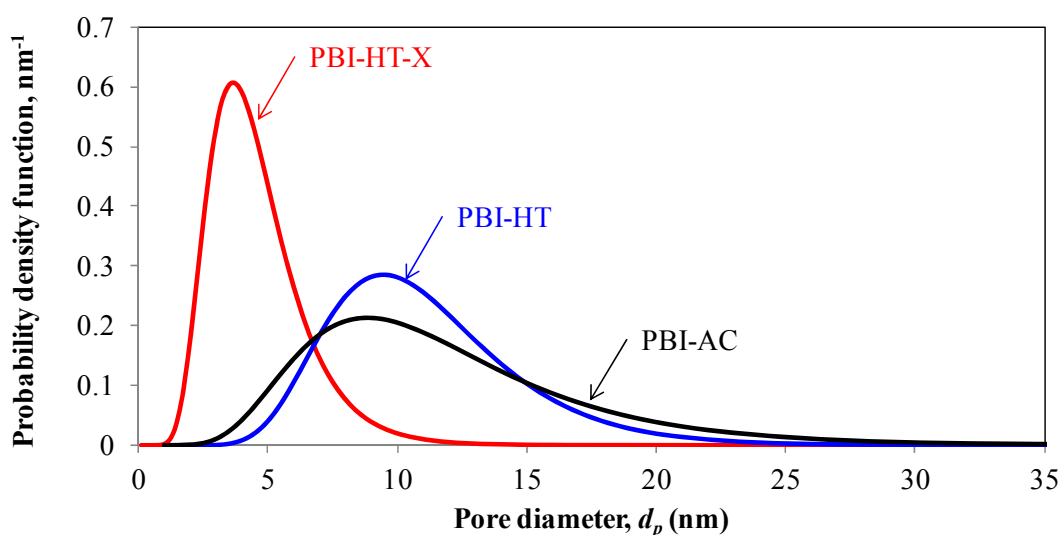
**Figure 5-7** Pore size distribution curves of newly developed PBI membranes

Table 5-4 shows the performance of both PBI-HT and PBI-HT-X membranes to separate BSA/Hb binary mixtures at different pH. It is obvious that PBI-HT-X membranes exhibit a much higher separation factor than PBI-HT at both pH values. From the basic properties of the two proteins shown in Table 5-5, it is known that the molecular weights of BSA and Hb are quite similar; therefore it is necessary to utilize other means and

physical characteristics in order to separate them from each other. The equivalent ellipsoidal dimensions (nm) of BSA and Hb molecules are $4 \times 4 \times 14$ nm and $5.5 \times 5.5 \times 7$ nm, respectively [143]. Hence, the ideal pore size to separate them should be between 4 nm and 5.5 nm, which may allow BSA to pass through the membrane freely while completely reject Hb. When the pore has a size larger than 5.5 nm, it may provide passages for both BSA and Hb, resulting in a low separation factor. As the PBI-HT-X membranes have a mean effective pore diameter of 4.23 nm and a narrow pore size distribution, they exhibit an enhanced selectivity compared to PBI-HT membranes. In this aspect, size exclusion plays a key role in the separation of BSA/Hb mixtures.

Table 5-4 BSA/Hb separation performance of PBI membranes at different pH values

| | PH=4.8 | | | PH=6.8 | | |
|----------|-------------------|--|---|-------------------|--|---|
| | $\alpha_{BSA/Hb}$ | BSA sieving coefficient (%) $C_{BSA,p}/C_{BSA,f}$ | Hb sieving coefficient (%) $C_{Hb,p}/C_{Hb,f}$ | $\alpha_{BSA/Hb}$ | BSA sieving coefficient (%) $C_{BSA,p}/C_{BSA,f}$ | Hb sieving coefficient (%) $C_{Hb,p}/C_{Hb,f}$ |
| PBI-HT | 6.54 | 56.59 | 8.65 | 2.06 | 55.61 | 27.04 |
| PBI-HT-X | 94.55 | 77.50 | 0.82 | 14.09 | 69.25 | 4.92 |

Table 5-5 Basic properties of BSA and Hb

| | Bovine serum albumin (BSA) | Hemoglobin (Hb) |
|--|-----------------------------------|---------------------------|
| Molecular weight (kDa) | 66-68 | 64-67 |
| Equivalent ellipsoidal dimensions (nm) | $4 \times 4 \times 14$ | $5.5 \times 5.5 \times 7$ |
| Isoelectric point (pH) | 4.8 | 6.8 |

However, solute size is just one of the many factors that could be utilized for separation. Protein-protein interactions, protein-membrane interactions, the extent of concentration polarization and the predominant mode of protein transport are amongst several factors, which can be exploited for enhancement of protein fractionation [50]. In this case, the electrostatic interactions between PBI membranes and proteins also affect the separation performance [144], which is evidenced by the separation tests at pH=4.8 and pH=6.8. As shown in Table 5-4, the separation factors at pH=4.8 are higher than those at pH=6.8 for both of the PBI membranes. In order to explain this phenomenon, a schematic presentation of protein separation environments with PBI membranes at two pH values is illustrated in Figure 5-8. It is known that PBI membranes are almost neutral at pH=6.8, while get positive charges at pH=4.8 [118]. Considering the isoelectric points of the proteins, BSA is neutral and Hb carries positive charges at pH=4.8. At this time, the positive charged PBI membranes should allow the transport of BSA, yet confine the transport of Hb due to electronic repulsion as shown in Figure 5-8 (a). At pH=6.8, BSA becomes negative charged while Hb is neutral, the neutral PBI membranes would not provide much transport resistance resulted from no electronic interaction to both proteins, depicted in Figure 5-8 (b). As a result, for both the PBI-HT and PBI-HT-X membranes, BSA sieving coefficients were not altered obviously at different pH values, however, Hb sieving coefficients at pH=4.8 were much smaller than that at pH=6.8, indicating a strong rejection of Hb at pH=4.8 due to the electronic repulsion. This is the fact that contributes to a higher separation factor of BSA/Hb at pH=4.8. It is worth noting that PBI-HT-X membranes achieve a high separation factor of 94.55 at pH=4.8 due to both the size

exclusion and charge repulsion, indicating that the employed cross-linking method can significantly improve the BSA/Hb separation performance by enhancing the size exclusion effect of the charged PBI membranes.

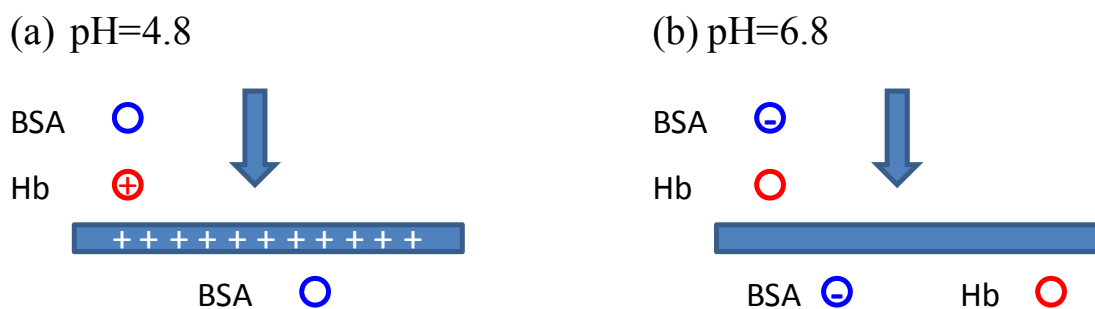


Figure 5-8 Schematic of protein separation environments with PBI membranes at (a) pH=4.8, (b) pH=6.8

5.4 Conclusions

In this work, we have provided an important insight into possible mechanisms of dissolving PBI in ionic liquids and discovered [EMIM]OAc as a strategic green solvent for the fabrication of PBI membranes in light of current environmental unfriendly organic solvents. The following conclusions can be made:

- (1) Compared to DMAc, [EMIM]OAc is superior in dissolving PBI under much lower temperature and pressure because it is inherently equipped with strong proton acceptor characteristics that can powerfully disrupt the original hydrogen bonding in PBI and effectively dissolve PBI even at high concentrations (up to 20 wt%).

(2) According to the molecular dynamic simulation, the PBI/[EMIM]OAc system intrinsically possesses the largest amount of hydrogen bonding and the lowest interaction energy out of three studied PBI/ionic liquid systems has, leading to the excellent solubility of PBI in [EMIM]OAc.

(3) The PBI/[EMIM]OAc solution exhibits discrepancy from the Cox-merz rule which generally apply well for flexible polymer systems, and an initial shear thinning behavior under low shear rates. These distinctive rheological properties correspond well to the ordered structure arose from the hydrogen bonding and coulombic interactions in the PBI/[EMIM]OAc system.

(4) PBI ultrafiltration membranes are prepared from PBI/[EMIM]OAc solutions by non-solvent induced phase separation method. The high dope viscosity and a high ratio of [EMIM]OAc outflow to water inflow facilitate the formation of a relatively thick sponge-like structure with a few macrovoids. After thermal treatment in ethylene glycol at 140°C and chemical cross-linking by dichloro p-xylene, the PBI membranes achieve a high separation factor of 94.55 for BSA/Hb binary protein mixtures with the aid of combined effects of size exclusion and charge repulsion.

As far as we know, this is the first work that employs ionic liquids as an effective solvent for fabrication of PBI membranes and successfully applied the resultant membranes for protein separation. Future work will focus on utilizing ionic liquids to prepare PBI membranes feasible for pharmaceutical separation and organic solvent recovery.

Chapter 6 Fabrication of porous and interconnected PBI/P84 ultrafiltration membranes using [EMIM]OAc as the green solvent

6.1 Introduction

The utilization of large quantities of traditional organic solvents during industrialization has led to severe waste solvent pollution and other adverse impacts on environments and public health. Hence, there is an intensifying need to seek for alternative green solvents in order to replace these traditional organic solvents. Room temperature ionic liquids have gained worldwide attention as green solvents in the past decade [124]. Various attempts of using ionic liquid for organic synthesis, catalysis and electrochemistry and membrane separation have been demonstrated [7, 9, 10, 145].

Directly using ionic liquids to fabricate polymeric membranes by the non-solvent induced phase inversion method only took place recently. Similar to conventional organic solvents, experience suggests that a physicochemical match between ionic liquids and polymers is needed to form homogenous solutions even though the dissolving mechanisms may be different. It has been reported that cellulose can dissolve in hydrophilic imidazolium-based ionic liquids under relatively milder conditions [30], polybenzimidazole in 1-butyl-3-methylimidazolium chloride ([BMIM]Cl) [126] and 1-ethyl-3-methylimidazolium acetate ([EMIM]OAc) [146] at the temperature of 120°C or higher. The strong ionic interaction is the driving force to break up the hydrogen bonding and the molecular π - π stacking in cellulose and polybenzimidazole, which is too complex to achieve in traditional organic solvents such as dimethyl sulfoxide (DMSO), *N,N*-dimethylacetamide (DMAc), *N,N*-dimethylformamide (DMF) under similar conditions

[36]. The other benefit of employing imidazolium-based ionic liquids comprising hydrophilic anions is the miscibility with water at any ratio [20]. As a result, this type of ionic liquids can be easily leached out from as-cast membranes, recycled and reused. They are suitable to replace organic solvents as green solvents for membrane fabrication. To the best of our knowledge, so far only hydrophilic imidazolium-based ionic liquids have been explored to fabricate polymeric membranes such as cellulose, cellulose acetate and polybenzimidazole membranes with different configurations for ultrafiltration [31, 108, 128, 146].

Several challenges have been encountered when replacing volatile organic solvents by ionic liquids for the fabrication of polybenzimidazole membranes, they are polybenzimidazole solubility, dope viscosity, membrane morphology and separation performance. So far, about 6 types of ionic liquids [126, 146] have been examined. Ionic liquid, 1-ethyl-3-methylimidazolium acetate ([EMIM]OAc), exhibits the best efficiency in dissolving PBI under much lower temperature and pressure compared to the traditional toxic DMAc because the acetate anions of [EMIM]OAc can form hydrogen bonding with PBI chains and effectively break up the interchain hydrogen bonding in PBI molecules [146]. However, similar to membrane formation using conventional solvents [147], several drawbacks were also observed during the fabrication of ultrafiltration membranes using this ionic liquid such as (1) high viscosity of PBI solutions, (2) weak mechanical properties of the resultant membranes, and (3) relatively low water flux because of tight morphology. In order to overcome these shortcomings, our strategy is to employ a binary

blend system with the aid of additional polymer to modify the dope properties, manipulate their morphology and enhance their mechanical strength and water flux.

Since PBI and polyimide have strong interactions, and some of them form miscible or partial miscible blends [148-153], a variety of commercially available high performance polyimides and polyamide-imides such as Matrimid[®], Ultem[®], Extem[®], Torlon[®], and P84 were therefore screened. Firstly, the chosen polyimide must be soluble in [EMIM]OAc. Secondly, it must have super thermal stability and chemical resistance in order not to sacrifice the same advantages of PBI [119, 148, 154]. Thirdly, it must have good mechanical properties to supplement the strength of blend membranes. Recognizing the aforementioned concerns, the objectives of this study are to (1) choose the best candidate for PBI blends and fundamentally understand the molecular interaction among [EMIM]OAc, PBI and the blend material; (2) investigate the rheological properties and microstructure of the blend solutions; (3) study the effects of process parameters on morphological characteristics and ultrafiltration performance of the blend membranes. This work may provide basic insights of molecular interactions between ionic liquids and polymers, and lay the preliminary foundation for the fabrication of next-generation membranes in a “green” process using ionic liquids.

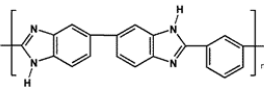
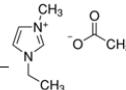
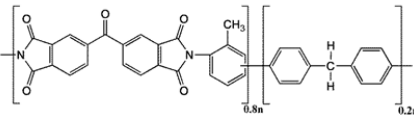
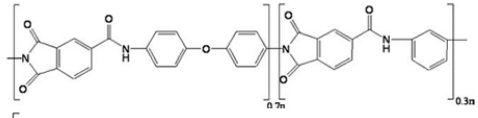
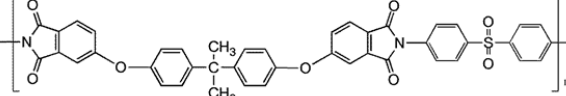
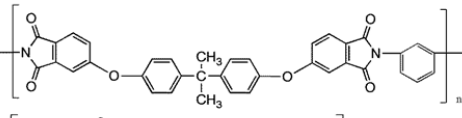
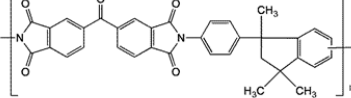
6.2 Experimental

6.2.1 Materials

The P84 co-polyimide (BTDA-TDI/MDI, co-polyimide of 3,3',4,4'-benzophenone tetracarboxylic dianhydride and 80% methylphenylenediamine + 20%

methylenediamine) was purchased from HP Polymer GmbH (Austria), Torlon[®] 4000T polyamide-imide from Solvay Advanced Polymers, Extem[®] XH 1015 and Ultem[®] 1010 polyetherimide from GE plastics, and Matrimid 5218 (3,3',4,4'-benzophenone tetracarboxylic dianhydride and diamino-phenylindane) powder from Ciba Polymers (Hawthorne, New York). The ionic liquid, 1-ethyl-3-methylimidazolium acetate ([EMIM]OAc), was provided by BASF (Germany). Table 6-1 summarizes their chemical structures. Poly(ethylene glycol) (PEG) of different molecular weights were purchased from Sigma-Aldrich. All the materials were used as received.

Table 6-1 Solubilities of PBI, polyimides and polyamide-imides in [EMIM]OAc at 120 °C

| Studied polymers | Solubility in [EMIM]OAc |
|---|---|
| PBI  |  ~ 20 wt% PBI can dissolve. |
| P84 co-polyimide  | ~ 20 wt% P84 can dissolve. |
| Torlon[®] 4000T  | ~ 10 wt% Torlon can dissolve. |
| Extem[®] XH1015  | Cannot dissolve |
| Ultem[®] 1010  | Cannot dissolve |
| Matrimid[®] 5218  | Cannot dissolve |

6.2.2 Dope characterizations - Rheological measurements, phase inversion kinetics of PBI/ionic liquid solutions

All polymers were dried in a vacuum oven at 120°C overnight to remove moisture before use. Mixtures of PBI, [EMIM]OAc and the blend polymer were prepared by adding desirable amounts of polymer powder to glass vials containing [EMIM]OAc, and then heated with stirring in an oil bath.

The rheological measurements of blend solutions and pure [EMIM]OAc were conducted by a rotational cone and plate rheometer (AR-G2 rheometer, TA instruments, USA). The shear viscosities were measured using a 20-mm or 40-mm, 1° cone geometry at required temperatures under a steady state flow mode.

The light transmittance experiments were conducted to study the phase inversion kinetics of blend solutions with different polymer compositions in water. The dope was firstly cast on a glass slide using a casting knife with a thickness of 100 μm at 80 °C. The glass slide was immediately put into a plastic cuvette holding water at room temperature, and the transmittance T at 600 nm (water has no absorbance at this wavelength) was monitored and recorded by a UV-vis scanning spectrophotometer (Libra S32, Biochrom Ltd., England) and its built-in software. A relative light transmittance T_r was calculated as indicated in section 4.2.2.

6.2.3 Fabrication of flat asymmetric membranes

The non-solvent induced phase inversion method was employed to fabricate a flat asymmetric membrane. The casting method was described in section 5.2.5 but using PBI blend solutions at desired temperatures. The developed asymmetric membranes were designated by the polymer ratio in the dope solution, i.e. 10/10 wt% PBI/P84, 15/5 wt% PBI/P84 and 20 wt% PBI. They were then immersed in water for at least 3 days to remove the residual solvents. The morphology and ultrafiltration performances of resultant membranes were also explored.

6.2.4 Fourier transformed infrared spectroscopy (FTIR)

A Bio-Rad FTIR FTS 135 was used to analyze pure [EMIM]OAc and the blend solutions over the range of 1000-4000 cm^{-1} in the attenuated total reflectance (ATR) mode. The chemical structure changes of dry asymmetric membranes were studied under a FTIR transmission mode in potassium bromide pellets. The number of scans for each sample was 32 under nitrogen flow (5 mL/min).

6.2.5 Differential Scanning Calorimetry (DSC)

The glass transition temperature (T_g) of developed membranes was measured by a PerkinElmer Pyris-1 differential scanning calorimeter. Two heat cycles from 25 °C to 450 °C of each membrane in nitrogen atmosphere were performed to remove the thermal history and the T_g was determined from the second cycle.

6.3 Results and discussion

6.3.1 Solubility of selected polyimides in [EMIM]OAc

In order to identify a suitable polymer to blend with PBI in [EMIM]OAc, the solubilities of a series of polyimides and polyimide-amides were examined. Table 6-1 summarizes their chemical structures and solubilities. For each polymer, a 10/90 wt% polymer/[EMIM]OAc mixture was prepared in a glass vial and stirred overnight at room temperature, but none of them dissolved in [EMIM]OAc. When temperature was elevated to 120 °C, both P84 and Torlon[®] 4000T dissolved in [EMIM]OAc and formed homogeneous solutions, while Extem[®] XH1015, Ultem[®] 1010, Matrimid[®] 5218 did not dissolve. Therefore, only P84 and Torlon[®] were possible candidates to blend with PBI. Flat sheet membranes were then cast from both 15/5/80 wt% PBI/P84/[EMIM]OAc and PBI/Torlon[®]/[EMIM]OAc solutions. Interestingly, membranes made of PBI/P84 blends appeared to be much sturdier than those from PBI/Torlon[®] blends. Therefore, the PBI/P84/[EMIM]OAc system was chosen for investigation in the subsequent sections.

6.3.2 Interactions in the P84/[EMIM]OAc solution

Figure 6-1 presents the FTIR spectra of the P84 co-polyimide, [EMIM]OAc and their solutions. The typical imide peaks of P84 are located at 1782 cm⁻¹ for symmetric C=O stretching, 1721 cm⁻¹ for asymmetric C=O stretching and 1362 cm⁻¹ for C-N stretching. As for the spectrum of [EMIM]OAc, the assignment for wave numbers below 1500 cm⁻¹ mainly arises from the imidazolium cations [155]. Other characteristic peaks at 1558 cm⁻¹, approximately 2980 cm⁻¹ and 3100 cm⁻¹ correspond to C=O stretching of acetate anions, -C-H stretching and =C-H stretching, respectively.

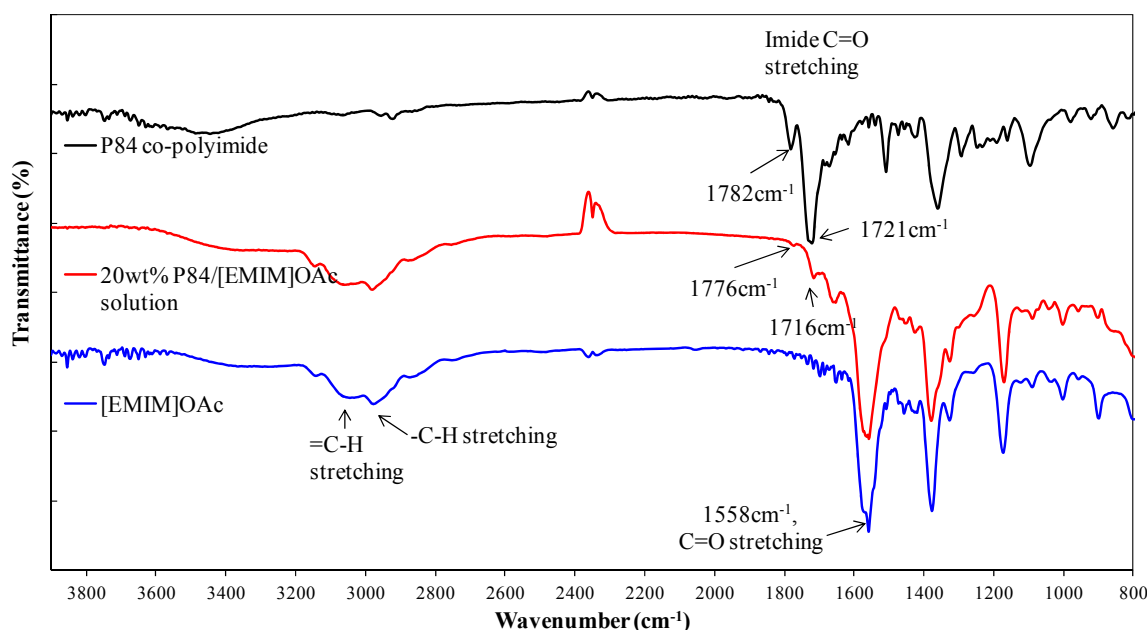


Figure 6-1 The FTIR spectra of P84 co-polyimide, [EMIM]OAc and their solution

It is noted that the C=O stretching peaks of P84 apparently shifted to lower wave numbers in the 20wt% P84/[EMIM]OAc solution, which indicates specific interactions between P84 co-polyimide and [EMIM]OAc. Both experimental and simulation research reported that hydrogen bonding between the anions (proton acceptor) and the hydrogen of the imidazolium cations (proton donor) existed in imidazolium-based ionic liquids due to the nature of electrostatic interactions among these ions [13, 18, 103, 156]. Therefore, when P84 and [EMIM]OAc are well mixed, the imidazolium hydrogen of [EMIM]OAc may provide protons, while the C=O groups of P84 accept protons. This leads to the formation of hydrogen bonding between P84 and [EMIM]OAc, facilitating the dissolution of P84 in [EMIM]OAc.

6.3.3 Miscibility of P84 and PBI in [EMIM]OAc

In order to examine the miscibility of P84 and PBI after dissolving in [EMIM]OAc, the glass transition temperature (T_g) of the PBI/P84 blend membranes was determined by DSC. Interestingly, the PBI/P84 blend membranes display one single intermediate T_g at each composition as summarized in Table 6-2. The single T_g indicates good miscibility between PBI and P84 molecules at the molecular level [148, 157]. According to the Fox equation [158], the T_g of miscible blends can be predicted as following:

$$\frac{1}{T_g} = \frac{w_1}{T_{g1}} + \frac{w_2}{T_{g2}} \quad (8)$$

where W_1 and W_2 represent the mass fractions, T_{g1} and T_{g2} refer to the glass transition temperatures (Kelvin) of polymers 1 and 2, respectively.

Table 6-2 T_g values of the PBI/P84 blend systems from the Fox equation and experimental results

| | T_g from the Fox equation (°C) | T_g from DSC (°C) | Deviation (%) ^a |
|------------------|----------------------------------|---------------------|----------------------------|
| P84 | 315 | | |
| 10/10wt% P84/PBI | 361.9 | 331.4 | 8.43 |
| 15/5wt% P84/PBI | 388.3 | 397.6 | 2.39 |
| PBI | 417.1 | | |

^a Deviation based on T_g calculated from the Fox equation.

Table 6-2 also compares the T_g calculated by the Fox equation with the one measured by DSC as a function of blend composition. The experimental values are relatively consistent with the calculated results by the Fox equation. The T_g deviation between the experimental and the calculated values is smaller for the 15/5 PBI/P84 membrane than the 10/10 PBI/P84 membrane, which may indicate a better miscibility at the molecular scale among PBI and P84 polymer chains when the blended ratio is 15/5.

It has been explored in previous studies that the miscibility of binary polymer blends always arises from the existence of specific intermolecular interactions between the blend polymers [150]. For the blends of PBI and polyimides, it has been known that the carbonyl groups $>C=O$ of polyimides have a strong tendency to form hydrogen bonding with the $>N-H$ groups of PBI, which greatly facilitate the formation of the miscible blends [111, 151, 159]. To verify the existence of specific interactions between PBI and P84, FTIR of PBI/P84 blend membranes with two different polymer compositions was conducted and their spectra are illustrated in Figure 6-2. The maximum wave number of $C=O$ stretching of the pure P84 apparently shifted from 1721 cm^{-1} to 1716 cm^{-1} for the PBI/P84 blend membranes as depicted in Figure 6-2(a). Meanwhile, the hydrogen bonded $N-H$ stretching band of pure PBI also shifted from about 3180 cm^{-1} to lower wave numbers for the PBI/P84 blend membranes as shown in Figure 6-2(b). The band shift indicates that interactions between PBI and P84 have occurred. In other words, the efficient formation of $N-H\cdots O=C$ hydrogen bonding between the benzimidazole and the phthalimide demonstrates the good miscibility of PBI/P84 blends.

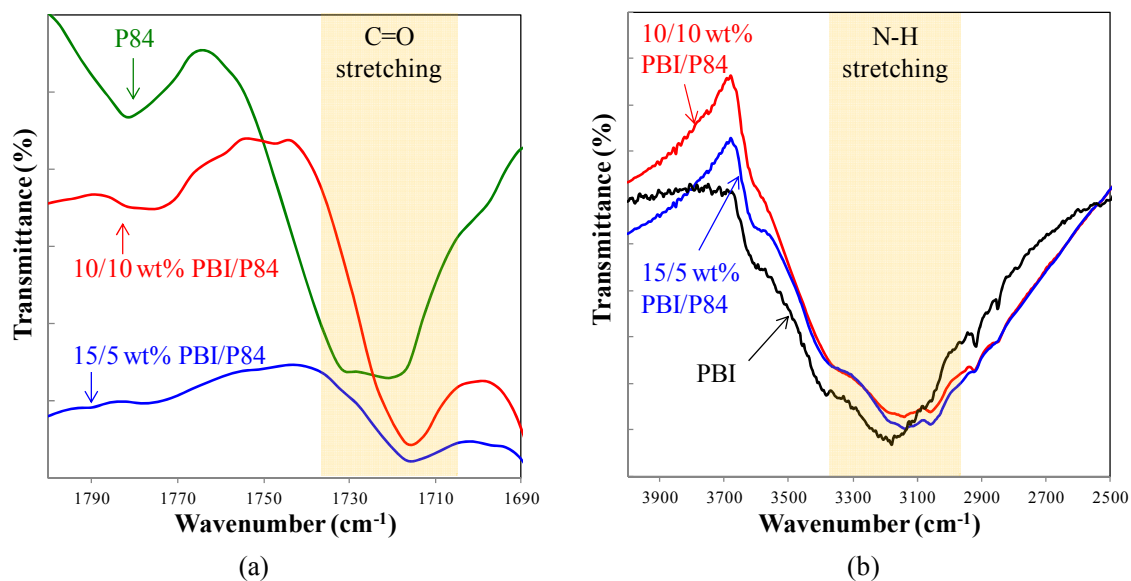


Figure 6-2 The enlarged FTIR spectra of PBI/P84 blend membranes at wave numbers of (a) 1690 – 1800 cm^{-1} and (b) 2500 – 4000 cm^{-1}

Therefore, an interconnected network may exist from inter- and intra-molecular hydrogen bonding and coulombic forces in the PBI/P84/[EMIM]OAc system. Figure 6-3 schematically elucidates the possible intermolecular hydrogen bonding in this system from different factors. Firstly, it has been found that ionic liquids possess very long-range ordering resulting from the long-range nature of the coulombic interactions among the ions. This charge-induced ordering facilitates the development of self-organized network in ionic liquids [11, 13]. Since [EMIM]OAc is the major and continuous phase while PBI and P84 are minor phases surrounded by cations and anions, the charge-ordered network of [EMIM]OAc would still play an overwhelming role in determining the microstructure of the PBI/P84/[EMIM]OAc system [128]. Secondly, as aforementioned, [EMIM]OAc is self-equipped with both proton donors (hydrogen of imidazolium rings) and acceptors (carbonyl groups of acetate anions). As a proton donor, the $>\text{C}=\text{O}$ groups of [EMIM]OAc

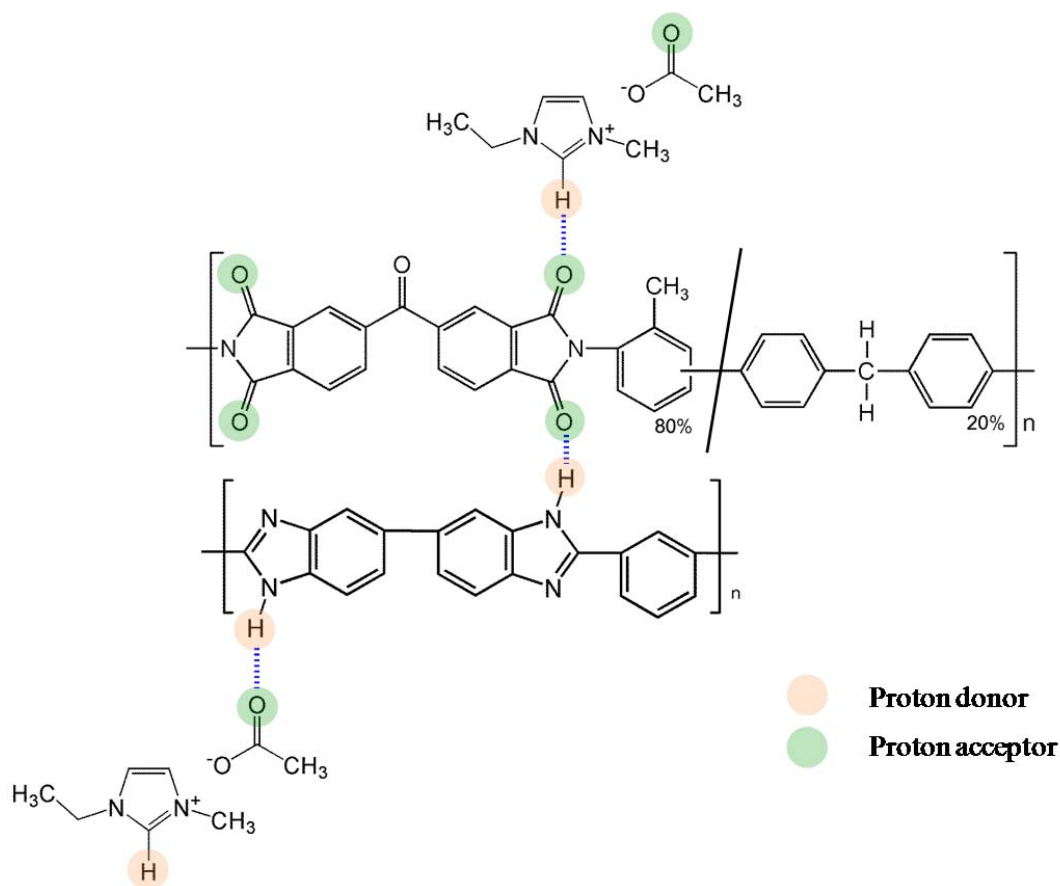


Figure 6-3 Possible intermolecular hydrogen bonding among PBI, P84 and [EMIM]OAc

may effectively form hydrogen bonding with the $>N-H$ groups of PBI, which could break up the interchain hydrogen bonding in the PBI molecules and lead to the rapid dissolution of PBI in [EMIM]OAc [146]. On the other hand, as a proton acceptor, the imidazolium hydrogen of [EMIM]OAc and the carbonyl groups of P84 can form hydrogen bonding as well. Therefore, [EMIM]OAc can interact with both PBI and P84 at the molecular level on different sites. Additionally, PBI is a polymer that possesses both proton donors ($>N-H$) and acceptors ($=N-$) [111, 121, 131, 132] by which PBI chains are expected to form intra-molecular hydrogen bonding as well as inter-molecular hydrogen bonding with P84 and [EMIM]OAc. As a result, it is believed that the ternary system of

PBI/P84/[EMIM]OAc may form a hydrogen-bonded interconnect network based on the highly charge-ordered structure of [EMIM]OAc. This unique interconnect network may influence the rheological behavior of PBI/P84/[EMIM]OAc solutions and affect the microstructure of the resultant membranes.

6.3.4 The rheological behavior of PBI/P84/[EMIM]OAc solutions

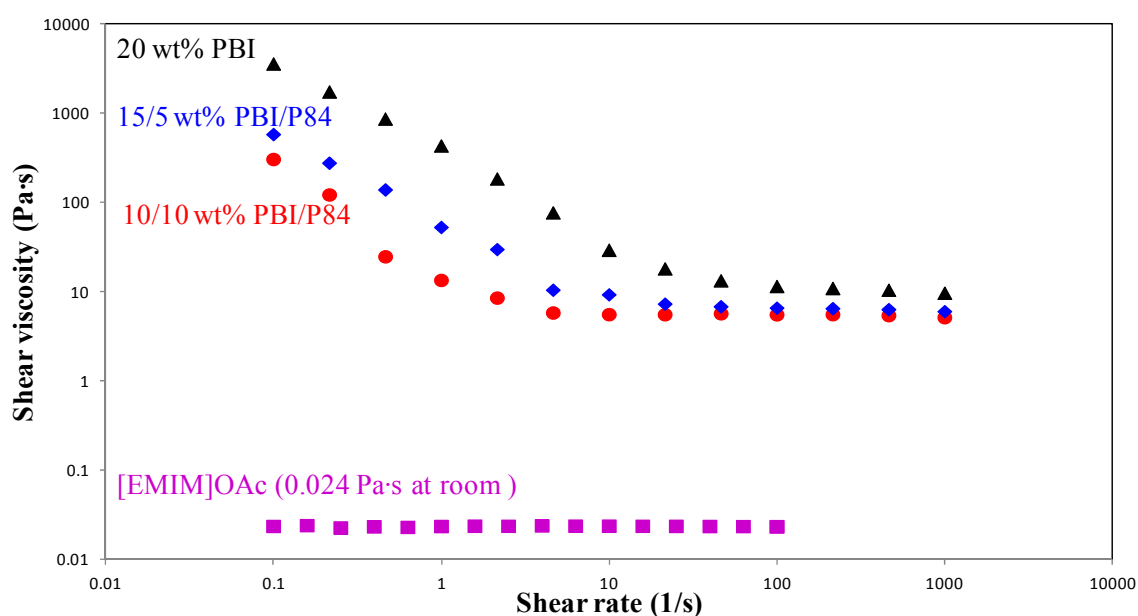


Figure 6-4 Shear viscosity of PBI/P84/[EMIM]OAc solution with different polymer ratios at 80°C

Figure 6-4 shows the shear viscosities of PBI/P84/[EMIM]OAc solutions as a function of polymer composition and shear rate at 80 °C. Since viscosity reflects the resistance of a fluid against the deformation, the PBI/[EMIM]OAc solution has the highest viscosity because of the stiffness of PBI chains [121] and because both PBI and [EMIM]OAc

possess unique characteristics of proton donors and acceptors. As a result, the incorporation of P84 into the PBI/[EMIM]OAc solution decreases the overall molecular stiffness and charge-induced interactions, and lowers the shear viscosity. On the other hand, the lower viscosity would make the membrane fabrication process more viable due to lower energy consumption for spinning or casting.

All tested solutions displayed a shear thinning behavior at low shear rates ($< 20 \text{ s}^{-1}$) which gradually evolved into a Newtonian plateau at higher shear rates within the measurable range which is apparently different from the rheology of conventional polymeric solutions. Such rheological behavior has never been reported for PBI, P84 and their blended solutions in traditional organic solvents. So far, this unique phenomenon has been reported for polymer/ionic solutions such as cellulose [160], cellulose acetate [128] and PBI [146] dissolved in ionic liquids. The hydrogen-bonded interconnected network of the ternary solution and the charge-ordered structure of [EMIM]OAc may be accountable for the rheological behavior at the low and high shear rate regions. Under low shear rates, the highly interconnected and entangled microstructures of PBI/P84/[EMIM]OAc solutions would begin to distort and deform, leading to a decreased flow resistance and a lower viscosity, thereby presenting a shear thinning behavior [78, 106]. When the shear rate is further raised, contributions from disentangled PBI and P84 chains to the shear viscosity become weak and minimal, while the interconnected affinity among PBI, P84 and [EMIM]OAc stays the same. As a result, the PBI/P84/[EMIM]OAc solution shows a Newtonian behavior as pure [EMIM]OAc but with a higher viscosity.

6.3.5 Morphology and ultrafiltration performance of PBI/P84 blend membranes

6.3.5.1 Effects of polymer composition

Figure 6-5 depicts the effects of polymer composition on the morphology of PBI/P84 flat sheet membranes cast on non-woven fabrics. All membranes consist of a relatively dense top layer, a microporous sponge-like structure, and some macrovoids near the bottom above the fabrics. With an increase in P84 ratio in polymer blends, the membrane thickness reduces from 119.6 μm to 39.4 μm , while the sponge-like region shifts toward a 3-dimensional open-cell silk-like structure. These morphological changes are caused by the following factors arising from different phase inversion kinetics and precipitation paths.

Table 6-3 Physicochemical properties of [EMIM]OAc and water

| Chemicals | Diffusion coefficients (cm^2/s) | Solubility parameter δ ($\text{MPa}^{1/2}$) | Density ρ (g/cm^3) (20°C) |
|-----------|--|---|---|
| [EMIM]OAc | 7.56 ^a | 32.8 ^c | 1.042 |
| Water | 0.52 ^b | 47.8 | 0.998 |

^a The diffusion coefficient of [EMIM]OAc into almost pure water;

^b The diffusion coefficient of water into almost pure [EMIM]OAc;

^c Calculation using Material studio.

One major factor is the different diffusion coefficients. The diffusion coefficient of [EMIM]OAc into water is much larger than that of water into [EMIM]OAc as calculated by the Wilke-Chang equation [80] and listed in Table 6-3. Therefore, the [EMIM]OAc outflows faster than water inflow during phase inversion. As the dope viscosity decreased

with increasing P84 ratio, the [EMIM]OAc would leach out to the external coagulant (i.e., water) with less flow resistance resulting in the formation of a thinner and porous PBI/P84 blend membrane on top of the fabric is therefore formed. The addition of P84, the PBI/P84 blend solution easily penetrated into the non-woven fabrics due to the decreased dope viscosity, resulting in a thinner membrane.

Figure 6-6 shows the light transmittance results as a function of polymer composition. The phase inversion of the PBI/[EMIM]OAc solution happens immediately as indicated by a rapid decrease in light transmittance. With an increase in P84 content in blend solutions, there was an obvious slowing down of the phase inversion process. A longer duration is an indication of delayed demixing which not only allows the nascent membrane to adjust its thickness and contour during the outflow of [EMIM]OAc [108] but also often forms an open-cell and porous morphology. It is also known that interactions and affinity between materials will greatly affect the phase inversion path [64]. The total solubility parameters of PBI and P84 were calculated according to Hoy's table [161], Fedors' method [162] and Matsuura's work [2], as summarized in Table 6-4. A significant divergence is found among these values because they were estimated using different methods. However, P84 always displays a slightly larger solubility parameter than PBI and the solubility parameter differences between P84 and PBI in all three cases are quite small that corresponds well to their excellent miscibilities. Since the incorporation of P84 into the PBI/[EMIM]OAc system slows down the phase inversion process as illustrated in Figure 6-6, the solubility parameters calculated from the Hoy's table is most likely closest to the real situation. Compared to PBI, P84 has a closer

solubility parameter to [EMIM]OAc and water as indicated in Tables 6-3 and 6-4. Therefore, P84 can tolerate more water than PBI and the phase inversion of the PBI/P84 blend system is slower than that of the plain PBI system.

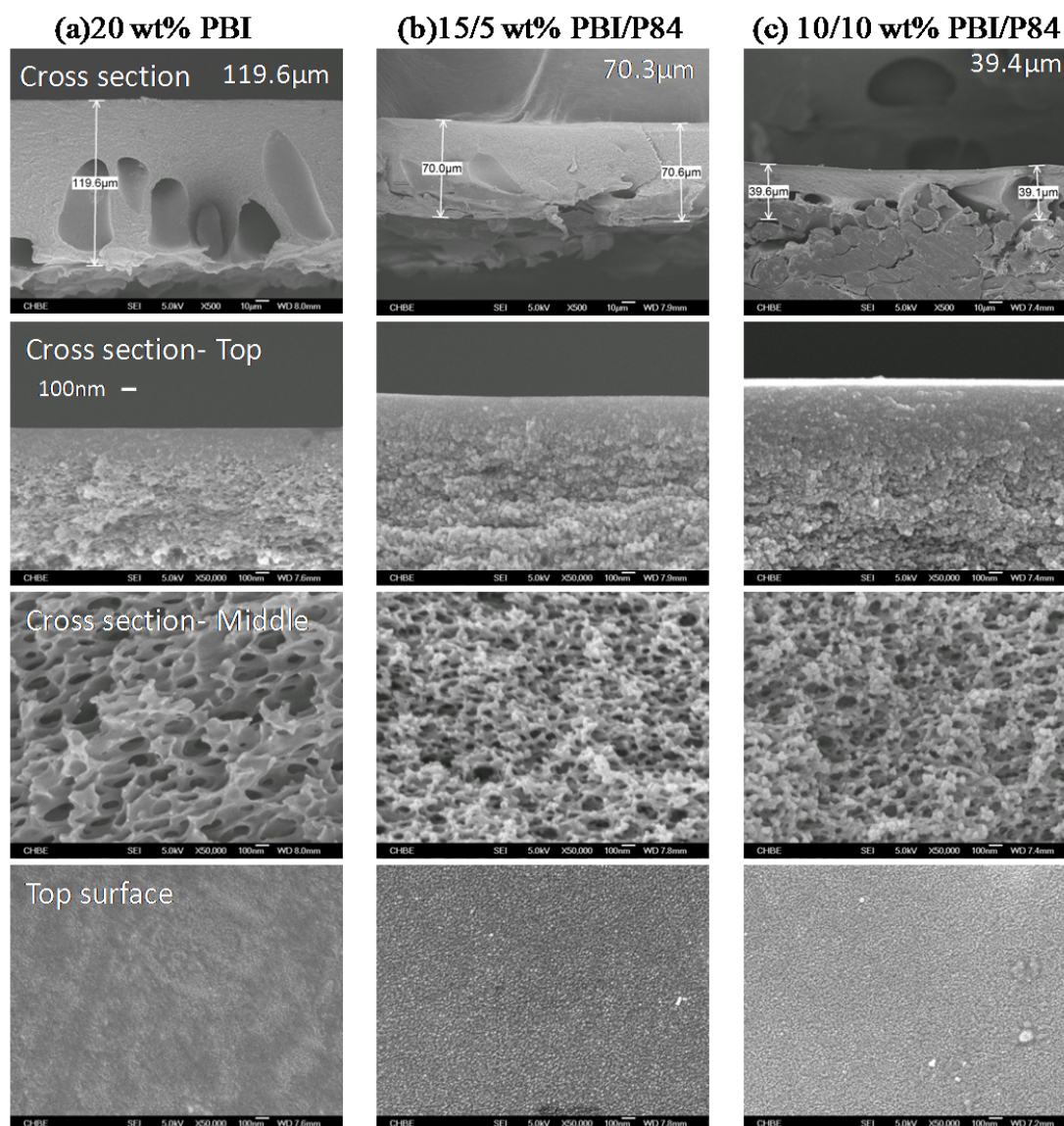


Figure 6-5 Comparison of the morphology of PBI/P84 blend membranes prepared at 80 °C

Table 6-4 Solubility parameters of PBI and P84 at 298K calculated according to Hoy's table, Fedors' and Matsuura's methods

| Methods | Solubility parameter δ of PBI (MPa ^{1/2}) | Solubility parameter δ of P84 (Mpa ^{1/2}) |
|-----------------------|--|--|
| Hoy's table [163] | 23.90 | 24.36 |
| Fedors' method [164] | 31.13 | 32.14 |
| Matsuura's method [2] | 34.70 | 34.74 |

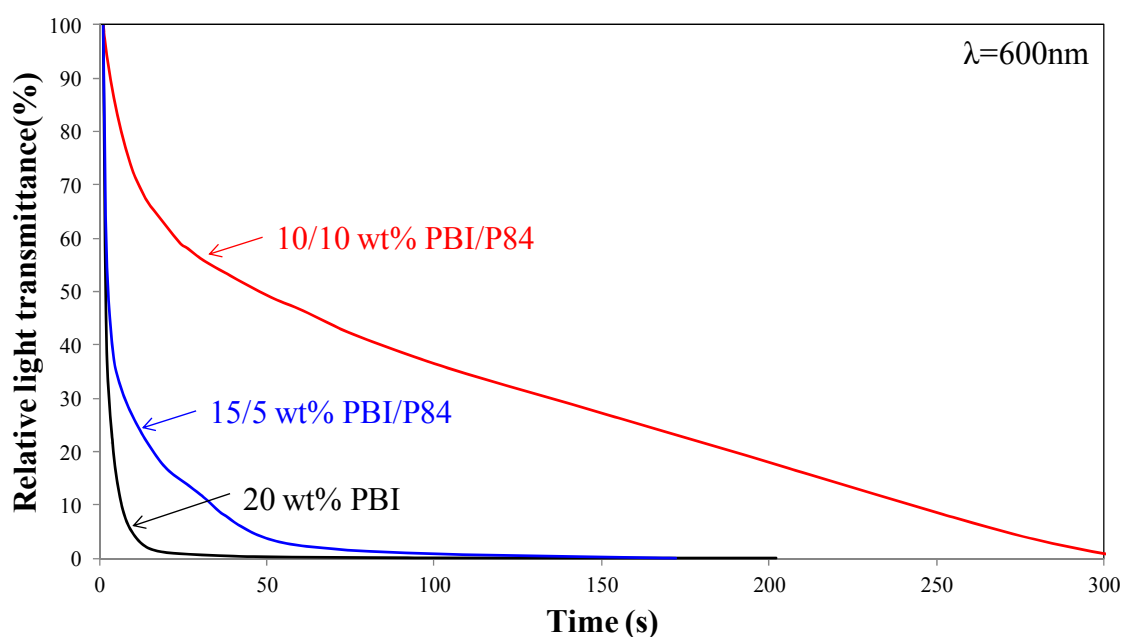


Figure 6-6 The phase inversion kinetics of PBI/P84/[EMIM]OAc solutions in water (casting temperature 80°C)

Similarly, the enhanced affinity among P84, [EMIM]OAc and water, the reduced viscosity of the blend system, and the high ratio of [EMIM]OAc outflow to water inflow

also facilitate the formation of a thinner PBI/P84 blend membrane with an open cell structure that favors a high water flux. Table 6-5 illustrates the effects of polymer composition and casting temperature on the ultrafiltration performance of PBI/P84 blend membranes, while Figure 6-7 shows the mean effective pore diameter and pore size distributions of these membranes cast at 80°C. Consistent with previous discussion, an increase in P84 ratio in blend solutions gave rise to an increase of the PWP to around 200 (L/m² bar h) as compared to 141.3 (L/m² bar h) of plain PBI membranes, as well as the increase of the mean effective pore diameter of the blended membranes. This result not only shows that PWP values can be apparently increased, but that the pore properties of membranes are easily manipulated by blending P84 in PBI systems.

Table 6-5 Comparison of PWP values and pore diameters of PBI/P84 blend membranes

| Membranes | Casting temperature | PWP (L/[m² bar h]) | μ_p (nm) | σ_p |
|-----------------------|----------------------------|--------------------------------------|--------------------------------|------------------------------|
| 20 wt% PBI | 80°C | 141.3 ± 5.4 | 10.75 | 1.56 |
| 15/5 wt% PBI/P84 | 80°C | 215.9 ± 20.4 | 12.79 | 1.33 |
| 10/10 wt% PBI/P84 | 80°C | 184.0 ± 11.4 | 15.80 | 1.55 |
| 10/10 wt% PBI/P84 -60 | 60°C | 67.5 ± 3.6 | 8.13 | 1.96 |

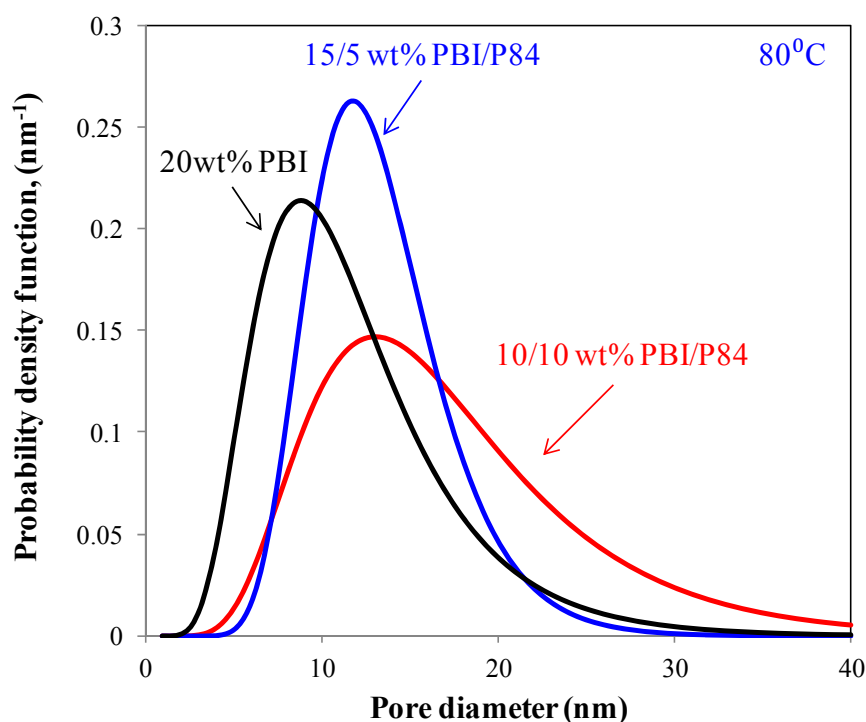
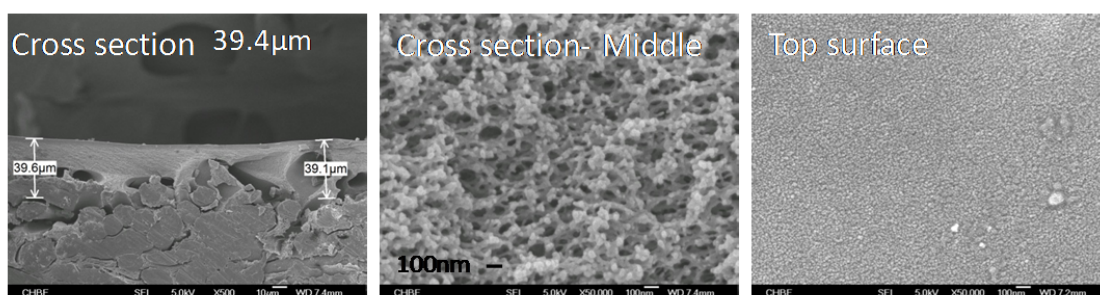


Figure 6-7 Pore size distribution curves of developed PBI/P84 blend membranes (casting temperature 80°C)

6.3.5.2 Effects of casting temperatures

Figure 6-8 compares the cross-sections and surface morphologies of the 10/10 wt% PBI/P84 membranes cast at two different temperatures. The membrane cast at 60 °C has a thicker and denser cross-section and surface morphology than the membrane cast at 80 °C. In addition, the former has no macrovoid, while the latter has. This interesting phenomenon arises from the fact that the former has a high viscosity than the latter as shown in Figure 6-9. In addition, the mutual diffusion coefficients between [EMIM]OAc and water became lower at lower temperatures [65]. Therefore, the higher dope viscosity and slower diffusion coefficients prevented the rapid water intrusion into the nascent membrane and thus eliminated any chance of local surface instability [83, 163, 164] for

10/10 wt% PBI/P84 cast at 80°C



10/10 wt% PBI/P84 cast at 60°C

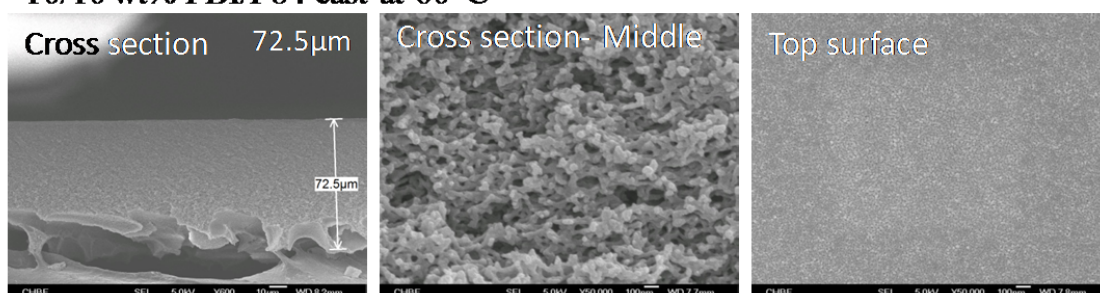


Figure 6-8 Comparison of the morphology of 10/10 wt% PBI/P84 blend membranes cast at different temperatures

the macrovoid formation. Since the binodal curve would shift toward the polymer-solvent axis at lower temperatures, less water is required to initiate the phase inversion [91]. Consequently, the stiff surface of the nascent membranes along with their high dope viscosities at 60 °C helped to tighten the bulk membrane, resulting in a less porous structure. Table 6-5 confirms our hypotheses and shows that both of the PWP value and the mean effective pore diameter of the 10/10 wt% PBI/P84 blend membranes cast at 60 °C are much smaller than that cast at 80 °C.

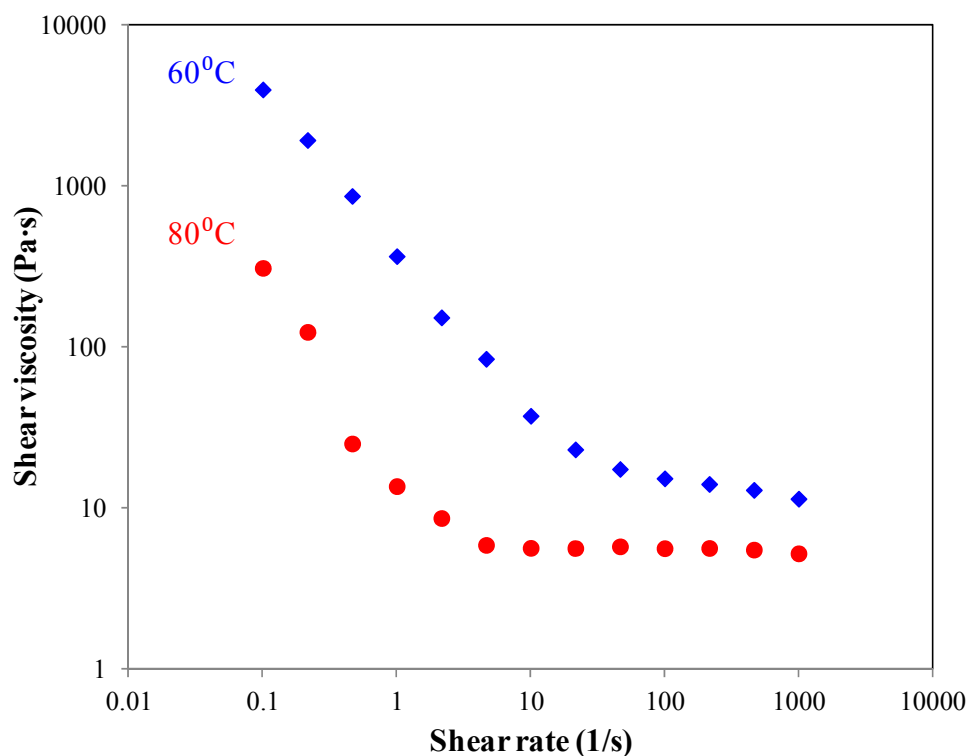


Figure 6-9 Shear viscosity of 10/10/80 wt% PBI/P84/[EMIM]OAc solution at different temperatures

6.4 Conclusions

In this study, we have fabricated PBI blend membranes for ultrafiltration with (1) a higher water flux, (2) consumption of reduced amount the expensive PBI material, and (3) replacement of toxic DMAc by an environmentally friendly ionic liquid. We have screened five commercially available high performance polyimides and polyimide-amides and found P84 to be the most suitable blend material with PBI in [EMIM]OAc. As confirmed by FTIR spectra, PBI and P84 not only formed miscible blends, but P84 also interacted with PBI and [EMIM]OAc closely via hydrogen bonding because both PBI and [EMIM]OAc have characteristics of proton donors and acceptors. As a result,

PBI, P84 and [EMIM]OAc constructed an interconnected network based on highly charge-ordered characteristics of [EMIM]OAc in the ternary system. The PBI/P84/[EMIM]OAc solution displays an initial shear thinning behavior under low shear rates followed by a Newtonian plateau, which verifies the existence of the interconnect ordered microstructure. The incorporation of P84 into the PBI system not only reduces the dope viscosity for a more viable membrane fabrication process but also alters the phase inversion path. The newly developed PBI/P84 blend membranes exhibited an open cell structure and ultrafiltration characteristics with pure water permeability up to 50% higher than the plain PBI asymmetric membranes. These new membranes may be suitable for recovering and concentrating pharmaceuticals and other valuable products from organic solvents due to their outstanding chemical and thermal stabilities.

Chapter 7 Conclusions and recommendations

This study has examined, from the molecular level, the interactions between ionic liquids and polymeric materials interrelated to the chemical structure and properties of the employed ionic liquids. It was found that in the CA/[EMIM]SCN solution, the highly charge-ordered ionic structure remained in the mixture with the inclusion of CA molecules. This may be attributed to the hydrogen bonding and coulombic forces existed in the CA/[EMIM]SCN solution. The ordered structure was further proved by the rheology of CA/[EMIM]SCN solutions which was demonstrated as a three-region flow curve under shear stress. This unique rheological characterization possibly arises from the competition between the charged-ordered structure and polymer chain entanglements in the CA/[EMIM]SCN solution. The interactions between [EMIM]SCN and CA play important roles in dissolving CA as well as in the membrane formation process.

This study then proceeded to explore the feasibility of using ionic liquids to replace the organic solvent to prepare asymmetric flat sheet membranes and hollow fiber membranes using the phase inversion method. It was found that the ionic liquids studied in this work showed an excellent capacity to dissolve CA. The results also suggested that CA flat membranes cast from the 10/90wt% CA/[BMIM]SCN solution exhibited a macrovoid-free and a relatively dense structure full of nodules. That is because the phase inversion of the CA/[BMIM]SCN system most likely occurred through nucleation growth and gelation, and was followed possibly by spinodal demixing and then solidification, which was quite dissimilar with the mechanisms for membranes cast from organic solvent. This

study contributes to understanding the key factors affecting the membrane formation for flat asymmetric membranes using environmental-benign ionic liquids as the solvent and cellulose acetate as the polymer via phase inversion.

This study also explored the effects of dope flow rate, dope temperature and air-gap distance on hollow fiber formation correlated to the interaction between CA and ionic liquids and the phase inversion mechanisms. By alteration of the spinning conditions, CA hollow fiber membranes were successfully fabricated for ultrafiltration with a PWP value of 90.10 (L/m² bar h) and a mean effective pore diameter of 16.68nm. It was also found that the resultant hollow fiber had an asymmetric structure consisting of a porous inner surface and a relative dense outer surface, but the cross-section was macrovoid-free and full of nodules. As far as we know, this is the first work that applies hollow fibers fabricated from polymer/ionic liquid solution in water treatment.

This study further provided an important insight into possible mechanisms of dissolving PBI in ionic liquids and discovered [EMIM]OAc as a strategic green solvent for the fabrication of PBI membranes in light of current environmental unfriendly organic solvents. Compared to DMAc, [EMIM]OAc is superior in dissolving PBI under much lower temperature and pressure because it is inherently equipped with strong proton acceptor characteristics that can powerfully disrupt the original hydrogen bonding in PBI and effectively dissolve PBI even at high concentrations (up to 20 wt%). According to the molecular dynamic simulation, the PBI/[EMIM]OAc system intrinsically possesses the largest amount of hydrogen bonding and the lowest interaction energy out of three

studied PBI/ionic liquid systems, leading to the excellent solubility of PBI in [EMIM]OAc. In addition, the PBI/[EMIM]OAc solution exhibits discrepancy from the Cox-merz rule which generally apply well for flexible polymer systems, and an initial shear thinning behavior under low shear rates. These distinctive rheological properties correspond well to the ordered structure arose from the hydrogen bonding and coulombic interactions in the PBI/[EMIM]OAc system.

Furthermore, this study proceeded to conquer the difficulties in the fabrication of PBI membranes from [EMIM]OAc. P84 co-polyimide was chosen out of five commercially available polyimides and polyimide-amides to blend with PBI in [EMIM]OAc because P84 interacted with PBI and [EMIM]OAc closely via hydrogen bonding. As a result, the newly developed PBI/P84 blend membranes exhibited an open cell structure and ultrafiltration characteristics with pure water permeability up to 50% higher than the plain PBI asymmetric membranes. The developed CA membranes and PBI blend membranes with porous and macrovoid-free morphology are favorable for ultrafiltration processes for water reuse as well as pharmaceutical separations from different sources, even under harsh conditions.

This work contributes to the understanding of fundamental and mechanisms of membrane formation by the phase inversion method based on polymer/ionic liquid solutions. It also demonstrates the feasibility of using ionic liquids to replace traditional solvents in membrane fabrication processes for the sake of environmental protection. Based on this work, future work is needed to optimize spinning conditions to fabricate hollow fiber

membranes with desirable properties for different applications. It should be acknowledged that ionic liquids are not applicable to all polymer materials for membrane formation. Future work is needed to search for other ionic liquid to dissolve polymers, especially those that are difficult to prepare using traditional solvents. Another area of future work is to apply ionic liquids not only as a solvent but also as other media, such as porogen, separation carrier or functional groups to improve the performance of membranes.

Given recycling and reuse of ionic liquids, evaporating water from the mixture of water and ionic liquids was employed in this work. Due to low concentration of ionic liquids in the mixture, this method is feasible; however, is very energy intensive. To contribute to a green life circle of ionic liquids, other methods for recycling ionic liquids are urgently needed. Membrane technology may be developed to separate ionic liquid from water.

Chapter 8 References

- [1] S.P. Nunes, K.V. Peinemann, Membrane technology in the chemical industry, Wiley-VCH, 2006.
- [2] T. Matsuura, Synthetic Membranes and Membrane Separation Processes, CRC Press, 1994.
- [3] S. Loeb, S. Sourirajan, Sea Water Demineralization by Means of an Osmotic Membrane, in: Adv. Chem. Ser., ACS, 1963, pp. 117-132.
- [4] N. Peng, T.S. Chung, K.Y. Wang, Macrovoid evolution and critical factors to form macrovoid-free hollow fiber membranes, J. Membr. Sci., 318 (2008) 363-372.
- [5] K.Y. Wang, T. Matsuura, T.S. Chung, W.F. Guo, The effects of flow angle and shear rate within the spinneret on the separation performance of poly (ethersulfone) (PES) ultrafiltration hollow fiber membranes, J. Membr. Sci., 240 (2004) 67-79.
- [6] S.P. Sun, K.Y. Wang, N. Peng, T.A. Hatton, T.S. Chung, Novel polyamide-imide/cellulose acetate dual-layer hollow fiber membranes for nanofiltration, J. Membr. Sci., 363 (2010) 232-242.
- [7] R.D. Noble, D.L. Gin, Perspective on ionic liquids and ionic liquid membranes, J. Membr. Sci., 369 (2011) 1-4.
- [8] M.J. Earle, K.R. Seddon, Ionic liquids: Green solvents for the future, in: M.A. Abraham, L. Moens (Eds.) Clean Solvents: Alternative Media for Chemical Reactions and Processing, 2002, pp. 10-25.
- [9] R.D. Rogers, K.R. Seddon, Ionic liquids - Solvents of the future?, Science, 302 (2003) 792-793.

- [10] O.A. El Seoud, A. Koschella, L.C. Fidale, S. Dorn, T. Heinze, Applications of ionic liquids in carbohydrate chemistry: A window of opportunities, *Biomacromolecules*, 8 (2007) 2629-2647.
- [11] J.D. Martin, Structure-property relationships in ionic liquids, in: R.D. Rogers, K.R. Seddon (Eds.) *Ionic Liquids - Industrial Applications for Green Chemistry*, American Chemical Society, Washington, 2002, pp. 413-427.
- [12] I. Krossing, J.M. Slattery, C. Daguene, P.J. Dyson, A. Oleinikova, H. Weingärtner, Why are ionic liquids liquid? A simple explanation based on lattice and solvation energies, *J. Am. Chem. Soc.*, 128 (2006) 13427-13434.
- [13] J. Dupont, On the solid, liquid and solution structural organization of imidazolium ionic liquids, *J. Braz. Chem. Soc.*, 15 (2004) 341-350.
- [14] M. Revere, M.P. Tosi, Structure and dynamics of molten salts, *Rep. Prog. Phys.*, 49 (1986) 1001.
- [15] S. Biggin, J.E. Enderby, Comments on the structure of molten salts, *Journal of Physics C: Solid State Physics*, 15 (1982) L305.
- [16] J. Dupont, P.A.Z. Suarez, Physico-chemical processes in imidazolium ionic liquids, *Phys. Chem. Chem. Phys.*, 8 (2006) 2441-2452.
- [17] S. Saha, S. Hayashi, A. Kobayashi, H. Hamaguchi, Crystal structure of 1-butyl-3-methylimidazolium chloride. A clue to the elucidation of the ionic liquid structure, *Chem. Lett.*, 32 (2003) 740-741.
- [18] E.J. Maginn, Molecular simulation of ionic liquids: current status and future opportunities, *J. Phys.: Condens. Matter*, 21 (2009).

- [19] J.N.A.C. Lopes, A.A.H. Padua, Nanostructural organization in ionic liquids, *J. Phys. Chem. B*, 110 (2006) 3330-3335.
- [20] J.G. Huddleston, A.E. Visser, W.M. Reichert, H.D. Willauer, G.A. Broker, R.D. Rogers, Characterization and comparison of hydrophilic and hydrophobic room temperature ionic liquids incorporating the imidazolium cation, *Green Chem.*, 3 (2001) 156-164.
- [21] Y. Cao, J. Wu, J. Zhang, H. Li, Y. Zhang, J. He, Room temperature ionic liquids (RTILs): A new and versatile platform for cellulose processing and derivatization, *Chem Eng J*, 147 (2009) 13-21.
- [22] T. Welton, Room-Temperature Ionic Liquids. Solvents for Synthesis and Catalysis, *Chem. Rev.*, 99 (1999) 2071-2084.
- [23] V.I. Parvulescu, C. Hardacre, Catalysis in Ionic Liquids, *ChemInform*, 38 (2007) no-no.
- [24] A. Lewandowski, A. Świdorska, New composite solid electrolytes based on a polymer and ionic liquids, *Solid State Ionics*, 169 (2004) 21-24.
- [25] J. Lu, F. Yan, J. Texter, Advanced applications of ionic liquids in polymer science, *Progress in Polymer Science*, 34 (2009) 431-448.
- [26] J. Fuller, A.C. Breda, R.T. Carlin, Ionic liquid-polymer gel electrolytes, *J Electrochem Soc*, 144 (1997) L67-L70.
- [27] A. Noda, M. Watanabe, Highly conductive polymer electrolytes prepared by in situ polymerization of vinyl monomers in room temperature molten salts, *Electrochimica Acta*, 45 (2000) 1265-1270.

- [28] M. Yoshio, T. Kagata, K. Hoshino, T. Mukai, H. Ohno, T. Kato, One-Dimensional Ion-Conductive Polymer Films: Alignment and Fixation of Ionic Channels Formed by Self-Organization of Polymerizable Columnar Liquid Crystals, *Journal of the American Chemical Society*, 128 (2006) 5570-5577.
- [29] F. Yan, J. Texter, Surfactant ionic liquid-based microemulsions for polymerization, *Chem. Commun.*, (2006) 2696-2698.
- [30] S. Zhu, Y. Wu, Q. Chen, Z. Yu, C. Wang, S. Jin, Y. Ding, G. Wu, Dissolution of cellulose with ionic liquids and its application: a mini-review, *Green Chem.*, 8 (2006) 325-327.
- [31] R.P. Swatloski, S.K. Spear, J.D. Holbrey, R.D. Rogers, Dissolution of cellose with ionic liquids, *J. Am. Chem. Soc.*, 124 (2002) 4974-4975.
- [32] J.S. Moulthrop, R.P. Swatloski, G. Moyna, R.D. Rogers, High-resolution ¹³C NMR studies of cellulose and cellulose oligomers in ionic liquid solutions, *Chem. Commun.*, (2005) 1557-1559.
- [33] H. Zhang, J. Wu, J. Zhang, J. He, 1-Allyl-3-methylimidazolium Chloride Room Temperature Ionic Liquid: A New and Powerful Nonderivatizing Solvent for Cellulose, *Macromolecules*, 38 (2005) 8272-8277.
- [34] H. Zhang, Z.G. Wang, Z.N. Zhang, J. Wu, J. Zhang, J.S. He, Regenerated-Cellulose/Multiwalled- Carbon-Nanotube Composite Fibers with Enhanced Mechanical Properties Prepared with the Ionic Liquid 1-Allyl-3-methylimidazolium Chloride, *Advanced Materials*, 19 (2007) 698-704.

- [35] F. Hermanutz, F. Gaehr, E. Uerdingen, F. Meister, B. Kosan, New developments in dissolving and processing of cellulose in ionic liquids, *Macromol Symp*, 262 (2008) 23-27.
- [36] K.V. Peinemann, S.P. Nunes, *Membranes for Energy Conversion*, Wiley-VCH, 2008.
- [37] T.S. Chung, Fabrication of hollow-fiber membranes by phase Inversion, in: N.N. Li, A.G. Fane, W.S. Winston Ho, T. Matsuura (Eds.) *Advanced Membrane Technology and Applications*, John Wiley & Sons, Inc., 2008, pp. 821-839.
- [38] X. Feng, R.Y.M. Huang, Liquid separation by membrane pervaporation: A review, *Industrial and Engineering Chemistry Research*, 36 (1997) 1048-1066.
- [39] P. Snedden, A.I. Cooper, K. Scott, N. Winterton, Cross-Linked Polymer-Ionic Liquid Composite Materials, *Macromolecules*, 36 (2003) 4549-4556.
- [40] L.A. Neves, J. Benavente, I.M. Coelho, J.G. Crespo, Design and characterisation of Nafion membranes with incorporated ionic liquids cations, *J. Membr. Sci.*, 347 (2010) 42-52.
- [41] M.L. Guo, J. Fang, H.K. Xu, W. Li, X.H. Lu, C.H. Lan, K.Y. Li, Synthesis and characterization of novel anion exchange membranes based on imidazolium-type ionic liquid for alkaline fuel cells, *J. Membr. Sci.*, 362 (2010) 97-104.
- [42] P. Scovazzo, D. Havard, M. McShea, S. Mixon, D. Morgan, Long-term, continuous mixed-gas dry fed CO₂/CH₄ and CO₂/N₂ separation performance and selectivities for room temperature ionic liquid membranes, *J. Membr. Sci.*, 327 (2009) 41-48.
- [43] J.E. Bara, E.S. Hatakeyama, D.L. Gin, R.D. Noble, Improving CO₂ permeability in polymerized room-temperature ionic liquid gas separation membranes through the

formation of a solid composite with a room-temperature ionic liquid, *Polym. Adv. Technol.*, 19 (2008) 1415-1420.

[44] H.Z. Chen, P. Li, T.S. Chung, PVDF/ionic liquid polymer blends with superior separation performance for removing CO₂ from hydrogen and flue gas, *Int. J. Hydrogen Energy*, 37 (2012) 11796-11804.

[45] P. Li, D.R. Paul, T.S. Chung, High performance membranes based on ionic liquid polymers for CO₂ separation from the flue gas, *Green Chem.*, 14 (2012) 1052-1063.

[46] W.S.W. Ho, K.K. Sirkar, *Membrane Handbook*, Kluwer Academic Pub., 1992.

[47] M. Mulder, *Basic principles of membrane technology*, Kluwer Academic, 1996.

[48] W.J. Koros, Evolving beyond the thermal age of separation processes: Membranes can lead the way, *AIChE J.*, 50 (2004) 2326-2334.

[49] D.R. Trettin, M.R. Doshi, LIMITING FLUX IN ULTRAFILTRATION OF MACROMOLECULAR SOLUTIONS, *ChEnC*, 4 (1980) 507-522.

[50] R. Ghosh, *Protein Bioseparation Using Ultrafiltration: Theory, Applications and New Developments*, Imperial College Press, 2003.

[51] K.Y. Wang, Fabrication and characterization of ultrafiltration and nanofiltration membranes, in: *Ph.D Thesis*, National University of Singapore, 2005.

[52] O. Olabisi, L.M. Robeson, M.T. Shaw, *Polymer-polymer miscibility*, Academic Press, 1979.

[53] T.S. Chung, X.D. Hu, Effect of air-gap distance on the morphology and thermal properties of polyethersulfone hollow fibers, *J. Appl. Polym. Sci.*, 66 (1997) 1067-1077.

- [54] D. Li, T.S. Chung, J. Ren, R. Wang, Thickness Dependence of Macrovoid Evolution in Wet Phase-Inversion Asymmetric Membranes, *Ind. Eng. Chem. Res.*, 43 (2004) 1553-1556.
- [55] A.F. Ismail, I.R. Dunkin, S.L. Gallivan, S.J. Shilton, Production of super selective polysulfone hollow fiber membranes for gas separation, *Polymer*, 40 (1999) 6499-6506.
- [56] L. Yilmaz, A.J. McHugh, Analysis of nonsolvent–solvent–polymer phase diagrams and their relevance to membrane formation modeling, *J. Appl. Polym. Sci.*, 31 (1986) 997-1018.
- [57] L. Yilmaz, A.J. McHugh, Modeling of asymmetric membrane formation. II. The effects of surface boundary conditions, *J. Appl. Polym. Sci.*, 35 (1988) 1967-1979.
- [58] S.S. Prakash, L.F. Francis, L.E. Scriven, Microstructure evolution in dry–wet cast polysulfone membranes by cryo-SEM: A hypothesis on macrovoid formation, *J. Membr. Sci.*, 313 (2008) 135-157.
- [59] J.W. Cahn, Phase Separation by Spinodal Decomposition in Isotropic Systems, *JChPh*, 42 (1965) 93-&.
- [60] T.S. Chung, The limitations of using Flory-Huggins equation for the states of solutions during asymmetric hollow-fiber formation, *J. Membr. Sci.*, 126 (1997) 19-34.
- [61] R.E. Kesting, A.K. Fritzsche, *Polymeric gas separation membranes*, Wiley, 1993.
- [62] J.A. van't Hof, A.J. Reuvers, R.M. Boom, H.H.M. Rolevink, C.A. Smolders, Preparation of asymmetric gas separation membranes with high selectivity by a dual-bath coagulation method, *J. Membr. Sci.*, 70 (1992) 17-30.
- [63] H. Yanagishita, T. Nakane, H. Yoshitome, Selection Criteria for Solvent and Gelation Medium in the Phase Inversion Process, *J. Membr. Sci.*, 89 (1994) 215-221.

- [64] R.-C. Ruaan, T. Chang, D.-M. Wang, Selection criteria for solvent and coagulation medium in view of macrovoid formation in the wet phase inversion process, *J. Polym. Sci., Part B: Polym. Phys.*, 37 (1999) 1495-1502.
- [65] N. Peng, T.S. Chung, K.Y. Li, The role of additives on dope rheology and membrane formation of defect-free Torlon[®] hollow fibers for gas separation, *J. Membr. Sci.*, 343 (2009) 62-72.
- [66] N. Widjojo, T.S. Chung, Thickness and air gap dependence of macrovoid evolution in phase-inversion asymmetric hollow fiber membranes, *Ind. Eng. Chem. Res.*, 45 (2006) 7618-7626.
- [67] P.I. Flory, Thermodynamics of high polymer solutions, *JChPh*, 10 (1942) 51-61.
- [68] P. Aptel, N. Abidine, F. Ivaldi, J.P. Lafaille, Polysulfone hollow fibers — effect of spinning conditions on ultrafiltration properties, *Journal of Membrane Science*, 22 (1985) 199-215.
- [69] A.F. Ismail, S.J. Shilton, I.R. Dunkin, S.L. Gallivan, Direct measurement of rheologically induced molecular orientation in gas separation hollow fibre membranes and effects on selectivity, *Journal of Membrane Science*, 126 (1997) 133-137.
- [70] A.F. Ismail, P.Y. Lai, Effects of phase inversion and rheological factors on formation of defect-free and ultrathin-skinned asymmetric polysulfone membranes for gas separation, *Separation and Purification Technology*, 33 (2003) 127-143.
- [71] T.S. Chung, S.K. Teoh, W.W.Y. Lau, M.P. Srinivasan, Effect of shear stress within the spinneret on hollow fiber membrane morphology and separation performance (vol 37, pg 3936, 1998), *Ind. Eng. Chem. Res.*, 37 (1998) 4903-4903.

- [72] T.S. Chung, W.H. Lin, R.H. Vora, The effect of shear rates on gas separation performance of 6FDA-durene polyimide hollow fibers, *Journal of Membrane Science*, 167 (2000) 55-66.
- [73] C. Cao, T.-S. Chung, S.B. Chen, Z. Dong, The study of elongation and shear rates in spinning process and its effect on gas separation performance of Poly(ether sulfone) (PES) hollow fiber membranes, *Chem. Eng. Sci.*, 59 (2004) 1053-1062.
- [74] J.J. Qin, J. Gu, T.S. Chung, Effect of wet and dry-jet wet spinning on the shear-induced orientation during the formation of ultrafiltration hollow fiber membranes, *J. Membr. Sci.*, 182 (2001) 57-75.
- [75] N. Peng, T.S. Chung, J.Y. Lai, The rheology of Torlon (R) solutions and its role in the formation of ultra-thin defect-free Torlon (R) hollow fiber membranes for gas separation, *J. Membr. Sci.*, 326 (2009) 608-617.
- [76] A.F.M. Barton, *CRC Handbook of Solubility Parameters and Other Cohesion Parameters*, Second Edition, Taylor & Francis, 1991.
- [77] J.-J. Shieh, T.S. Chung, Effect of liquid-liquid demixing on the membrane morphology, gas permeation, thermal and mechanical properties of cellulose acetate hollow fibers, *J. Membr. Sci.*, 140 (1998) 67-79.
- [78] T.S. Chung, J.J. Qin, A. Huan, K.C. Toh, Visualization of the effect of die shear rate on the outer surface morphology of ultrafiltration membranes by AFM, *J. Membr. Sci.*, 196 (2002) 251-266.
- [79] A.J. Reuvers, C.A. Smolders, Formation of membranes by means of immersion precipitation : Part II. the mechanism of formation of membranes prepared from the system cellulose acetate-acetone-water, *J. Membr. Sci.*, 34 (1987) 67-86.

- [80] C.R. Wilke, P. Chang, Correlation of diffusion coefficients in dilute solutions, *AICHE J.*, 1 (1955) 264-270.
- [81] C. Blicke, K.-V. Peinemann, S. Pereira Nunes, Ultrafiltration membranes from poly(ether sulfonamide)/poly(ether imide) blends, *J. Membr. Sci.*, 79 (1993) 83-91.
- [82] H.A. Tsai, C.Y. Kuo, J.H. Lin, D.M. Wang, A. Deratani, C. Pochat-Bohatier, K.R. Lee, J.Y. Lai, Morphology control of polysulfone hollow fiber membranes via water vapor induced phase separation, *J. Membr. Sci.*, 278 (2006) 390-400.
- [83] H. Strathmann, K. Kock, The formation mechanism of phase inversion membranes, *Desalination*, 21 (1977) 241-255.
- [84] Č. Stropnik, V. Kaiser, Polymeric membranes preparation by wet phase separation: mechanisms and elementary processes, *Desalination*, 145 (2002) 1-10.
- [85] R.J. Ray, W.B. Krantz, R.L. Sani, Linear stability theory model for finger formation in asymmetric membranes, *J. Membr. Sci.*, 23 (1985) 155-182.
- [86] F.G. Paulsen, S.S. Shojaie, W.B. Krantz, Effect of evaporation step on macrovoid formation in wet-cast polymeric membranes, *J. Membr. Sci.*, 91 (1994) 265-282.
- [87] Y. Li, T.S. Chung, Exploration of highly sulfonated polyethersulfone (SPES) as a membrane material with the aid of dual-layer hollow fiber fabrication technology for protein separation, *J. Membr. Sci.*, 309 (2008) 45-55.
- [88] T.S. Chung, S.K. Teoh, X. Hu, Formation of ultrathin high-performance polyethersulfone hollow-fiber membranes, *J. Membr. Sci.*, 133 (1997) 161-175.
- [89] Y.E. Santoso, T.S. Chung, K.Y. Wang, M. Weber, The investigation of irregular inner skin morphology of hollow fiber membranes at high-speed spinning and the solutions to overcome it, *J. Membr. Sci.*, 282 (2006) 383-392.

- [90] A.J. Reuvers, F.W. Altena, C.A. Smolders, Demixing and Gelation Behavior of Ternary Cellulose-Acetate Solutions, *Journal of Polymer Science Part B-Polymer Physics*, 24 (1986) 793-804.
- [91] T.S. Chung, E.R. Kafchinski, The effects of spinning conditions on asymmetric 6FDA/6FDAM polyimide hollow fibers for air separation, *J. Appl. Polym. Sci.*, 65 (1997) 1555-1569.
- [92] K.Y. Lin, D.M. Wang, J.Y. Lai, Nonsolvent-induced gelation and its effect on membrane morphology, *Macromolecules*, 35 (2002) 6697-6706.
- [93] Y. Su, G.G. Lipscomb, H. Balasubramanian, D.R. Lloyd, Observations of recirculation in the bore fluid during hollow fiber spinning, *AIChE J.*, 52 (2006) 2072-2078.
- [94] Y.H. See-Toh, M. Silva, A. Livingston, Controlling molecular weight cut-off curves for highly solvent stable organic solvent nanofiltration (OSN) membranes, *J. Membr. Sci.*, 324 (2008) 220-232.
- [95] J.T. Tsai, Y.S. Su, D.M. Wang, J.L. Kuo, J.Y. Lai, A. Deratani, Retainment of pore connectivity in membranes prepared with vapor-induced phase separation, *J. Membr. Sci.*, 362 (2010) 360-373.
- [96] H. Matsuyama, M. Teramoto, R. Nakatani, T. Maki, Membrane formation via phase separation induced by penetration of nonsolvent from vapor phase. II. Membrane morphology, *J. Appl. Polym. Sci.*, 74 (1999) 171-178.
- [97] L. Setiawan, R. Wang, K. Li, A.G. Fane, Fabrication of novel poly(amide-imide) forward osmosis hollow fiber membranes with a positively charged nanofiltration-like selective layer, *J. Membr. Sci.*, 369 (2011) 196-205.

- [98] C. Rauwendaal, Polymer extrusion, Hanser Gardner Publications, 2001.
- [99] S. Bonyadi, T.S. Chung, W.B. Krantz, Investigation of corrugation phenomenon in the inner contour of hollow fibers during the non-solvent induced phase-separation process, *J. Membr. Sci.*, 299 (2007) 200-210.
- [100] B. Derescker, A. Derecsker-Kovacs, Molecular modelling simulations to predict density and solubility parameter of ionic liquids, *Mol. Simul.*, 34 (2008) 1167-1175.
- [101] J. Sadlej, A. Jaworski, K. Miaskiewicz, A theoretical study of the vibrational spectra of imidazole and its different forms, *Journal of Molecular Structure*, 274 (1992) 247-257.
- [102] A. Chowdhury, S.T. Thynell, Confined rapid thermolysis/FTIR/ToF studies of imidazolium-based ionic liquids, *Thermochimica Acta*, 443 (2006) 159-172.
- [103] K.M. Dieter, C.J. Dymek, N.E. Heimer, J.W. Rovang, J.S. Wilkes, Ionic structure and interactions in 1-methyl-3-ethylimidazolium chloride- AlCl_3 molten-salts, *J. Am. Chem. Soc.*, 110 (1988) 2722-2726.
- [104] K.F. Wissbrun, Rheology of Rod-Like Polymers in the Liquid-Crystalline State, *J. Rheol.*, 25 (1981) 619-662.
- [105] T.S. Chung, The recent developments of thermotropic liquid crystalline polymers, *Polymer Engineering & Science*, 26 (1986) 901-919.
- [106] C.W. Macosko, *Rheology: Principles, Measurements, and Applications*, Wiley-VCH, 1994.
- [107] T.H. Young, L.W. Chen, Pore formation mechanism of membranes from phase inversion process, *Desalination*, 103 (1995) 233-247.

- [108] D.Y. Xing, N. Peng, T.S. Chung, Formation of cellulose acetate membranes via phase inversion using ionic liquid, [BMIM]SCN, as the solvent, *Ind. Eng. Chem. Res.*, 49 (2010) 8761-8769.
- [109] I.M. Wienk, R.M. Boom, M.A.M. Beerlage, A.M.W. Bulte, C.A. Smolders, H. Strathmann, Recent advances in the formation of phase inversion membranes made from amorphous or semi-crystalline polymers, *J. Membr. Sci.*, 113 (1996) 361-371.
- [110] R.E. Kesting, *Synthetic polymeric membranes: a structural perspective*, Wiley, 1985.
- [111] T.S. Chung, A critical review of polybenzimidazoles: Historical development and future R&D, *J. Macromol. Sci. Rev. Macromol. Chem. Phys.*, C37 (1997) 277-301.
- [112] Y. Wang, S.H. Goh, T.S. Chung, Miscibility study of Torlon (R) polyamide-imide with Matrimid (R) 5218 polyimide and polybenzimidazole, *Polymer*, 48 (2007) 2901-2909.
- [113] D.J. Jones, J. Roziere, Recent advances in the functionalisation of polybenzimidazole and polyetherketone for fuel cell applications, *J. Membr. Sci.*, 185 (2001) 41-58.
- [114] D. Mecerreyes, H. Grande, O. Miguel, E. Ochoteco, R. Marcilla, I. Cantero, Porous polybenzimidazole membranes doped with phosphoric acid: Highly proton-conducting solid electrolytes, *Chem Mater*, 16 (2004) 604-607.
- [115] Q. Li, R. He, J.O. Jensen, N.J. Bjerrum, PBI-Based Polymer Membranes for High Temperature Fuel Cells – Preparation, Characterization and Fuel Cell Demonstration, *Fuel Cells*, 4 (2004) 147-159.

- [116] K.Y. Wang, T.-S. Chung, R. Rajagopalan, Novel Polybenzimidazole (PBI) Nanofiltration Membranes for the Separation of Sulfate and Chromate from High Alkalinity Brine To Facilitate the Chlor-Alkali Process, *Ind. Eng. Chem. Res.*, 46 (2007) 1572-1577.
- [117] L.C. Sawyer, R.S. Jones, Observations on the structure of first generation polybenzimidazole reverse osmosis membranes, *J. Membr. Sci.*, 20 (1984) 147-166.
- [118] K.Y. Wang, Y.C. Xiao, T.S. Chung, Chemically modified polybenzimidazole nanofiltration membrane for the separation of electrolytes and cephalexin, *Chem. Eng. Sci.*, 61 (2006) 5807-5817.
- [119] K.Y. Wang, T.S. Chung, J.J. Qin, Polybenzimidazole (PBI) nanofiltration hollow fiber membranes applied in forward osmosis process, *J. Membr. Sci.*, 300 (2007) 6-12.
- [120] Y. Wang, M. Gruender, T.S. Chung, Pervaporation dehydration of ethylene glycol through polybenzimidazole (PBI)-based membranes. 1. Membrane fabrication, *J. Membr. Sci.*, 363 (2010) 149-159.
- [121] J.R. Klaehn, T.A. Luther, C.J. Orme, M.G. Jones, A.K. Wertsching, E.S. Peterson, Soluble N-substituted organosilane polybenzimidazoles, *Macromolecules*, 40 (2007) 7487-7492.
- [122] R. Hausman, B. Digman, I.C. Escobar, M. Coleman, T.-S. Chung, Functionalization of polybenzimidazole membranes to impart negative charge and hydrophilicity, *J. Membr. Sci.*, 363 (2010) 195-203.
- [123] Z.X. Li, J.H. Liu, S.Y. Yang, S.H. Huang, J.D. Lu, J.L. Pu, Synthesis and characterization of novel hyperbranched polybenzimidazoles based on an AB₂ monomer

containing four amino groups and one carboxylic group, *J. Polym. Sci., Part A: Polym. Chem.*, 44 (2006) 5729-5739.

[124] R. Renner, Ionic liquids: An industrial cleanup solution, *Environ. Sci. Technol.*, 35 (2001) 410a-413a.

[125] C.L. Li, D.M. Wang, A. Deratani, D. Quemener, D. Bouyer, J.Y. Lai, Insight into the preparation of poly(vinylidene fluoride) membranes by vapor-induced phase separation, *J. Membr. Sci.*, 361 (2010) 154-166.

[126] B. Wang, Y.F. Tang, Z.W. Wen, H.P. Wang, Dissolution and regeneration of polybenzimidazoles using ionic liquids, *Eur. Polym. J.*, 45 (2009) 2962-2965.

[127] R. Shukla, M. Balakrishnan, G.P. Agarwal, Bovine serum albumin-hemoglobin fractionation: significance of ultrafiltration system and feed solution characteristics, *Bioseparation*, 9 (2000) 7-19.

[128] D.Y. Xing, N. Peng, T.S. Chung, Investigation of unique interactions between cellulose acetate and ionic liquid [EMIM]SCN, and their influences on hollow fiber ultrafiltration membranes, *J. Membr. Sci.*, 380 (2011) 87-97.

[129] Z. Luo, J. Jiang, Molecular dynamics and dissipative particle dynamics simulations for the miscibility of poly(ethylene oxide)/poly(vinyl chloride) blends, *Polymer*, 51 (2010) 291-299.

[130] S. Li, J.R. Fried, J. Colebrook, J. Burkhardt, Molecular simulations of neat, hydrated, and phosphoric acid-doped polybenzimidazoles. Part 1: Poly(2,2'-m-phenylene-5,5'-bibenzimidazole) (PBI), poly(2,5-benzimidazole) (ABPBI), and poly(p-phenylene benzobisimidazole) (PBBI), *Polymer*, 51 (2010) 5640-5648.

- [131] A. Sannigrahi, D. Arunbabu, R.M. Sankar, T. Jana, Aggregation behavior of polybenzimidazole in aprotic polar solvent, *Macromolecules*, 40 (2007) 2844-2851.
- [132] P. Musto, F.E. Karasz, W.J. Macknight, Hydrogen-bonding in polybenzimidazole poly(ether imide) blends - a spectroscopic study, *Macromolecules*, 24 (1991) 4762-4769.
- [133] Y. Iwakura, K. Uno, Y. Imai, Polyphenylenebenzimidazoles, *J. Polym. Sci., Part A: General Papers*, 2 (1964) 2605-2615.
- [134] C.B. Shogbon, J.L. Brousseau, H.F. Zhang, B.C. Benicewicz, Y.A. Akpalu, Determination of the molecular parameters and studies of the chain conformation of polybenzimidazole in DMAc/LiCl, *Macromolecules*, 39 (2006) 9409-9418.
- [135] D.T. Bowron, C. D'Agostino, L.F. Gladden, C. Hardacre, J.D. Holbrey, M.C. Lagunas, J. McGregor, M.D. Mantle, C.L. Mullan, T.G.A. Youngs, Structure and Dynamics of 1-Ethyl-3-methylimidazolium Acetate via Molecular Dynamics and Neutron Diffraction, *J. Phys. Chem. B*, 114 (2010) 7760-7768.
- [136] W.P. Cox, E.H. Merz, Correlation of Dynamic and Steady Flow Viscosities, *J. Polym. Sci.*, 28 (1958) 619-622.
- [137] L.A. Utracki, R. Gendron, PRESSURE OSCILLATION DURING EXTRUSION OF POLYETHYLENES .2, *J. Rheol.*, 28 (1984) 601-623.
- [138] R.G. Larson, CONSTITUTIVE RELATIONSHIPS FOR POLYMERIC MATERIALS WITH POWER-LAW DISTRIBUTIONS OF RELAXATION-TIMES, *Rheol. Acta.*, 24 (1985) 327-334.
- [139] J.R. Gillmor, R.H. Colby, E. Hall, C.K. Ober, Viscoelastic Properties of a Model Main-Chain Liquid-Crystalline Polyether, *J. Rheol.*, 38 (1994) 1623-1638.

- [140] D.W. Mead, R.G. Larson, Rheoptical Study of Isotropic Solutions of Stiff Polymers, *Macromolecules*, 23 (1990) 2524-2533.
- [141] S. Bonyadi, T.S. Chung, Flux enhancement in membrane distillation by fabrication of dual layer hydrophilic–hydrophobic hollow fiber membranes, *J. Membr. Sci.*, 306 (2007) 134-146.
- [142] Q. Yang, K.Y. Wang, T.S. Chung, Dual-layer hollow fibers with enhanced flux as novel forward osmosis membranes for water production, *Environ. Sci. Technol.*, 43 (2009) 2800-2805.
- [143] Y. Li, S.C. Soh, T.S. Chung, S.Y. Chan, Exploration of Ionic Modification in Dual-Layer Hollow Fiber Membranes for Long-Term High-Performance Protein Separation, *AICHE J.*, 55 (2009) 321-330.
- [144] D.B. Burns, A.L. Zydney, Contributions to electrostatic interactions on protein transport in membrane systems, *AICHE J.*, 47 (2001) 1101-1114.
- [145] R.D. Rogers, K.R. Seddon, A.C.S.D.o. Industrial, E. Chemistry, A.C.S. Meeting, *Ionic liquids: Industrial Applications for Green Chemistry*, American Chemical Society, 2002.
- [146] D.Y. Xing, S.Y. Chan, T.S. Chung, Molecular interactions between polybenzimidazole and [EMIM]OAc, and derived ultrafiltration membranes for protein separation, *Green Chem.*, 14 (2012) 1405-1412.
- [147] A. Moriya, T. Maruyama, Y. Ohmukai, T. Sotani, H. Matsuyama, Preparation of poly(lactic acid) hollow fiber membranes via phase separation methods, *J. Membr. Sci.*, 342 (2009) 307-312.

- [148] M. Jaffe, P. Chen, E.W. Choe, T.S. Chung, S. Makhija, High performance polymer blends, in: P. Hergenrother (Ed.) High Performance Polymers, Springer Berlin / Heidelberg, 1994, pp. 297-327.
- [149] T.S. Chung, W.F. Guo, Y. Liu, Enhanced Matrimid membranes for pervaporation by homogenous blends with polybenzimidazole (PBI), *J. Membr. Sci.*, 271 (2006) 221-231.
- [150] G. Guerra, S. Choe, D.J. Williams, F.E. Karasz, W.J. MacKnight, Fourier transform infrared spectroscopy of some miscible polybenzimidazole/polyimide blends, *Macromolecules*, 21 (1988) 231-234.
- [151] E. Foldes, E. Fekete, F.E. Karasz, B. Pukanszky, Interaction, miscibility and phase inversion in PBI/PI blends, *Polymer*, 41 (2000) 975-983.
- [152] Y. Wang, S.H. Goh, T.S. Chung, Miscibility study of Torlon[®] polyamide-imide with Matrimid[®] 5218 polyimide and polybenzimidazole, *Polymer*, 48 (2007) 2901-2909.
- [153] S.S. Hosseini, T.S. Chung, Carbon membranes from blends of PBI and polyimides for N₂/CH₄ and CO₂/CH₄ separation and hydrogen purification, *J. Membr. Sci.*, 328 (2009) 174-185.
- [154] M. Flanagan, R. Hausman, B. Digman, I.C. Escobar, M. Coleman, T.S. Chung, Surface functionalization of polybenzimidazole membranes to increase hydrophilicity and charge, in: *Modern Applications in Membrane Science and Technology*, American Chemical Society, 2011, pp. 303-321.
- [155] J. Kiefer, K. Obert, A. Bösmann, T. Seeger, P. Wasserscheid, A. Leipertz, Quantitative analysis of alpha-D-glucose in an ionic liquid by using infrared spectroscopy, *ChemPhysChem*, 9 (2008) 1317-1322.

- [156] H. Liu, K.L. Sale, B.M. Holmes, B.A. Simmons, S. Singh, Understanding the interactions of cellulose with ionic liquids: A molecular dynamics study, *J. Phys. Chem. B*, 114 (2010) 4293-4301.
- [157] R.S. Porter, L.-H. Wang, Compatibility and transesterification in binary polymer blends, *Polymer*, 33 (1992) 2019-2030.
- [158] K.A. Schult, D.R. Paul, Water sorption and transport in blends of polyethyloxazoline and polyethersulfone, *J. Polym. Sci., Part B: Polym. Phys.*, 35 (1997) 993-1007.
- [159] T.S. Chung, Z.L. Xu, Asymmetric hollow fiber membranes prepared from miscible polybenzimidazole and polyetherimide blends, *J. Membr. Sci.*, 147 (1998) 35-47.
- [160] M. Gericke, K. Schluffer, T. Liebert, T. Heinze, T. Budtova, Rheological properties of cellulose/ionic liquid solutions: from dilute to concentrated states, *Biomacromolecules*, 10 (2009) 1188-1194.
- [161] D.R. Paul, S. Newman, *Polymer Blends*, Academic Press, 1978.
- [162] R.F. Fedors, A method for estimating both the solubility parameters and molar volumes of liquids, *Polym. Eng. Sci.*, 14 (1974) 147-154.
- [163] L. Broens, F.W. Altena, C.A. Smolders, D.M. Koenhen, Asymmetric membrane structures as a result of phase separation phenomena, *Desalination*, 32 (1980) 33-45.
- [164] J.-Y. Lai, F.-C. Lin, T.-T. Wu, D.-M. Wang, On the formation of macrovoids in PMMA membranes, *J. Membr. Sci.*, 155 (1999) 31-43.